On the effects of an azimuth offset in the MBC-transformation used by IPC for wind turbine fatigue load reductions

Gianmarco Emilio Disario

Master of Science Thesis

Delft University of Technology

Delft Center for Systems and Control

On the effects of an azimuth offset in the MBC-transformation used by IPC for wind turbine fatigue load reductions

Master of Science Thesis

For the degree of Master of Science in Systems and Control at Delft University of Technology

Gianmarco Emilio Disario

July 16, 2018

Faculty of Mechanical, Maritime and Materials Engineering (3mE) · Delft University of Technology

Delft University of Technology
Department of
Delft Center for Systems and Control (dcsc)

The undersigned hereby certify that they have read and recommend to the Faculty of Mechanical, Maritime and Materials Engineering (3mE) for acceptance a thesis entitled

On the effects of an azimuth offset in the MBC-transformation used by IPC for wind turbine fatigue load reductions

by

Gianmarco Emilio Disario

in partial fulfillment of the requirements for the degree of

Master of Science Systems and Control

Dated: July 16, 2018

Supervisor(s):

Prof. dr. ir. Jan-Willem van Wingerden

Ir. Sebastiaan P. Mulders

Reader(s):

Dr. ir. Carlas S. Smith

Abstract

Wind energy currently is one of the most attractive solutions to help in the goal of switching to a more sustainable way of energy production. To stay competitive with other forms of energy production, the reduction of the Levelized Cost of Energy (LCoE) is an important indicator. One way of achieving this goal is by increasing the size of the wind turbine. As a result, the increased blade length also comes with a significant increase in fatigue loads present on the wind turbine's rotating and fixed structure.

Individual Pitch Control (IPC) forms an interesting opportunity in attenuating these fatigue loads. IPC is generally applied with the help of the Multi-Blade Coordinate (MBC-) transformation. The IPC control strategy uses the Out-of-Plane (OoP) bending moments measured on each blade. The MBC-transformation transforms the measured OoP bending moments towards the non-rotating reference frame. As a result the OoP bending moments are transformed into non-rotating yaw- and tilt-moments. The minimisation of these signals is then used as a control objective. Subsequently, the provided non-rotating control signals are then transformed back to the rotating domain to obtain the implementable individual pitch signals.

In the literature this controller synthesis is often employed by two separately operating Single-Input Single-Output (SISO) control loops. Whereby implicitly (or sometimes explicitly) assuming that the yaw- and tilt-moments are sufficiently decoupled to make this type of control viable. In the literature, a recent frequency domain analysis has shown that the coupling is non-neglible. Literature suggests that the introduction of an offset in the inverse MBC-transformation can help decouple these yaw- and tilt-moments, although this offset is usually found in an heuristic manner and its real effects are unknown.

In this study a thorough analysis on the effects of the azimuth offset is given on simplified and high-fidelity models. It is shown that the choice of blade-dynamic model structures has a significant effect on the analysis for maximum decoupling. It is also shown that a first-order model approximation is able to locate the ideal offset of a complex high-fidelity non-linear wind turbine model, which is subsequently verified by simulations and a sensitivity function analysis.

Table of Contents

Acknowledgements

First and foremost, I would like to thank my supervisor, Ir. Sebastiaan P. Mulders for all his assistance and his open attitude towards the many questions I posed. Furthermore, his enthusiasm and friendly attitude have motivated me throughout the year.

Secondly, I would like to thank Prof. dr. ir. Jan-Willem van Wingerden for his assistance throughout the master program. I am very grateful that I could be a teaching assistant for his courses. I have thoroughly enjoyed helping him with these courses and have gotten a deeper appreciation for the field of control as a result.

Thirdly, I would like to thank the department of DCSC for providing a stimulating learning environment and for the opportunity and support they have provided in the foundation of Delft Student Association Rudolf Kalman.

Finally, I would like to thank my parents in supporting me all throughout my educational career and making sure I always foster my curiosity.

Delft, University of Technology
July 16, 2018

Gianmarco Emilio Disario

Chapter 1

Introduction

As the worldwide demand for sustainable energy production grows, the demand for wind energy also increases, because wind turbines are seen as a long-term trustworthy investment for a steady supply of sustainable energy [1]. The Global Wind Energy Council (GWEC) every year publishes statistics on wind energy, where the latest figures from 2001-2017 show a more than 20 fold increase in the production of wind energy in 16 years [2]. The year-to-year numbers are given by Figure 1-1.

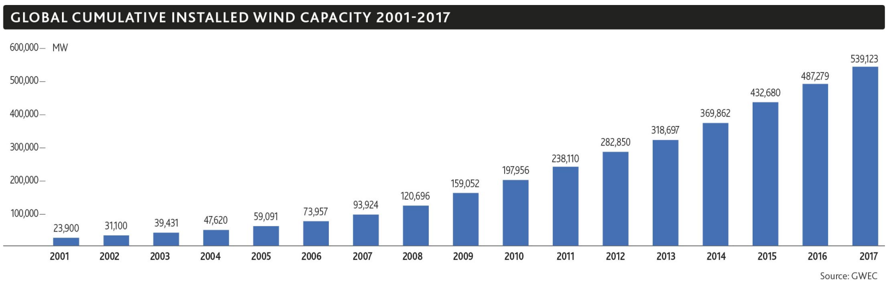

Figure 1-1: Global Cumulative Installed Wind Capacity 2001-2017. An exponential increase in the total amount of wind capacity can be observed [2].

The exponential growth in wind energy production is a strong motivation for production of ever larger, more efficient, and longer lasting wind turbines. This puts a demand on many different research fields to improve the overall performance and durability of a wind turbine. The aim of most of this research is to contribute to the reduction of the Levelized Cost of Energy (LCoE) of wind turbines, making wind turbines a more sustainable alternative to traditional oil-based power production. This is in line with the goals stated in the Paris Agreement [3].

Control of wind turbines

Control is one of the wind energy research fields. Wind turbine control aims to optimize wind turbine performance of a current design. This is done through power maximization and (fatigue) load minimization [4].

The focus of the control objectives differ depending on the operating conditions of the wind turbine, which is usually divided in 3 or 4 regions.

- **Region 1** is when the wind speed is below the cut-in wind speed. In this region the wind turbine is usually kept at a standstill by supervisory control [4].
- **Region 2** is referred to as the below-rated region. It is operates between the cut-in and the rated speed. In this region, maximization of power production by operating the rotor at the maximum power coefficient/efficiency is the main goal. For variable speed turbines, this is done through torque control [5].
- **Region 3** is the so-called above-rated region. In the above-rated region power production is limited to make sure that no excessive stresses occur on the wind turbine. For a variable pitch wind turbine, this is done through Collective Pitch Control (CPC), altering the aerodynamic rotor characteristics and efficiency [5].
- **Region 4** is the region where the wind speed is above the cut-out wind speed and the wind turbine is shut down by supervisory control.

Another possibility is the individual control of the blades. This is a very active research area and is usually referred to as Individual Pitch Control (IPC). IPC can help reduce loads, by focussing on asymmetric loads. Although this is usually employed in region 3, it is also a viable control strategy in region 2 [6].

It is also possible that an intermediate region is considered between region 2 and region 3 to assist in the transition from the different types of control [1]. In such a case it could be referred to as region 2.5.

Developments in wind turbines

A way for LCoE reduction is by is by the increase in size of the individual turbines. This is reflected by the prediction of the European Wind Energy Association (EWEA) in Figure 1-2 [7]. One of the reasons that this increase is being made is that the power produced by wind turbines is directly dependent on the area spanned by the rotor blades: a linear increase in wind turbine blade length corresponds to a squared increase in the area covered by the blades [1].

The increasing size of wind turbines also comes with its challenges. The wind field hitting the wind turbine becomes less homogeneous with an increasing area. As a result, the asymmetric once per revolution (1P) periodic (fatigue) loads on the wind turbine blades increase

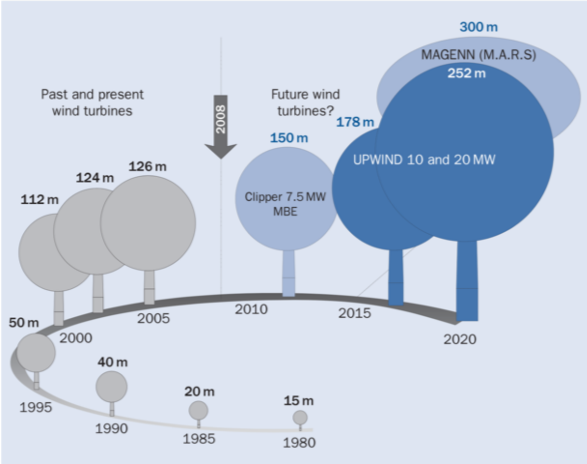

Figure 1-2: An overview of the history of the size of wind turbines is presented as well as the forecasts for the foreseeable future [7].

significantly [6]. The higher harmonics also show increases in their loads (2P, 3P, . . .). This is due to the combined effects of yaw-misalignment, wind shear, turbulence and tower shadow [8].

It is desirable to mitigate these loads on the blades as much as possible. As mentioned earlier, IPC shows great potential to aid in the reduction of these loads. A major advantage is that many Horizontal Axis Wind Turbines (HAWTs) already have individual pitch actuators installed on them. Furthermore, trying to reduce these loads through control is more economical than creating new mechanical systems to cope with heavy loads [6].

1-1 Related Research

To mitigate periodic fatigue loads with the use of IPC, it should be clear what loads are experienced by which components. The blades of the wind turbine mainly experience 1P harmonic loads. The structural components of the wind turbine are mainly affected by n_bP harmonic loads, where n_b are the number of blades of the wind turbine [8]. From this point on, a 3-bladed HAWT will be considered.

To decompose the 1P loads towards a constant load the Multi-Blade Coordinate (MBC-) transformation is employed [6]. This allows to perform control techniques directly in the low-frequency region where it is desired [9]. It does this by transforming the loads from a rotating frame of reference towards a non-rotating frame of reference which is solely dependent on the azimuth angle of the blades.

To be precise, the MBC-transformation allows for the decomposition of many different types of eigenmodes of the wind turbine [8]. Usually for control the ones considered are the Out-of-Plane (OoP) bending moments on the blades [10]. This in turn transforms them in a time-independent tilt- and yaw-moments present on the wind turbine structure.

The paper [11] extended this framework towards the control of 2P and 3P harmonics with the use of the MBC-transformation. This was done by simultaneously incorporating separate control loops for 1P, 2P and 3P harmonics. It is based on the fact that the MBC-transformation maps the 1P harmonics in the rotating frame towards the 0P harmonics in the non-rotating frame, and it moves the 2P harmonics in the rotating frame towards the 3P harmonics in the non-rotating frame [12].

Even though many HAWTs have the possibility of pitching each blade individually, the implementation of advanced IPC is currently still limited. This is likely due to the combination of pitch actuator loadings induced by continuous pitch action and difficult maintenance of sensors on the blades [13, 14]. As a result, most of the research is currently based on simulation results.

As these simulations provide promising results, several field tests have been carried out to verify the promising simulation results [15, 16]. For a 3-bladed turbine [15] managed to reduce the 1P loads on the blades significantly through MBC-transformation based IPC. The 3P structural loads were also reduced by method of applying the MBC-transformation on the 2P harmonics. Although significant reductions were made on different harmonics this came at the cost of a $4° - 5°$ per second pitch rate induced by IPC. Which was for their particular turbine well within the actuator range, but it should be a consideration on larger turbines.

The conventional IPC is inherently a Multiple-Input Multiple-Output (MIMO) control system, because of the actuation of the 3 different blades. Even when using the MBC-transformation it remains a 2-input, 2-output control system. Nevertheless several papers assume that the dynamics are sufficiently decoupled to allow for two separate Single-Input Single-Output (SISO) control loops. This has resulted in a variety of control techniques being implemented for IPC, this variety includes Linear Quadratic Gaussian (LQG) and Proportional Integral (PI) [6], as well as the more modern Model Predictive Control (MPC) [17]. But because of this inherent MIMO system, MIMO H_∞ techniques usually result in better performing controllers [18, 19].

Suggestions have been made that it is possible to present an offset in the MBC-transformation in order to increase the performance and/or decoupling of the system. The first suggestion is made in [6] to include a constant offset in the reverse MBC-transformation to take the coupling between the two transformed axes into account. In a subsequent paper the same author suggests to introduce an offset to compensate for the phase lag between the controller and the pitch actuator [20]. This is later corroborated by [21], where two offsets were introduced for two parallel IPCs on the 1P and 2P harmonics. These offsets were determined by looking at the phase lag in the bode plots of the linearised plant (including the addition of their filters). These offsets are not compared to other offsets.

During the field tests of [16] it is noted that an offset can indeed compensate for delays and the offset is found experimentally. In the other field tests of [15] the usefulness of these offsets (as well as for different harmonics) is also validated. The offsets are also determined experimentally but it was mentioned that they are too big to only represent the frequency dependent actuator delay. Here it is suggested that the offset mainly could help to compensate for cross-coupling between the MBC-transformed axis. It is also stated that it might be possible to determine the offsets in advance.

An extensive frequency-domain analysis of the workings of the MBC-transformation is given in [18]. This frequency-domain analysis shows some of the effect of the cross-coupling present. This cross-coupling is subsequently considered in the design of a controller using H_∞ techniques, but the effect of an azimuth offset is further left unconsidered. It should also be noted that [18], in its framework assumes fully decoupled blade dynamics (i.e. the pitching of the blades does not effect the loads on the other blades), which is not fully justifiable but allows for an understandable analysis.

The first proper analysis focussed on understanding the offset in the MBC-transformation is given in [22]. Here the author incorporates it in the framework set up by [18]. The effect of the offset on the gain of the system as well as its effect on the stability of the system is elaborated upon.

Summarizing, the introduction of an offset has been eluded to for several years. It has been incorporated several times in manners that make use of ad-hoc reasoning without a proper understanding of its effects. A first step has been taken to understand the effects of the offset in the reverse MBC-transformation, and its influence on the stability of the system. Therefore, this thesis will focus on expanding the understanding and framework related to the offset in the MBC-transformation.

1-2 Problem Statement & Research Goal

There seems to be a lack of understanding on the effects of the introduction of an offset in the MBC-transformation. More specifically, there currently exists a narrow framework based on fully decoupled blade dynamics and introducing the offset in the reverse transformation without clear reasoning for both of these implementations.

This thesis sets out to make an extensive analysis of the introduction of an offset in the MBC-transformation. This analysis will be made to gain an insight into the properties of the offset, aiming to clarify the different statements made in the literature. To date, the literature's main suggestion is that the offset is able to reduce the cross-coupling of the MBC-transformed system, which in turn allows for more convenient controller synthesis for IPC.

In setting up the analysis, several sub-goals need to be stated to set clear focus areas where the analysis can provide actual insights:

1. First of, the exact structure of the MBC-transformation together with (the validity of) its assumptions is analysed. More elaborately, it has been stated in the literature that the azimuth offset in the MBC-transformation should specifically be applied to

the reverse/inverse MBC-transformation without clear justification. A justification or rebuttal of this claim is a goal of this thesis.

2. The validity of the fully decoupled blade-dynamic model structure will be investigated to see if it is indeed a valid assumption for the MBC-transformation and if it also provides an appropriate model for determining the offset in the MBC-transformation.

3. As most claims with respect to the offset in the MBC-transformation relate to different type wind turbine model types, it is hard to make a general claim about its properties. To help in the analysis, this thesis applies the analysis first on a very basic model to gain a preliminary insight.

4. The basic model is then extended to a more complex model. It is then investigated whether the preliminary insights translate to the more complex model, whereby looking out for possible generalisations.

5. The final aim is to use the different insights gained to perform a simulation study to see whether the results from the different linear analyses can be extended to the non-linear domain. In this final section also the exact effects of the introduction of the azimuth offset on the controller performance is investigated.

1-3 Report Structure

This master's thesis presents six chapters. After this first introductory chapter, the second chapter derive the MBC-transformation in the way it will be used throughout the thesis. Different parts of the derivation are needed for alterations in the subsequent sections and chapters. In the second chapter, an offset is introduced in the MBC-transformation and different variations of the blade-dynamic models will be considered.

In chapter 3 a first-order model is considered for the blade-dynamics, which is a very rough approximation of the real dynamics, but it allows for an insightful analytic analysis. Chapter 4 will then use the results from chapters 2 and 3 to apply the MBC-transformation on linearisations of a high-fidelity non-linear wind turbine model. The first-order model approximation of chapter 3 will subsequently be applied to see if the insights of chapter 3 can be extended to the high-fidelity model.

Chapter 5 applies the previously obtained knowledge to apply this on a simulation of a non-linear wind turbine model. First, the found ideal decoupling for the linearisation is validated to a spectral estimate of the non-linear model. After which a time-marching simulation is run with and without the offset to see its effects on the non-linear controlled model. The chapter is then concluded with an explanation of the effect of the azimuth offset on the controller performance.

Finally, chapter 6 combines all the results in a final conclusion and gives recommendations for possibilities of future research.

Chapter 2

Multi-Blade Coordinate Transformation

In the analysis of different structural loads on HAWTs, there is an interplay between the rotating frame in which the individual blades are modeled and the fixed frame of the nacelle and support structure. The MBC-transformation allows to combine these different frames such that the structural loads can be analyzed in a single coordinate frame. This chapter first provides an introduction to the MBC-transformation and, subsequently, the transformation is derived for a linear wind turbine model. After which an azimuth offset is introduced in the transformation. Finally, one of the main assumptions on which conventional IPC is based (a fully decoupled blade-dynamic model structure) is alleviated and will be changed to see its influence on the MBC-transformation.

2-1 Introduction to the transformation

In this introduction, the history related to the MBC-transformation is set out, after which the application to wind turbine load control is explained. When the characteristics of the transformation become clear, the possibility of exploiting possible arises.

2-1-1 History

The design and dynamics of a wind turbine closely resemble the ones of a helicopter [23]. In this regard, one might take a look at the classic helicopter literature to see if the analyses on helicopter blades is also applicable to the wind turbine rotor. The first occurrence of an analysis of the dynamics of helicopter rotor blades through a decoupling of eigenmodes was carried out in [24]. It was referred to as the Multi-Blade Coordinate transformation, and it was used to analyze the stability related to flap-motion of the blades. In two subsequent papers, [25, 26] the mathematical basis has been set out to decompose the blades from a rotating frame to a frame where the eigenmodes could be analyzed. As Coleman was one of its founders, it is also referred to as the Coleman transformation [25].

2-1-2 Application on wind turbines

Now that the origins of the MBC-transformation are known, its application to wind turbines is assessed. The MBC-transformation can be applied to different modes of the wind turbine. The most mathematically general form is presented in [10], where the author allows for the analysis of different eigenmodes of the wind turbine and also for a different number of blades of the turbine. The eigenmodes of the turbines analysed by [10] correspond to the analysis of the loads made on the turbine by [8]. In the paper of [8] a large variety of loads present on the wind turbine are explained with the help of the MBC-transformation. It also provides a framework to analyse these eigenmodes in a non-rotating frame of reference. By exploiting this frame of reference different (frequency dependent) properties of these loads are set out. This thesis will focus on the application of the MBC-transformation on the Out-of-Plane bending moments.

2-1-3 Control using the MBC-transformation

The MBC-transformation allows for a decoupling of the Out-of-Plane bending moments on the blades in a rotating frame of reference towards structural yaw and tilt moments in a non-rotating frame of reference. This results in yaw and tilt moments which are a function of rotational speed. The resulting functions depending on rotational speed then allow for frequency analysis, which in turn proves being useful for application of classic control techniques. Combining this property with individual blade load measurements, the loads can be reduced by controlling the individual blades. This field of research is generally referred to as individual pitch control.

The first application of research in this topic is performed in [27], where different control techniques are applied to asses the proper application of IPC for load reductions. Another seminal paper in the research of IPC is [6], where the MBC-Transformation is used, although the writer refers to it as the d-q transformation. An LQG controller is applied and a considerable improvement in fatigue load reduction as compared to solely applying CPC is found. In the paper, CPC is used to optimise for power output, and the IPC is applied in parallel to reduce the loads on the individual blades as well as other harmonic loads. Except for an LQG control implementation, also PI-controllers are used on different parts of the turbine for comparison to the LQG controller. The results in the paper are shown in Figure 2-1.

Figure 2-1 shows the differences in loads on the system for different type of controllers. A big reduction at the rotor speed frequency can be seen by introducing IPC for the shaft bending moment and the Out-of-Plane bending moments measured at the root of the blade. The difference in the yaw-bearing moment is mainly experienced as a reduction of the DC-gain. This is due to the fact that the MBC-transformation maps the once per revolution harmonics towards the 0P or DC-gain of the system. The difference between only collective pitch and the introduction of the individual pitch is most significant. The reduction between the different IPC strategies is less significant. These IPC strategies include LQG control as well as PI control based on different sensors on the turbine (blade, shaft, and yaw bearing sensors).

Recently, more advanced control implementations are applied using the MBC framework. In [18], the MBC-transformation is employed using linear blade models. The paper synthesises

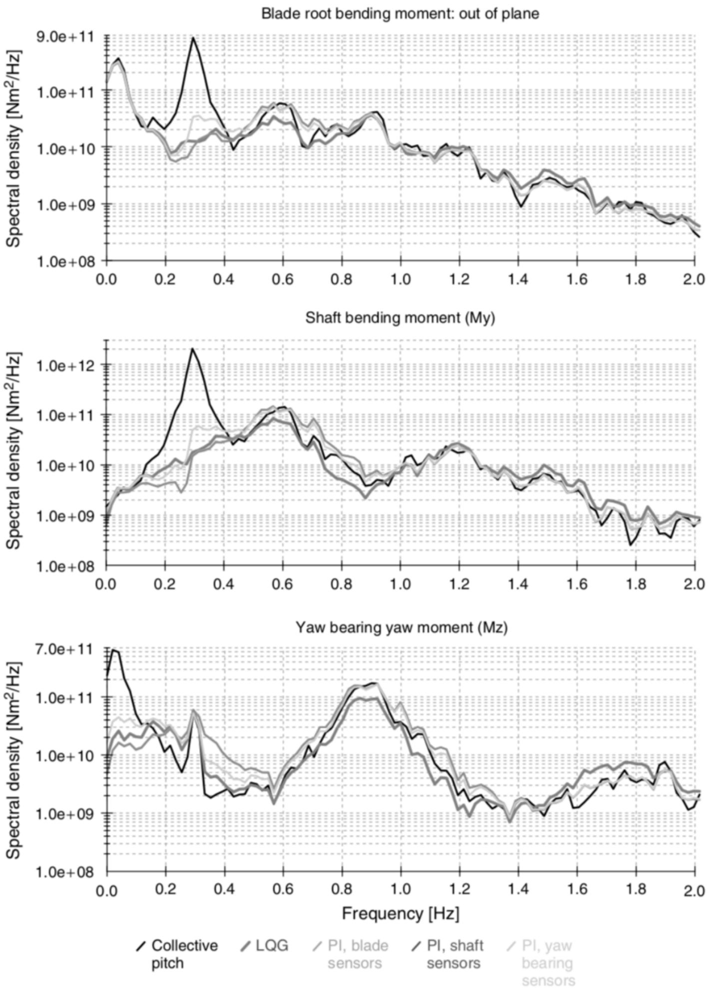

Figure 2-1: The application of different IPC controllers compared to a CPC controller. A significant drop in loads present on the turbine can be seen at the 1P frequency for the OoP bending moment and shaft bending moment for the IPC as opposed to CPC. For the yaw moment this reduction is at the DC-gain, because of the properties of the MBC-transformation. The difference between the different IPC strategies is not very significant. [6]

different SISO controllers and a robust MIMO controller based on H_∞ loop shaping for IPC. The H_∞ controller proved to be most successful in the reduction of most bending moments, which was discussed to be true because of the coupling between tilt- and yaw-moments.

In 2016, [19] elaborates on [18], where the MIMO H_∞ synthesis is done more elaborately and subsequently gives more insight into the sensitivity function analysis as well as the weight selection in the model. Another improvement is the bound that is put on the input control action to the specific blades (in other words, limiting how far the blades physically are able to pitch). Furthermore, the use of a linearized model is analyzed and compared to a non-linear model and the limitations show that a reduction of loads at higher frequencies is hard to achieve using the linear model. It was discussed that this is due to the impossibility of incorporating the higher order dynamics in the linear model. This means that based on linearizations, significant reductions of 1P harmonic blade loads are attainable, but negligible reductions are attained for 2P and higher harmonics.

The MBC-transformation nevertheless gives insight into the specific loads on the turbine, and proves to be a useful tool for analysis and further controller synthesis.

2-2 Derivation of the MBC-transformation

This section presents a mathematical derivation for the MBC-transformation. As was noted before by Bir and Hansen [10, 8], the MBC-transformation can be performed for a variety of eigenmodes and number of blades of the wind turbine. This section will only cover the Out-of-Plane bending moments on the blades. The focus on this specific mode for the MBC-transformation gives the opportunity to show more specific properties of the MBC-transformation as opposed to the more generic form.

2-2-1 Basic setup of the MBC-transformation

The main setup for MBC-transformation based IPC can be seen in Figure 2-2. From the turbine one can measure the bending moments on the specific blades, these are denoted as $M_1(t)$, $M_2(t)$, $M_3(t)$. Furthermore, the rotational speed of the wind turbine, $\omega_0(t)$ (in [rad/s.]) is normally used for CPC, which then, in turn, provides a mean pitch actuation angle for all the blades to turn to $\bar{\theta}(t)$. When the bending moments are fed through the MBC-transformation, this results in the separation of the average bending moment $\bar{M}(t)$ and a separate yaw-, and tilt-moment $M_{\text{yaw}}(t)$, $M_{\text{tilt}}(t)$, respectively. When these are fed through the IPC, two abstract and non-intuitive pitch angles are obtained, which are referred to as $\theta_{\text{yaw}}(t)$, $\theta_{\text{tilt}}(t)$ respectively. These are then combined with the CPC mean pitch actuation of all the pitch angles $\bar{\theta}(t)$ and fed back through the inverse MBC-transformation where blade-specific pitch angles $\tilde{\theta}_1(t)$, $\tilde{\theta}_2(t)$, $\tilde{\theta}_3(t)$ are obtained.

Any additional terms which are not of specific interest are captured in the term $f(t)$. This includes among other things wind loading and generator torque. Furthermore, $\phi(t)$ refers to the azimuth angle of the first blade of the wind turbine. The azimuth angle in this case is defined to be the angle between the top of the wind turbine and the current position of the first blade. This means the azimuth angles of the second and third blade can be characterised by the azimuth of the first blade with the addition of $\frac{2}{3}\pi$ and $\frac{4}{3}\pi$ respectively. The rotational speed of the wind turbine, ω_0, will be assumed to be constant. This results in an azimuth angle of the form $\phi(t) = \omega_0 t$.

The transformation from the separate moments on the blades to the average, tilt- and yaw-moments is through a matrix multiplication,

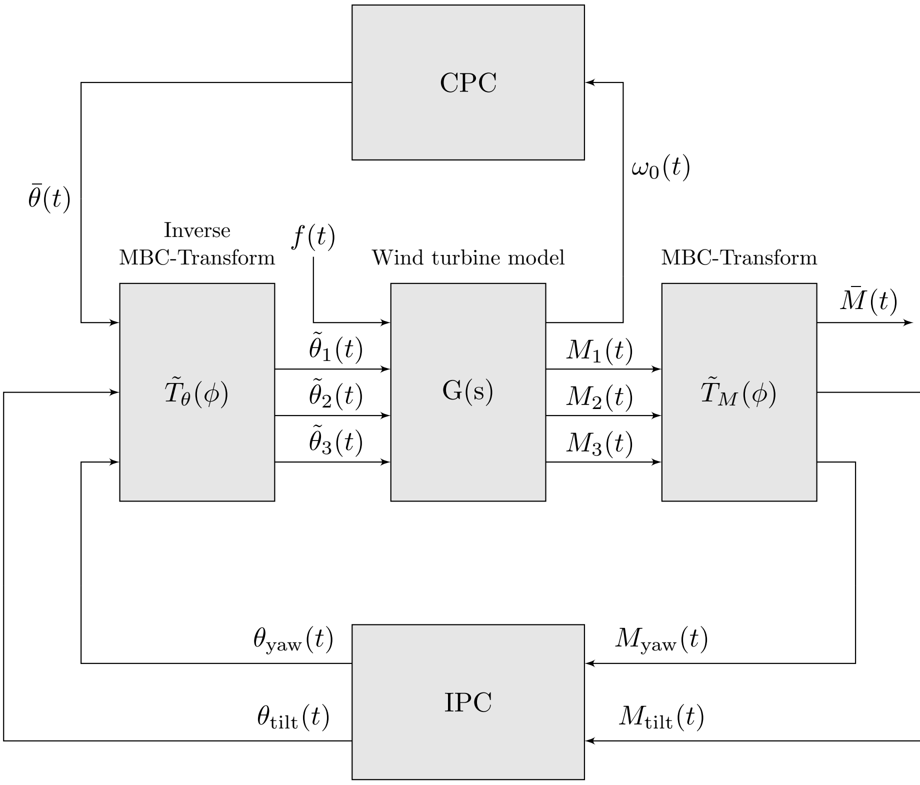

Figure 2-2: The basic model how the MBC-transformation is used in IPC. The wind turbine model gets input signals $\tilde{\theta}_i(t)$ for the blade $i \in \{1, 2, 3\}$. All other inputs are captured in $f(t)$. The outputs of interest of the wind turbine model are the OoP bending moments $M_i(t)$ (for the blades $i \in \{1, 2, 3\}$), as well as the rotor speed ω_0. For CPC, generally only ω_0 is used, which subsequently provides a mean pitch actuation signal $\bar{\theta}(t)$. The MBC-transform transforms the blade moments into three new signals, $\bar{M}(t)$, $M_{\text{yaw}}(t)$, and $M_{\text{tilt}}(t)$. Where the tilt- and yaw-signals are utilised for IPC. This then provides the signals $\theta_{\text{yaw}}(t)$ and $\theta_{\text{yaw}}(t)$. Which are subsequently combined with the mean pitch signal to be transformed back by the inverse MBC-transformation towards the pitch input signals.

$$\begin{bmatrix} \bar{M}(t) \\ M_{\text{tilt}}(t) \\ M_{\text{yaw}}(t) \end{bmatrix} = \underbrace{\begin{bmatrix} \frac{1}{3} & \frac{1}{3} & \frac{1}{3} \\ \frac{2}{3}\cos\phi(t) & \frac{2}{3}\cos\left(\phi(t) + \frac{2}{3}\pi\right) & \frac{2}{3}\cos\left(\phi(t) + \frac{4}{3}\pi\right) \\ \frac{2}{3}\sin\phi(t) & \frac{2}{3}\sin\left(\phi(t) + \frac{2}{3}\pi\right) & \frac{2}{3}\sin\left(\phi(t) + \frac{4}{3}\pi\right) \end{bmatrix}}_{\tilde{T}_M(\phi)} \begin{bmatrix} M_1(t) \\ M_2(t) \\ M_3(t) \end{bmatrix}. \tag{2-1}$$

This can be verified by decomposing the bending moments in a classical statics/mechanics of materials framework and decomposing the blade moments in their respective horizontal and vertical moments. In Figure 2-2 it can be seen that the average moment $\bar{M}(t)$ is not of interest for IPC. This means that the first row from Eq. (2-1) can be omitted. This leaves the form which is generally considered in IPC, namely

$$\begin{bmatrix} M_{\text{tilt}}(t) \\ M_{\text{yaw}}(t) \end{bmatrix} = \underbrace{\begin{bmatrix} \frac{2}{3}\cos\phi(t) & \frac{2}{3}\cos\left(\phi(t)+\frac{2}{3}\pi\right) & \frac{2}{3}\cos\left(\phi(t)+\frac{4}{3}\pi\right) \\ \frac{2}{3}\sin\phi(t) & \frac{2}{3}\sin\left(\phi(t)+\frac{2}{3}\pi\right) & \frac{2}{3}\sin\left(\phi(t)+\frac{4}{3}\pi\right) \end{bmatrix}}_{T_M(\phi)} \begin{bmatrix} M_1(t) \\ M_2(t) \\ M_3(t) \end{bmatrix}. \tag{2-2}$$

The inverse transformation for the pitch angles has a similar derivation. It adds the mean actuation of all pitch angles, $\bar{\theta}(t)$ with a cosine and sine multiplication of the tilt- and yaw-pitch actuation angles respectively. In this manner the transformation conforms with the mechanics of materials theory once again. This results in

$$\begin{bmatrix} \tilde{\theta}_1(t) \\ \tilde{\theta}_2(t) \\ \tilde{\theta}_3(t) \end{bmatrix} = \underbrace{\begin{bmatrix} 1 & \cos\phi(t) & \sin\phi(t) \\ 1 & \cos\left(\phi(t)+\frac{2}{3}\pi\right) & \sin\left(\phi(t)+\frac{2}{3}\pi\right) \\ 1 & \cos\left(\phi(t)+\frac{4}{3}\pi\right) & \sin\left(\phi(t)+\frac{4}{3}\pi\right) \end{bmatrix}}_{\tilde{T}_\theta(\phi)} \begin{bmatrix} \bar{\theta}(t) \\ \theta_{\text{tilt}}(t) \\ \theta_{\text{yaw}}(t) \end{bmatrix}. \tag{2-3}$$

It can be verified quite quickly that $\tilde{T}_M(\phi)$ from Eq. (2-1) and $\tilde{T}_\theta(\phi)$ from Eq. (2-3) are each others' inverses. This is the reason they are commonly referred to as the MBC-transformation and the inverse MBC-transformation. The IPC only provides an actuation of the pitch angles on top of the mean actuation which comes from the CPC. This means that the different pitch angles can be decomposed into

$$\begin{cases} \tilde{\theta}_1(t) & = \bar{\theta}(t) + \theta_1(t), \\ \tilde{\theta}_2(t) & = \bar{\theta}(t) + \theta_2(t), \\ \tilde{\theta}_3(t) & = \bar{\theta}(t) + \theta_3(t). \end{cases} \tag{2-4}$$

As the interest currently lies in discovering the properties of the IPC, the mean term will be dropped out and the only term for interest is the blade-specific pitch angles. This means that the first column of Eq. (2-3) can be omitted, which leaves

$$\begin{bmatrix} \theta_1(t) \\ \theta_2(t) \\ \theta_3(t) \end{bmatrix} = \underbrace{\begin{bmatrix} \cos\phi(t) & \sin\phi(t) \\ \cos\left(\phi(t)+\frac{2}{3}\pi\right) & \sin\left(\phi(t)+\frac{2}{3}\pi\right) \\ \cos\left(\phi(t)+\frac{4}{3}\pi\right) & \sin\left(\phi(t)+\frac{4}{3}\pi\right) \end{bmatrix}}_{T_\theta(\phi)} \begin{bmatrix} \theta_{\text{tilt}}(t) \\ \theta_{\text{yaw}}(t) \end{bmatrix}. \tag{2-5}$$

It is now interesting to see how the yaw- and tilt-moments are related to the yaw- and tilt-pitch angles. This can be done by assuming a linear model for the blade-dynamics and setting up a transfer function from $(M_{\text{tilt}}(t),\ M_{\text{yaw}}(t))$ to $(\theta_{\text{tilt}}(t),\ \theta_{\text{yaw}}(t))$. This linear model will relate the pitch blade actuation to the moments on the blades. It will be referred to as $G : \mathbb{C}^{3\times 3} \to \mathbb{C}^{3\times 3}$. Please note that the terms "wind turbine model" and "blade-dynamics model" will be used intermittently throughout this thesis, but both relate to $G(s)$. This is done because from time to time it might be better for the understanding of the reader to refer to it as a wind turbine model or a blade-dynamics model. It should of course be clear that it does not fully describe all the dynamics of the entire wind turbine, but only the ones that relate pitch angles to the moments.

Now that the characteristics of interest are described for IPC, the full framework can be set up which will allow an in-depth analysis. This framework combines Eq. (2-2), Eq. (2-5) and the assumption of a linear model $G(s)$ which described the blade-dynamics. A block-diagram of this framework is shown in Figure 2-3. In essence, the IPC-loop present in Figure 2-2 is extracted in Figure 2-3. This allows for more efficient analysis of only the IPC part.

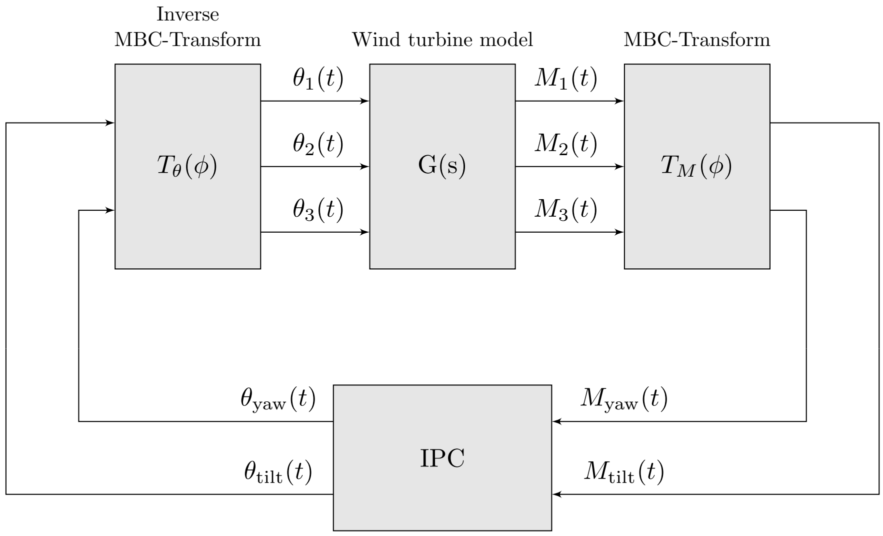

Figure 2-3: The block-diagram model describing the IPC framework under consideration. This is a reduced form of Figure 2-3.

The use of the linearized wind turbine model $G(s)$ will prove to be very useful to gain an insight into the offsets, gains, and couplings present in the turbine. The azimuth angle in Figure 2-3 is dependent on time, $\phi(t)$. Figure 2-3 also shows that the mean moment and average pitch angle coming from the CPC are omitted compared to Figure 2-2. They can easily be incorporated again later to provide full detail in their interactions, but for the derivation, they would only prove to make it harder to follow.

2-2-2 Deriving the MBC-transformation

In classical controller design it is interesting to have a good picture of the dynamics between the input and output. In Figure 2-3 the controller is situated in the IPC block. This means that it is interesting to see the dynamics from $\begin{bmatrix} \theta_{\text{tilt}} \\ \theta_{\text{yaw}} \end{bmatrix} \rightarrow \begin{bmatrix} M_{\text{tilt}} \\ M_{\text{yaw}} \end{bmatrix}$. In Eq. (2-2) this is already done to go from the specific blade moments to the generalised tilt- and yaw-moments. The same has been done in Eq. (2-5) for the pitch angles. This means one step is missing which is to go from pitch angles to the moments. Depending on the model it is described by

$$\begin{bmatrix} M_1(t) \\ M_2(t) \\ M_3(t) \end{bmatrix} = G(s) \begin{bmatrix} \theta_1(t) \\ \theta_2(t) \\ \theta_3(t) \end{bmatrix}. \tag{2-6}$$

Combining Eq. (2-2), Eq. (2-5) and Eq. (2-6) into one equation results in the full interaction from tilt- and yaw-pitch angles to tilt- and yaw-moments,

$$\begin{bmatrix} M_{\text{tilt}}(t) \\ M_{\text{yaw}}(t) \end{bmatrix} = T_\theta(\phi(t))G(s)T_M(\phi(t)) \begin{bmatrix} \theta_{\text{tilt}}(t) \\ \theta_{\text{yaw}}(t) \end{bmatrix}. \tag{2-7}$$

The sub-dependencies on 't' of the MBC-transformation are specifically indicated in Eq. (2-7) to indicate that this is the time-domain interaction of the pitch angles and moments. For controller design it is desired that this is transferred into the frequency-domain, because it allows for a more insightful picture of the exact frequency dependent dynamics of the system. Hereby the gain and phase properties on specific frequencies might indicate high loads in certain regions which can be mitigated by the controller.

Eq. (2-7) can be transferred into the frequency-domain by a classical Laplace transformation. This Laplace transformation is not as straightforward as it seems, because of the time-dependencies within the arguments of the sines and cosines in Eq. (2-2) and Eq. (2-5). Furthermore, the choice of blade-dynamics model structure is also very important for the resulting final description of the system. This will be discussed in detail in Chapter 2-4. For now an assumption is made that there is no interaction in the dynamics between the different blades and that the dynamics of every blade are the same. This allows for a fully decoupled system and provides a clear and concise foundation for the derivation before expanding on it in Chapter 2-4. This means that $G(s)$ can be described by,

$$\begin{bmatrix} M_1(t) \\ M_2(t) \\ M_3(t) \end{bmatrix} = \underbrace{\begin{bmatrix} g_b(s) & 0 & 0 \\ 0 & g_b(s) & 0 \\ 0 & 0 & g_b(s) \end{bmatrix}}_{G_b(s)} \begin{bmatrix} \theta_1(t) \\ \theta_2(t) \\ \theta_3(t) \end{bmatrix}. \tag{2-8}$$

Which in turn allows for a system where $M_i(t) = g_b(s)\theta_i(t),\ i \in \{1, 2, 3\}$. This changes the general form of Figure 2-3 into the specific form of Figure 2-4.

The full in-depth mathematical details of the derivation of the MBC-transformation can be found in Appendix A. The resulting frequency-domain description of Eq. (2-7) is

$$\begin{bmatrix} M_{\text{tilt}}(s) \\ M_{\text{yaw}}(s) \end{bmatrix} = \begin{bmatrix} \frac{g_b(s-j\omega_0)+g_b(s+j\omega_0)}{2} & j\frac{g_b(s-j\omega_0)-g_b(s+j\omega_0)}{2} \\ -j\frac{g_b(s-j\omega_0)-g_b(s+j\omega_0)}{2} & \frac{g_b(s-j\omega_0)+g_b(s+j\omega_0)}{2} \end{bmatrix} \begin{bmatrix} \Theta_{\text{tilt}}(s) \\ \Theta_{\text{yaw}}(s) \end{bmatrix}. \tag{2-9}$$

This results in a similar form as described in [18], although a sign change is noticed on the off-diagonal compared to the description of [18]. As that paper does not show its derivation, it is assumed to be an error in their derivation. From this point, the coupling between the yaw- and tilt-moments becomes clear since the off-diagonal components in Eq. (2-9) are not zero if $\omega_0 \neq 0$. This means that in case the rotor speed $\omega_0 = 0$ rad/s there is no coupling between the yaw- and tilt-moments, but as soon as the wind turbine starts rotating a coupling starts becoming apparent.

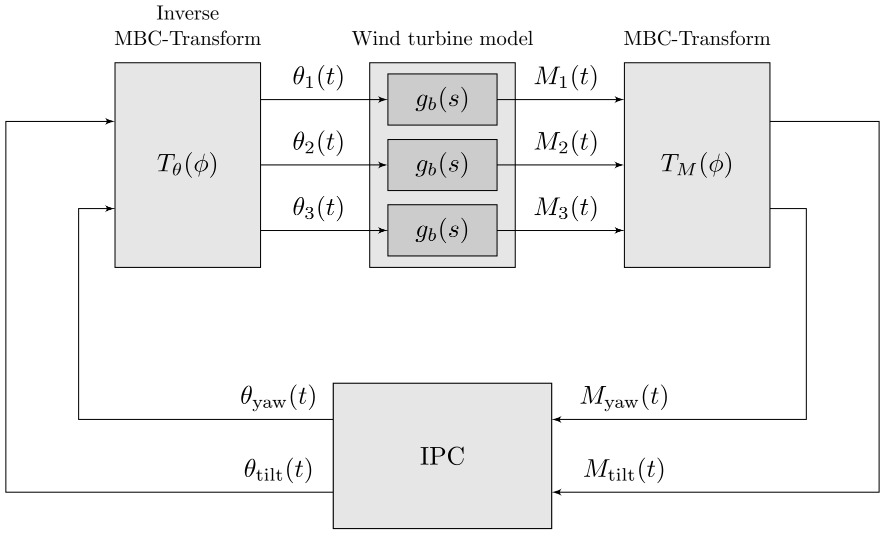

Figure 2-4: The block-diagram model describing the IPC framework for a fully decoupled blade-dynamic model structure $G_b(s)$. Here $g_b(s)$ describes the linear blade-dynamics from the pitch actuation towards the bending moments on the blades.

2-3 Introduction of an offset

As earlier discussed in Chapter 1-1, several reasons have been proposed why the introduction of an offset in the MBC-transformation can come in useful. First of all, it can help to compensate for the controller-actuator phase lag [6, 15, 16, 21]. During field testing it has been seen that significantly more offset is usually needed than expected to be induced by controller-actuator phase lag [20]. This offset might be explained by cross-coupling between the tilt- and yaw-moments. This cross-coupling can indeed be seen in Eq. (2-9).

Furthermore the offset has classically always been suggested to applied in $T_\theta(\phi)$ without clear justification why. This Section explains why this might be the case and see what the effect is if the offset is added either in $T_\theta(\phi)$, in $T_M(\phi)$, or in both. This will then also set the foundation for any further analysis that might make use of the offset in the MBC-transformation.

2-3-1 Offset in the inverse MBC-transformation

When introducing an offset in the inverse transform it means that a new term is introduced in the T_θ matrix of Eq. (2-5). This changes the model of Figure 2-3 into a model of the form which can be seen in Figure 2-5.

As a result, the derivation made in Chapter 2-2 changes slightly. The following terms will be introduced to mean the offset and will make clear that a different transformation is performed as opposed in the previous section. The offset is introduced in the form $\phi_\theta(t) = \omega_0 t + \psi_\theta$. Where ψ_θ is a constant offset. As can be seen in Figure 2-5 this offset is presented in T_θ which changes its dependency from $\phi(t)$ to $\phi_\theta(t)$. This also induces a change in Eq. (2-5) of the form

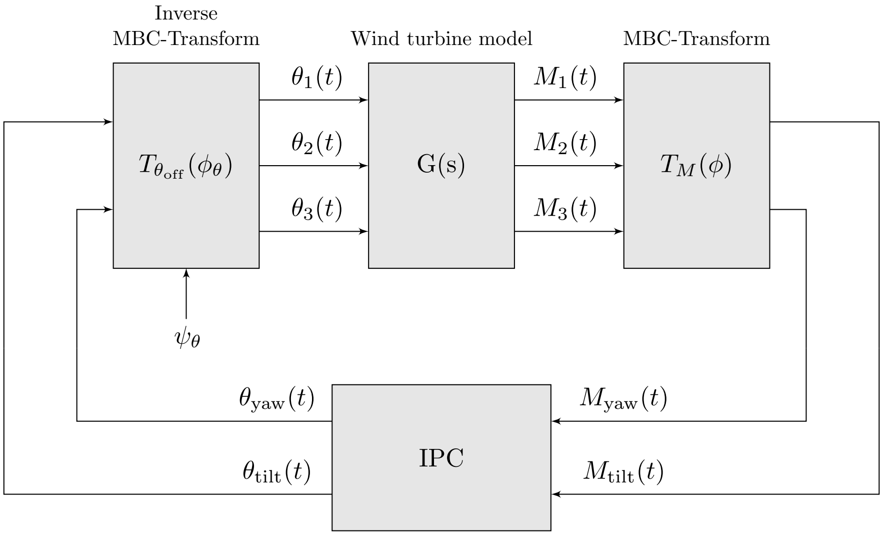

Figure 2-5: The block-diagram model describing the IPC framework with an offset inclusion of ψ_θ in T_θ.

$$\begin{bmatrix}\theta_1(t)\\ \theta_2(t)\\ \theta_3(t)\end{bmatrix} = \underbrace{\begin{bmatrix}\cos\phi_\theta(t) & \sin\phi_\theta(t)\\ \cos\left(\phi_\theta(t)+\frac{2\pi}{3}\right) & \sin\left(\phi_\theta(t)+\frac{2\pi}{3}\right)\\ \cos\left(\phi_\theta(t)+\frac{4\pi}{3}\right) & \sin\left(\phi_\theta(t)+\frac{4\pi}{3}\right)\end{bmatrix}}_{T_{\theta_{\mathrm{off}}}(\phi_\theta)} \begin{bmatrix}\theta_{\mathrm{tilt}}(t)\\ \theta_{\mathrm{yaw}}(t)\end{bmatrix}. \tag{2-10}$$

This has a considerable effect on the matrix multiplications in the derivation of the MBC-transformation. The exact mathematical details are described in Appendix B-1. When it is worked out in detail, the form of Eq. (2-9) changes into

$$\begin{bmatrix}M_{\mathrm{tilt}}(s)\\ M_{\mathrm{yaw}}(s)\end{bmatrix} = \begin{bmatrix}\frac{e^{-j\psi_\theta} g_b(s-j\omega_0)+e^{j\psi_\theta} g_b(s+j\omega_0)}{2} & j\frac{e^{-j\psi_\theta} g_b(s-j\omega_0)-e^{j\psi_\theta} g_b(s+j\omega_0)}{2}\\ -j\frac{e^{-j\psi_\theta} g_b(s-j\omega_0)-e^{j\psi_\theta} g_b(s+j\omega_0)}{2} & \frac{e^{-j\psi_\theta} g_b(s-j\omega_0)+e^{j\psi_\theta} g_b(s+j\omega_0)}{2}\end{bmatrix} \begin{bmatrix}\Theta_{\mathrm{tilt}}(s)\\ \Theta_{\mathrm{yaw}}(s)\end{bmatrix}. \tag{2-11}$$

Where a phase-shift of the different blade-dynamics is observed. As the phase-shift $e^{-j\psi_\theta}$ is applied on the argument shifted $g_b(s-j\omega_0)$ and the phase-shift $e^{j\psi_\theta}$ is applied on the argument shifted $g_b(s+j\omega_0)$, the effect on the full model description cannot not easily be interpreted without an explicit model description of $g_b(s)$.

2-3-2 Offset in the MBC-transformation

In case the offset is introduced in the MBC-transformation the change then occurs in T_M. This specific offset will be denoted as $\phi_M(t) = \omega_0 t + \psi_M$, where ψ_M is a constant. This means that diagram of Figure 2-3 changes into the form described in Figure 2-6.

As a result the derivation changes slightly once again, but this time the change of the derivation is due to the introduction of the offset in Eq. (2-2). The new form is described by

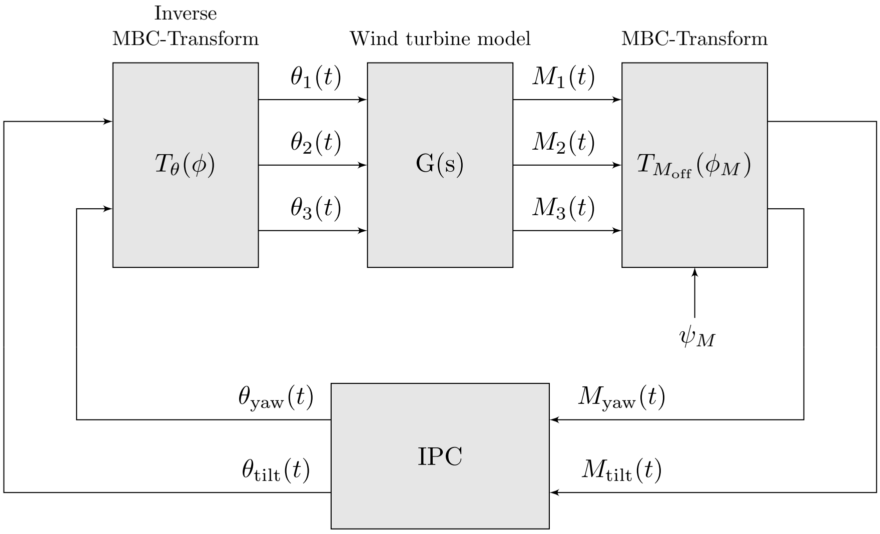

Figure 2-6: The block-diagram model describing the IPC framework with an offset inclusion of ψ_M in T_M.

$$\begin{bmatrix} M_{\text{tilt}}(t) \\ M_{\text{yaw}}(t) \end{bmatrix} = \frac{2}{3} \underbrace{\begin{bmatrix} \cos\phi_M(t) & \cos\left(\phi_M(t) + \frac{2\pi}{3}\right) & \cos\left(\phi_M(t) + \frac{4\pi}{3}\right) \\ \sin\phi_M(t) & \sin\left(\phi_M(t) + \frac{2\pi}{3}\right) & \sin\left(\phi_M(t) + \frac{4\pi}{3}\right) \end{bmatrix}}_{T_{M_{\text{off}}}(\phi_M)} \begin{bmatrix} \tilde{M}_1(t) \\ \tilde{M}_2(t) \\ \tilde{M}_3(t) \end{bmatrix}. \tag{2-12}$$

Once again the full mathematical consequences for the derivation are described in Appendix B-2. The resulting transfer function relating the pitches to the moments is described by

$$\begin{bmatrix} M_{\text{tilt}}(s) \\ M_{\text{yaw}}(s) \end{bmatrix} = \begin{bmatrix} \frac{e^{j\psi_M} g_b(s-j\omega_0)+e^{-j\psi_M} g_b(s+j\omega_0)}{2} & j\frac{e^{j\psi_M} g_b(s-j\omega_0)-e^{-j\psi_M} g_b(s+j\omega_0)}{2} \\ -j\frac{e^{j\psi_M} g_b(s-j\omega_0)-e^{-j\psi_M} g_b(s+j\omega_0)}{2} & \frac{e^{j\psi_M} g_b(s-j\omega_0)+e^{-j\psi_M} g_b(s+j\omega_0)}{2} \end{bmatrix} \begin{bmatrix} \Theta_{\text{tilt}}(s) \\ \Theta_{\text{yaw}}(s) \end{bmatrix}. \tag{2-13}$$

Eq. (2-13) shows that the offset introduced in the transformation makes a 180 degree phase shift as compared to the offset being in the inverse MBC-transformation (Eq. (2-11)).

2-3-3 Offset in both the MBC-transformations

The final case of an offset being present is the possiblity that an offset is induced in the regular MBC-transformation as well as in the inverse MBC-transformation. This means that the offsets of Figure 2-5 and Figure 2-6 can now be combined into one block scheme including both offsets. This is shown in Figure 2-7.

In case the derivation is made (as is done in Appendix B-3) the final form is obtained to be

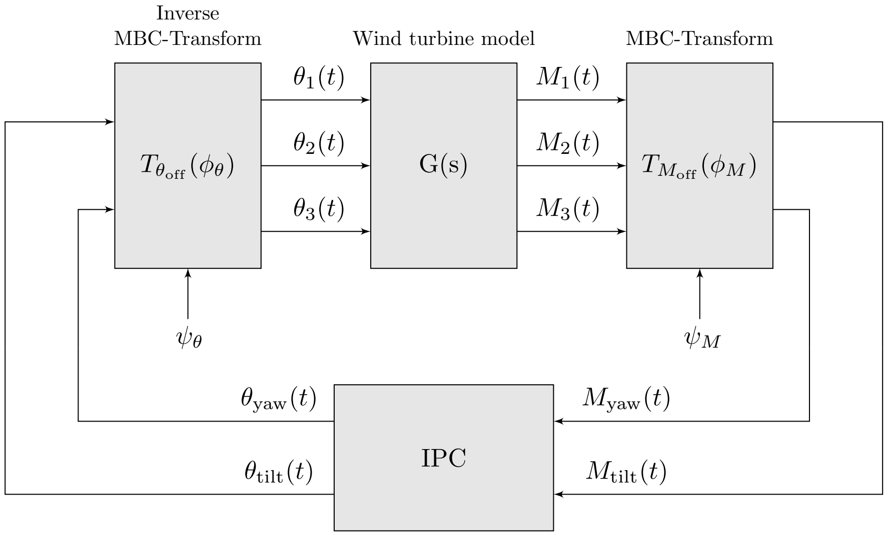

Figure 2-7: The block-diagram model describing the IPC framework with an offset inclusion of ψ_θ and ψ_M in T_θ and T_M respectively.

$$\begin{bmatrix} M_{\text{tilt}}(s) \\ M_{\text{yaw}}(s) \end{bmatrix} = \begin{bmatrix} \frac{e^{-j(\psi_\theta-\psi_M)}g_b(s-j\omega_0)+e^{j(\psi_\theta-\psi_M)}g_b(s+j\omega_0)}{2} & j\frac{e^{-j(\psi_\theta-\psi_M)}g_b(s-j\omega_0)-e^{j(\psi_\theta-\psi_M)}g_b(s+j\omega_0)}{2} \\ -j\frac{e^{-j(\psi_\theta-\psi_M)}g_b(s-j\omega_0)-e^{j(\psi_\theta-\psi_M)}g_b(s+j\omega_0)}{2} & \frac{e^{-j(\psi_\theta-\psi_M)}g_b(s-j\omega_0)+e^{j(\psi_\theta-\psi_M)}g_b(s+j\omega_0)}{2} \end{bmatrix} \begin{bmatrix} \Theta_{\text{tilt}}(s) \\ \Theta_{\text{yaw}}(s) \end{bmatrix}. \quad (2\text{-}14)$$

Where, in Eq. (2-14) the phase-shifts of Eq. (2-11) and Eq. (2-13) are combined. It is possible to define a new offset $\psi = \psi_\theta - \psi_M$ and rewrite it in a more concise way as follows,

$$\begin{bmatrix} M_{\text{tilt}}(s) \\ M_{\text{yaw}}(s) \end{bmatrix} = \begin{bmatrix} \frac{e^{-j\psi}g_b(s-j\omega_0)+e^{j\psi}g_b(s+j\omega_0)}{2} & j\frac{e^{-j\psi}g_b(s-j\omega_0)-e^{j\psi}g_b(s+j\omega_0)}{2} \\ -j\frac{e^{-j\psi}g_b(s-j\omega_0)-e^{j\psi}g_b(s+j\omega_0)}{2} & \frac{e^{-j\psi}g_b(s-j\omega_0)+e^{j\psi}g_b(s+j\omega_0)}{2} \end{bmatrix} \begin{bmatrix} \Theta_{\text{tilt}}(s) \\ \Theta_{\text{yaw}}(s) \end{bmatrix}. \quad (2\text{-}15)$$

Eq. (2-15) has the exact same form as Eq. (2-11). This means that instead of introducing an offset in both transformations a single offset can be introduced into $T_\theta(\phi)$ and make that $\psi = \psi_\theta - \psi_M$. This means that an offset being present in the inverse MBC-transformation suffices in the analysis. In case it is desired to have the offset be present in the MBC-Transform instead of the inverse MBC-Transform then the sign of ψ can simply be changed.

2-4 Effects of the choice of blade-dynamic model Structure on the MBC-transformation

During the derivation of a frequency domain representation of the MBC-transformation in Section 2-2-2, an assumption was made that the wind-turbine model was fully decoupled and equal for every $\theta_i(t) \rightarrow M_i(t),\ i \in \{1, 2, 3\}$. This led to a cancellation of different terms in Eq. (A-18) such that the final MBC-transformation loses its dependency on terms with the argument $(s \pm 2j\omega_0)$. This section will make a thorough analysis of different model structures of the blade-dynamics.

To prevent any confusion, the models indicated with a capital letter $G(s)$ refers to the matrix relating the pitch angles to the respective moments on the blades. Whereas the small letter $g(s)$ refers to the specific linear model relating the effects of one specific pitch angle (e.g. $\theta_1(t)$) to a specific moment on a blade (e.g. $M_2(t)$). This means that the most general form might be written as

$$\begin{bmatrix} M_1(t) \\ M_2(t) \\ M_3(t) \end{bmatrix} = G(s) \begin{bmatrix} \theta_1(t) \\ \theta_2(t) \\ \theta_3(t) \end{bmatrix} = \begin{bmatrix} g_{11}(s) & g_{12}(s) & g_{13}(s) \\ g_{21}(s) & g_{22}(s) & g_{23}(s) \\ g_{31}(s) & g_{32}(s) & g_{33}(s) \end{bmatrix} \begin{bmatrix} \theta_1(t) \\ \theta_2(t) \\ \theta_3(t) \end{bmatrix}. \tag{2-16}$$

In an ideal case, one would analyse the system described in Eq. (2-16) and from there make conclusions to simplifications based on the analytical analysis. As mentioned above, this is undesirable because certain cancellations would not occur in the mathematical derivation whereby making the general form not at all intuitive. This means that this section will restrict itself to simplified model structures which could bear resemblances to real-world wind turbine dynamics.

2-4-1 Decoupled blade-dynamic model structure

In the case that there is a negligible amount of interplay between pitch angles and loads on the different blades, a fully decoupled system might be the appropriate choice for analysis. This means that all off-diagonal terms in Eq. (2-16) are set to 0. There is then a second choice which has to be made and that is if all blade-dynamics are exactly the same, meaning that the interplay between $\theta_1(t) \rightarrow M_1(t) \sim \theta_2(t) \rightarrow M_2(t)$, or if that is not the case, $\theta_1(t) \rightarrow M_1(t) \nsim \theta_2(t) \rightarrow M_2(t)$.

All decoupled blade-dynamics are equal

In the case of decoupled blade models the model can be described by $g_{11}(s) = g_{22}(s) = g_{33}(s) = g_b(s)$, where $g_b(s)$ is referred to as the most general blade-dynamics model. This leaves the most simple description of the wind-turbine model relating the pitch angles to the moments in the form,

$$\begin{bmatrix} M_1(t) \\ M_2(t) \\ M_3(t) \end{bmatrix} = \underbrace{\begin{bmatrix} g_b(s) & 0 & 0 \\ 0 & g_b(s) & 0 \\ 0 & 0 & g_b(s) \end{bmatrix}}_{G_b(s)} \begin{bmatrix} \theta_1(t) \\ \theta_2(t) \\ \theta_3(t) \end{bmatrix}. \tag{2-17}$$

The analysis of this blade-dynamics model is made in the derivation of the MBC-transformation in Chapter 2-2. When the derivation is completely followed through including the azimuth offset inclusion, the model will be the same as was seen in Eq. (2-15). However, the notation that is used in this chapter is changed, as this improves readablity. The frequency shifted Laplace operators are changed to

$$\begin{cases} s_- &= s - j\omega_0, \\ s_+ &= s + j\omega_0. \end{cases} \tag{2-18}$$

This also changes the notation of the MBC-transformed model that results from choosing $G_b(s)$ from Eq. (2-15) into

$$\begin{bmatrix} M_{\text{tilt}}(s) \\ M_{\text{yaw}}(s) \end{bmatrix} = P_b(s) \begin{bmatrix} \Theta_{\text{tilt}}(s) \\ \Theta_{\text{yaw}}(s) \end{bmatrix} = \begin{bmatrix} \frac{e^{-j\psi} g_b(s_-) + e^{j\psi} g_b(s_+)}{2} & j \frac{e^{-j\psi} g_b(s_-) - e^{j\psi} g_b(s_+)}{2} \\ -j \frac{e^{-j\psi} g_b(s_-) - e^{j\psi} g_b(s_+)}{2} & \frac{e^{-j\psi} g_b(s_-) + e^{j\psi} g_b(s_+)}{2} \end{bmatrix} \begin{bmatrix} \Theta_{\text{tilt}}(s) \\ \Theta_{\text{yaw}}(s) \end{bmatrix} \tag{2-19}$$

.

An important remark is that this model structure has been the only model structure used for IPC to the present day. Although quite simplistic, and relying on many assumptions, it has already proved to be a useful blade-dynamic model structure for control. All further extensions of the model structure explained in the remainder of this section are therefore still very much experimental model structures.

Different decoupled blade-dynamics

The second case that can be made, is one that the blade-dynamics differ which means that the assumption $g_{11}(s) \neq g_{22}(s) \neq g_{33}(s)$ is made. In this case $g_{11}(s) = g_{b_1}(s),\ g_{22}(s) = g_{b_2}(s),\ g_{33}(s) = g_{b_3}(s)$. As a consequence the model in Eq. (2-17) changes into

$$\begin{bmatrix} M_1(t) \\ M_2(t) \\ M_3(t) \end{bmatrix} = \underbrace{\begin{bmatrix} g_{b_1}(s) & 0 & 0 \\ 0 & g_{b_2}(s) & 0 \\ 0 & 0 & g_{b_3}(s) \end{bmatrix}}_{G_{b_i}(s)} \begin{bmatrix} \theta_1(t) \\ \theta_2(t) \\ \theta_3(t) \end{bmatrix}. \tag{2-20}$$

This relatively minor change in the model as opposed to $G_b(s)$ makes the entire derivation as was performed in Appendices A and B much more cumbersome. The resulting MBC-transformed model has the form

$$\begin{bmatrix} M_{\text{tilt}}(s) \\ M_{\text{yaw}}(s) \end{bmatrix} = P_{b_i}(s) \begin{bmatrix} \Theta_{\text{tilt}}(s) \\ \Theta_{\text{yaw}}(s) \end{bmatrix} = \left[\begin{matrix} e^{-j\psi} \frac{g_{b_1}(s_-)+g_{b_2}(s_-)+g_{b_3}(s_-)}{6} + e^{j\psi} \frac{g_{b_1}(s_+)+g_{b_2}(s_+)+g_{b_3}(s_+)}{6} \\ -je^{-j\psi} \frac{g_{b_1}(s_-)+g_{b_2}(s_-)+g_{b_3}(s_-)}{6} + je^{j\psi} \frac{g_{b_1}(s_+)+g_{b_2}(s_+)+g_{b_3}(s_+)}{6} \end{matrix} \right. \cdots$$
$$\cdots \left. \begin{matrix} je^{-j\psi} \frac{g_{b_1}(s_-)+g_{b_2}(s_-)+g_{b_3}(s_-)}{6} - je^{j\psi} \frac{g_{b_1}(s_+)+g_{b_2}(s_+)+g_{b_3}(s_+)}{6} \\ e^{-j\psi} \frac{g_{b_1}(s_-)+g_{b_2}(s_-)+g_{b_3}(s_-)}{6} + e^{j\psi} \frac{g_{b_1}(s_+)+g_{b_2}(s_+)+g_{b_3}(s_+)}{6} \end{matrix} \right] \begin{bmatrix} \Theta_{\text{tilt}}(s) \\ \Theta_{\text{yaw}}(s) \end{bmatrix}. \tag{2-21}$$

It is verified that when $g_b(s) = g_{b_1}(s) = g_{b_2}(s) = g_{b_3}(s)$ Eq. (2-19) is equal to equal Eq. (2-21). Moreover, this shows that the interaction between tilt and yaw does not change significantly in the case of different blade dynamics. Although it should of course be taken into consideration that this is only the case if the blade dynamics are fully decoupled from each other. In the next section coupling in the blade-dynamic model structure is introduced.

2-4-2 Equal coupling between all blade-dynamics

In the case that the dominant blade-dynamics are on the diagonal it could be possible that the effects of pitching the off-diagonal and non-dominant blade models (i.e. $\theta_1(t) \to M_2(t)$ or $\theta_1(t) \to M_3(t)$) can be approximated by a single linear model. For the sake of simplicity and initial estimation, the blade-dynamics on the diagonal will be assumed to be equal to each other as was done for $G_b(s)$. In mathematical terms, this would change Eq. (2-16) into

$$\begin{bmatrix} M_1(t) \\ M_2(t) \\ M_3(t) \end{bmatrix} = \underbrace{\begin{bmatrix} g_b(s) & g_c(s) & g_c(s) \\ g_c(s) & g_b(s) & g_c(s) \\ g_c(s) & g_c(s) & g_b(s) \end{bmatrix}}_{G_{b_c}(s)} \begin{bmatrix} \theta_1(t) \\ \theta_2(t) \\ \theta_3(t) \end{bmatrix}, \tag{2-22}$$

where $g_c(s)$ is defined as the coupling model. As $g_b(s)$ is the dominant (diagonal) model the minor changes between the different off-diagonal models are assumed to be so minimal that one off-diagonal model in the form of $g_c(s)$ suffices to take the coupling into account. The resulting MBC-transformed plant is of the form

$$\begin{bmatrix} M_{\text{tilt}}(s) \\ M_{\text{yaw}}(s) \end{bmatrix} = P_{b_c}(s) \begin{bmatrix} \Theta_{\text{tilt}}(s) \\ \Theta_{\text{yaw}}(s) \end{bmatrix} = \begin{bmatrix} e^{-j\psi} \frac{g_b(s_-)-g_c(s_-)}{2} + e^{j\psi} \frac{g_b(s_+)-g_c(s_+)}{2} & \dots \\ -je^{-j\psi} \frac{g_b(s_-)-g_c(s_-)}{2} + je^{j\psi} \frac{g_b(s_+)-g_c(s_+)}{2} & \dots \end{bmatrix}$$
$$\begin{matrix} \dots & je^{-j\psi} \frac{g_b(s_-)-g_c(s_-)}{2} - je^{j\psi} \frac{g_b(s_+)-g_c(s_+)}{2} \\ \dots & e^{-j\psi} \frac{g_b(s_-)-g_c(s_-)}{2} + e^{j\psi} \frac{g_b(s_+)-g_c(s_+)}{2} \end{matrix} \Bigg] \begin{bmatrix} \Theta_{\text{tilt}}(s) \\ \Theta_{\text{yaw}}(s) \end{bmatrix}. \tag{2-23}$$

Eq. (2-23) shows that the model relates very much to the fully decoupled model of Eq. (2-19). The main difference is that all the off-diagonal terms are subtracted from the main diagonal models. This shows that in the case of a significant gain difference between the diagonal, and off-diagonal models the introduced complexity of $g_c(s)$ might be almost negligible in terms of the final structure. In the case that coupling is non-existent, Eq. (2-23) changes into Eq. (2-19).

A small stretch in assumptions can be made, when the diagonal terms are the dominant blade-dynamics and the off-diagonal terms might show approximately the same dynamics but on a smaller level. This would mean in the physical sense that the effect of pitching blade 1 has the most dominant effect on the moment of blade 1, but might have the same but severely reduced effect on the moment of blade 2 and 3. In this case $g_c(s) = \delta g_b(s),\ \delta \in \langle 0, 1\rangle$. This would result in the same model structure as Eq. (2-22), however, the MBC-transformed version could be rewritten in the form of Eq. (2-19),

$$\begin{bmatrix} M_{\text{tilt}}(s) \\ M_{\text{yaw}}(s) \end{bmatrix} = (1-\delta) P_b(s) \begin{bmatrix} \Theta_{\text{tilt}}(s) \\ \Theta_{\text{yaw}}(s) \end{bmatrix}. \tag{2-24}$$

This type of blade-dynamics model would therefore just lower the gain of a fully decoupled blade-dynamics model.

2-4-3 Equal coupling between different blade-dynamics

Another possibility is that the coupling is dependent on the previous and next blade dynamics. This is the most advanced model under consideration which still allows for the dropping out of the $(s \pm 2j\omega_0)$ terms in Eq. (A-18) and therefore make the MBC-transformed version a lot better workable and analysable is a more advanced model of coupling. In this model the effect of pitching blade i on moment of blade i is described by $g_b(s)$, but its effect on the moment of blade $i+1$ will be different from the effect on the moment of blade $i-1$. As this is an extension of model $G_{b_c}(s)$ it is assumed that all blade-dynamics are still equal.

This means that the diagonal terms will be $g_b(s)$. The effect of $\theta_1(t) \rightarrow M_2(t) \sim \theta_2(t) \rightarrow M_3(t) \sim \theta_3(t) \rightarrow M_1(t)$, as well as the effect of $\theta_1(t) \rightarrow M_3(t) \sim \theta_2(t) \rightarrow M_1(t) \sim \theta_3(t) \rightarrow M_2(t)$. For the sake completeness, it is assumed that $\theta_1(t) \rightarrow M_2(t) \nsim \theta_1(t) \rightarrow M_3(t)$ otherwise the model would be the same as G_{b_c}. Working all this out in the form of Eq. (2-16),

$$\begin{bmatrix} M_1(t) \\ M_2(t) \\ M_3(t) \end{bmatrix} = \underbrace{\begin{bmatrix} g_b(s) & g_p(s) & g_n(s) \\ g_n(s) & g_b(s) & g_p(s) \\ g_p(s) & g_n(s) & g_b(s) \end{bmatrix}}_{G_{b_{cc}}(s)} \begin{bmatrix} \theta_1(t) \\ \theta_2(t) \\ \theta_3(t) \end{bmatrix}, \tag{2-25}$$

where $g_n(s)$ signifies the effect of pitching on the next blade, and $g_p(s)$ the effect of pitching on the previous blade. To finalise this into the MBC-transformed model,

$$\begin{bmatrix} M_{\text{tilt}}(s) \\ M_{\text{yaw}}(s) \end{bmatrix} = P_{b_{cc}}(s) \begin{bmatrix} \Theta_{\text{tilt}}(s) \\ \Theta_{\text{yaw}}(s) \end{bmatrix} =$$
$$\left[\begin{matrix} e^{-j\psi}\left(\frac{2g_b(s_-)-g_p(s_-)-g_n(s_-)}{4} - j\sqrt{3}\frac{g_p(s_-)-g_n(s_-)}{4}\right) + e^{j\psi}\left(\frac{2g_b(s_+)-g_p(s_+)-g_n(s_+)}{4} + j\sqrt{3}\frac{g_p(s_+)-g_n(s_+)}{4}\right) \\ e^{-j\psi}\left(-j\frac{2g_b(s_-)-g_p(s_-)-g_n(s_-)}{4} - \sqrt{3}\frac{g_p(s_-)-g_n(s_-)}{4}\right) - e^{j\psi}\left(-j\frac{2g_b(s_+)-g_p(s_+)-g_n(s_+)}{4} + \sqrt{3}\frac{g_p(s_+)-g_n(s_+)}{4}\right) \end{matrix}\right. \cdots$$
$$\left.\begin{matrix} e^{-j\psi}\left(j\frac{2g_b(s_-)-g_p(s_-)-g_n(s_-)}{4} + \sqrt{3}\frac{g_p(s_-)-g_n(s_-)}{4}\right) - e^{j\psi}\left(j\frac{2g_b(s_+)-g_p(s_+)-g_n(s_+)}{4} - \sqrt{3}\frac{g_p(s_+)-g_n(s_+)}{4}\right) \\ e^{-j\psi}\left(\frac{2g_b(s_-)-g_p(s_-)-g_n(s_-)}{4} - j\sqrt{3}\frac{g_p(s_-)-g_n(s_-)}{4}\right) + e^{j\psi}\left(\frac{2g_b(s_+)-g_p(s_+)-g_n(s_+)}{4} + j\sqrt{3}\frac{g_p(s_+)-g_n(s_+)}{4}\right) \end{matrix}\right] \begin{bmatrix} \Theta_{\text{tilt}}(s) \\ \Theta_{\text{yaw}}(s) \end{bmatrix}. \tag{2-26}$$

In Eq. (2-26) an interesting property emerges from the coupling: somehow the difference in coupling between the blades introduces a phase-offset of the form $j\sqrt{3}\frac{g_p(s_-)-g_n(s_-)}{4}$. This means that a magnitude of the phase-offset is dependent on the difference in gain between interaction of the previous and the next blade.

For the decoupling of the tilt- and yaw-moments it is desired to decrease the magnitude of the off-diagonal terms by a considerable amount relative to the diagonal terms. As the off-diagonal terms have the introduction of a 90° phase-shift this cancels out against the $j\sqrt{3}\frac{g_p(s_-)-g_n(s_-)}{4}$ term and turns that part into $\sqrt{3}\frac{-g_p(s_-)+g_n(s_-)}{4}$. If these dynamics actually play a significant part in the real-world setup then this specific term could play a role in the choice of the azimuth-offset to decouple the system.

2-4-4 Conclusion

Most papers where MBC-transformation based IPC is applied, either implicitly or explicitly state the assumptions on which their model is based. Where one of the first assumptions is often the fact that a model structured of $G_b(s)$ is considered. In this Section, this assumption was let go, and the resulting blade dynamics model structure analysis has covered as many separate variations which bear a resemblance to real-world interactions of dynamics as possible.

The main result presented is that if a non-negligible amount of blade-dynamic coupling exists, that the model-structure on which the individual pitch controller is based can change considerably. As a consequence this means that assuming a model structure of $G_b(s)$ can limit the achievable performance of the controller.

Furthermore, this elaborate analysis shows how the generalised tilt- and yaw-moments on the wind turbine are very dependent on the dynamics of the blades and the interactions between them. It is therefore very important to carefully choose the proper blade-dynamics model in the linear model analysis.

Chapter 3

Effects on a First-Order System

The wind turbine model undergoes significant changes by application of the MBC-transformation, and it is not trivial how it relates to the characteristics of specific blade models (e.g. $g_b(s)$) themselves. In this chapter the focus is on the application of a basic blade-dynamic model and to investigate the effect of different extensions of the MBC-transformation. The basic blade-dynamic model considered in the chapter is assumed to be a classic first order system. Other models could also be considered, but would make the analysis more complex.

A basic first-order blade-dynamics model is of the form

$$H_b(s) = \frac{M_b(s)}{\Theta_b(s)} = \frac{K}{\tau s + 1}. \tag{3-1}$$

To see its frequency-domain characteristics a gain of $K = 10$ and time-constant of $\tau = 0.25$ are chosen. As a result, the DC-gain of the system is 10 (or $20\log_{10}(K) = 20$dB), and its pole is located at $s = -1/\tau = -4$. The corresponding frequency-domain characteristics are shown in Figure 3-1.

If the MBC-transformation including the azimuth offset, in conjunction with a fully decoupled blade-dynamic model is used (as described in Chapter 2-4-1), then the final form is described by Eq. (2-15). Which means that if an offset is introduced that it is solely introduced in T_θ. If $g_b(s) = H_b(s)$ then Eq. (2-15) can be written as

$$P(s) = \begin{bmatrix} \frac{e^{-j\psi}\frac{K}{\tau(s-j\omega_0)+1} + e^{j\psi}\frac{K}{\tau(s+j\omega_0)+1}}{2} & j\frac{e^{-j\psi}\frac{K}{\tau(s-j\omega_0)+1} - e^{j\psi}\frac{K}{\tau(s+j\omega_0)+1}}{2} \\ -j\frac{e^{-j\psi}\frac{K}{\tau(s-j\omega_0)+1} - e^{j\psi}\frac{K}{\tau(s+j\omega_0)+1}}{2} & \frac{e^{-j\psi}\frac{K}{\tau(s-j\omega_0)+1} + e^{j\psi}\frac{K}{\tau(s+j\omega_0)+1}}{2} \end{bmatrix}. \tag{3-2}$$

The terms in matrix $P(s)$ currently seem to become quite complicated if one would try to work them out, but if one is careful in its substitutions of Euler's formula ($e^{j\psi} = \cos\psi + j\sin\psi$) an easier form of $P(s)$ is available, namely

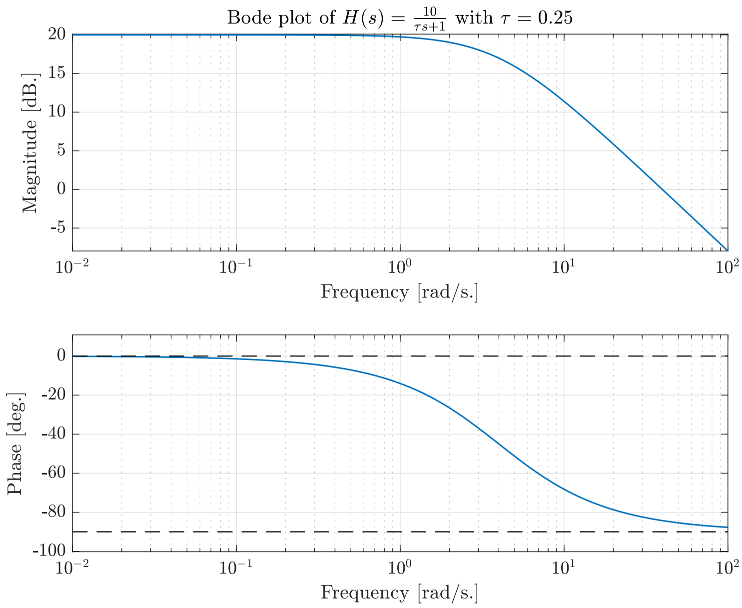

Figure 3-1: Bode plot of a first-order model with $K = 10$ and $\tau = 0.25$

$$P(s) = K \begin{bmatrix} \frac{(\tau s+1)\cos\psi + \tau\omega_0 \sin\psi}{(\tau s+1)^2+\tau^2\omega_0^2} & \frac{(\tau s+1)\sin\psi - \tau\omega_0 \cos\psi}{(\tau s+1)^2+\tau^2\omega_0^2} \\ \frac{-(\tau s+1)\sin\psi + \tau\omega_0 \cos\psi}{(\tau s+1)^2+\tau^2\omega_0^2} & \frac{(\tau s+1)\cos\psi + \tau\omega_0 \sin\psi}{(\tau s+1)^2+\tau^2\omega_0^2} \end{bmatrix}. \tag{3-3}$$

In Eq. (3-3) it is clear that the poles of all the different components of $P(s)$ are the same, because they have the same denominators. An analysis on the poles can be carried out by setting the denominator to zero and see how τ and ω_0 affect the poles of the system.

$$s = -\frac{1}{\tau} \pm j\omega_0. \tag{3-4}$$

It is clear that the pure pole that is present in the basic blade-dynamics model of Eq. (3-1) (pole at $s = -1/\tau$) becomes split up into a complex pole-pair for the MBC-transformed system, where the imaginary component is fully dependent on the rotational speed of the turbine ω_0. A visual representation of this is shown in Figure 3-2. As ω_0 increases, the poles start moving away further and further from the real axis.

3-1 Decoupling the system

In this section, the interest is focussed on finding out when decoupling occurs, or in other words, when the off-diagonal terms are minimal. This means finding $\min_\psi (|P_{12}(j\omega)|)$. As a

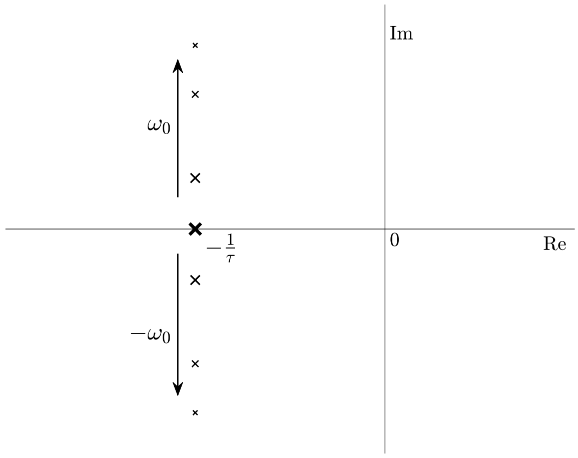

Figure 3-2: Poles of a MBC-transformed 1st-order system. As ω_0 increases, the poles start moving away further and further from the real axis.

consequence, it first has to be clear what the term exactly looks like before determining in what way it can be minimised. If it is worked out the following form is obtained,

$$|P_{12}(j\omega)| = \left|\frac{(\tau j\omega + 1)\sin\psi - \tau\omega_0\cos\psi}{(\tau j\omega + 1)^2 + \tau^2\omega_0^2}\right| = \frac{\sqrt{(\sin\psi - \tau\omega_0\cos\psi)^2 + (\tau\omega\sin\psi)^2}}{\sqrt{\left(\tau^2\left(\omega_0^2 - \omega^2\right) + 1\right)^2 + (2\tau\omega)^2}}. \tag{3-5}$$

For reference purposes, this derivation can be made for the entire $P(s)$. This means that if the same is done for $P_{11}(s), P_{21}(s), P_{22}(s)$, Eq. (3-3) can be turned into

$$|P(s)| = |K|\begin{bmatrix} \frac{\sqrt{(\cos\psi+\tau\omega_0\sin\psi)^2+(\tau\omega\cos\psi)^2}}{\sqrt{\left(\tau^2\left(\omega_0^2-\omega^2\right)+1\right)^2+(2\tau\omega)^2}} & \frac{\sqrt{(\sin\psi-\tau\omega_0\cos\psi)^2+(\tau\omega\sin\psi)^2}}{\sqrt{\left(\tau^2\left(\omega_0^2-\omega^2\right)+1\right)^2+(2\tau\omega)^2}} \\ \frac{\sqrt{(\tau\omega_0\cos\psi-\sin\psi)^2+(-\tau\omega\sin\psi)^2}}{\sqrt{\left(\tau^2\left(\omega_0^2-\omega^2\right)+1\right)^2+(2\tau\omega)^2}} & \frac{\sqrt{(\cos\psi+\tau\omega_0\sin\psi)^2+(\tau\omega\cos\psi)^2}}{\sqrt{\left(\tau^2\left(\omega_0^2-\omega^2\right)+1\right)^2+(2\tau\omega)^2}} \end{bmatrix}. \tag{3-6}$$

From the form presented in Eq. (3-5) it becomes clear that altering the offset ψ does not affect the denominator, and thus does not affect the poles of the system. This means that for decoupling, it suffices to minimise the numerator of $P_{12}(j\omega)$(, because $|P_{12}(j\omega)| = |P_{21}(j\omega)|$, whereby minimising the entire off-diagonal at once). In looking for the ideal offset three different cases can be considered.

1. One case where the frequency of the system is a lot smaller than the rotor speed, $\omega \ll \omega_0$.
2. The second case is when the system frequency is close to the rotor speed, $\omega \approx \omega_0$.
3. The third and final case is the system characteristics for higher frequencies, $\omega \gg \omega_0$.

The mathematical derivation of these offsets can be found in Appendix C. This derivation results in the ideal offsets for decoupling of

$$\begin{array}{rclllll} \psi &=& \tan^{-1}(\tau\omega_0), & \text{for}, & \omega & \ll & \omega_0, \quad \text{valid for } \psi \in \left[-\frac{\pi}{2}, \frac{\pi}{2}\right] \\ \psi &=& \frac{1}{2}\tan^{-1}(2\tau\omega_0), & \text{for}, & \omega & \approx & \omega_0, \quad \text{valid for } \psi \in \left[-\frac{\pi}{2}, \frac{\pi}{2}\right] \\ \psi &=& 0, & \text{for}, & \omega & \gg & \omega_0. \end{array} \tag{3-7}$$

It would be desired to decouple the system over the entire frequency spectrum, but the analysis just performed shows that one single offset is not able to decouple it over the entire frequency spectrum. This means that a deliberate choice has to be made as to which frequency region is of interest to decouple. This is fully dependent on the characteristics of the system under consideration and there is not one answer that will be sufficient for all systems.

What this exactly entails for a system can be seen in Figure 3-3. For this particular example $\tau = 0.2717$ and $\omega_0 \approx 1.2671$ rad/s, but τ and ω_0 can be chosen arbitrarily and the argumentation still holds. In the case that the offset is chosen to be as calculated in Eq. (C-1) Figure 3-3 shows that indeed in the lower frequency region there is a significant drop in magnitude. When $\psi = \frac{1}{2}\tan^{-1}(2\tau\omega_0)$, the drop magnitude around $\omega \approx \omega_0$ is visible, but the change is very small compared to the case off $\psi = \tan^{-1}(\tau\omega_0)$. The case where $\psi = 0°$ is clearly very useful for decoupling the high-frequency region.

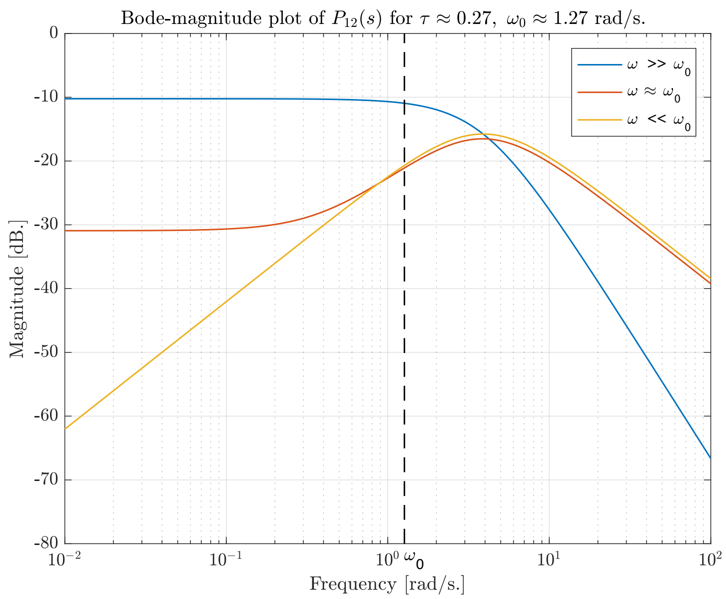

Figure 3-3: Bode magnitude plot to show the effectiveness regions for certain offsets. The yellow line provides maximum decoupling in the low-frequency region for $\omega \ll \omega_0$. The red line provides maximum in the region $\omega \approx \omega_0$. The difference between the red and yellow line around the frequency of ω_0 appears to be minimal. The blue line provides the maximum decoupling in the high-frequency region where $\omega \gg \omega_0$.

In the case of IPC for load mitigation on the blades of HAWTs, the MBC-transformation is generally applied on the 1P-frequency (i.e. at a frequency of ω_0) load spectrum. The MBC-transformation moves the 1P load harmonic in the rotating reference frame to a constant 0P signal in the non-rotating frame. Because 0P corresponds to DC or low-frequency signal content, it is desired to decouple the system at an as low a frequency as possible, which means that the DC-gain of $P_{12}(s)$ should be as low as possible. This is done by choosing $\psi = \tan^{-1}(\tau\omega_0)$ as was calculated in Eq. (C-1). The offset $\psi_d := \tan^{-1}(\tau\omega_0)$ to make future references to this low-frequency decoupling offset for a first-order system easy to refer to.

3-2 Effect of MBC-transformation on system zeros

The change in the numerator of Eq. (3-3) due to a change in the azimuth offset is the basis of the induced change which is seen in Figure 3-3. This change in gain due to a change in the numerator gives rise to the suspicion of an interplay between the gain of $P_{12}(s)$ and its zeros. The zeros of $P_{12}(s)$ are located at the roots of the numerator, and it can be found that

$$s = \frac{\omega_0}{\tan\psi} - \frac{1}{\tau}. \tag{3-8}$$

On careful inspection, a couple of interesting properties show up when taking this approach. The first one is when $\psi = 0°$, then in Eq. (3-3) the term with the s drops out, meaning that the zero completely disappears. In mathematical terms of Eq. (3-8) this is the same as taking $\lim_{\psi^+ \to 0} s = \infty$. In the case ψ is chosen relatively small, then the zero will be located at a high frequency resulting in a small change comparative to when no offset is present (or the blue line in Figure 3-3). When the offset is increased then the term $\omega_0 / \tan\psi$ of Eq. (3-8) starts to decrease, meaning the zero becomes located at a decreasing frequency.

As shown by Eq. (3-3) the ideal offset for decoupling in the low-frequency region was given by ψ_d. If this is substituted into Eq. (3-8) the resulting term for the zero becomes $s = 0$. Here it becomes clear that when increasing the offset from $0 \to \tan^{-1}(\tau\omega_0)$ the zero "travels" from ∞ (in the limit) to 0: an ideal differentiator is the result of the zero placed at 0 rad/s. This also proves that the yellow line of Figure 3-3 will keep decreasing for lower frequencies. The above described characteristics can be seen in a plot of the zeros in Figure 3-4.

Consequently, the DC-gain of $P_{12}(s)$ is 0 for $\psi = \psi_d$, this perfectly decouples the system. It is also important to know what the gains of other elements of Eq. (3-3) are with this specific offset compared to the case no offset is applied. If the same exemplary case is used (meaning $\tau = 0.2717$ and $\omega_0 \approx 1.2671$) then the DC-gains related are calculated to be

$$|P(j0)|_{\psi=0} = \begin{bmatrix} 0.8940 & -0.3078 \\ 0.3078 & 0.8940 \end{bmatrix}, \quad |P(j0)|_{\psi=\psi_d} = \begin{bmatrix} 0.9455 & 0 \\ 0 & 0.9455 \end{bmatrix}. \tag{3-9}$$

This shows an increase in the gain of $|P_{11}(j0)|_{\psi=\psi_d}$, which is not such a significant increase as the decrease in gain of $|P_{12}(j0)|_{\psi=\psi_d}$. This means that something different appears to be happening on the diagonal terms of $P(s)$.

The same analysis of zeros can be performed on $P_{11}(s)$ to see how these change and what effect this might have on the change in gain of the system by choosing $\psi = \psi_d$. In the case of

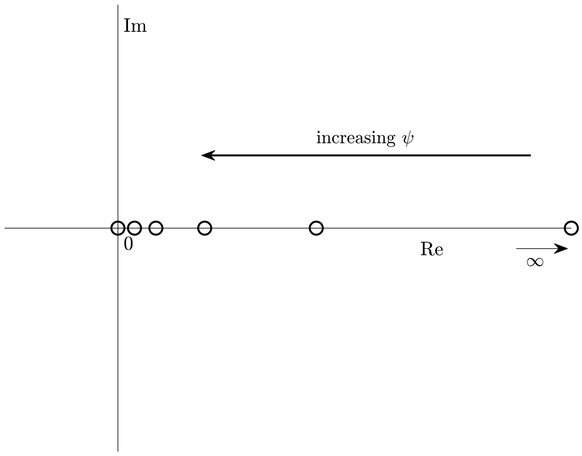

Figure 3-4: Zeros of a MBC-transformed 1st-order system. As the offset, ψ increases, the zeros travel from ∞ towards 0 for a value of $\psi_d = \tan^{-1}(\tau\omega_0)$. (If $\psi > \psi_d$ the zero moves into the left-half plane).

the location of the zero, this means the numerator of $P_{11}(s)$ in Eq. (3-5) can be set to zero to find its roots,

$$s = -\omega_0 \tan\psi - \frac{1}{\tau}. \tag{3-10}$$

This shows that in the case of decoupling, $s \overset{\psi=\psi_d}{=} -\omega_0^2\tau - 1/\tau$. This is a non-trivial location of the zero, but also does not pose any dangers to the system's stability. This is due to the fact that $\omega_0^2,\ \tau > 0$, meaning the location of the zero is always located in the complex left-half plane.

As a side note, the choice of $\psi = \tan^{-1}(-1/(\tau\omega_0))$ should be avoided, as this would place the zero of Eq. (3-10) at 0 rad/s (in effect creating an ideal differentiator in $P_{11}(s)$). As well as placing the zero of Eq. (3-8) at $-\omega_0^2\tau - 1/\tau$. This would make the yaw-moment fully dependent on the tilt-pitch and would result in inverse-coupling of the system in the low-frequency region.

Now that this has become clear for one specific τ, which corresponds to one specific time-constant coefficient, or one specific wind turbine. As the limitation of the applicability of $\psi \in \left[-\frac{\pi}{2}, \frac{\pi}{2}\right]$ due to the $\tan^{-1}$ function it is not at all trivial that this allows the applicability of the offsets in systems with arbitrary time-constants.

3-3 Analyzing the effects of DC-Gain, τ and ω_0.

In the previous section for exemplary purposes certain model parameters were chosen. Several effects were shown for these specific cases. It is interesting to see what how the decoupling changes if the wind turbine's characteristics change. In the case that the wind turbine blade-dynamics are approximated by a first order model this means that the characteristics are described as in Eq. (3-1). As a consequence, K and τ are the parameters which change the characteristics of the model. In Eq. (3-3) it was shown that the analysis of decoupling is irrespective of a change in K. This means that the most important characteristic is determined by the choice of τ.

Secondly, the MBC-transformation induces a term which is dependent on the rotational speed of the wind turbine, ω_0. As this term shows up in different places of $P(s)$ this might very well also play a role in decoupling the MBC-transformation as was seen in Eq. (3-5).

Before looking at the effect of changing these values, a proper metric has to be chosen to compare them to. As discussed earlier, the low-frequency properties are the most important properties for decoupling because of the shift of the 1P harmonics of the non-rotating frame to the 0P harmonics of the non-rotating frame. This coincides with the DC-gain. Therefore, first the exact changes in DC-gain are analyzed before changing the values of τ and ω_0.

3-3-1 DC-Gain change due to ψ_d

When changing the value of τ and to keep checking for decoupling in the low-frequency region, a more general form of $P_{12}(s)$ in Eq. (3-3) is set up. For this the identities of $\sin\left(\tan^{-1}(\tau\omega_0)\right) = \tau\omega_0/\sqrt{\tau^2\omega_0^2+1}$ and $\cos\left(\tan^{-1}(\tau\omega_0)\right) = 1/\sqrt{\tau^2\omega_0^2+1}$ come in very useful. The gain change for the off-diagonal is

$$P_{12_{\psi_d}}(s) = \frac{(\tau s+1)\sin\psi_d - \tau\omega_0\cos\psi_d}{(\tau s+1)^2+\tau^2\omega_0^2} = \underbrace{\frac{\tau\omega_0}{\sqrt{\tau^2\omega_0^2+1}}}_{K_{12_{\text{dec}}}} \frac{\tau s}{(\tau s+1)^2+\tau^2\omega_0^2}. \tag{3-11}$$

It is observed from Eq. (3-11) that a change in gain of magnitude $K_{12_{\text{dec}}}$ compared to the regular $P_{12}(s)$ is present. It has one zero in the origin. As was seen in Eq. (3-10) the zeros of P_{11} do have a different location. The change in the denominator might also result in a change in its gain. If the same substitution of Eq. (3-11) is done for $P_{11}(s)$ it becomes clear that

$$P_{11_{\psi_d}}(s) = \frac{(\tau s+1)\cos\psi_d + \tau\omega_0\sin\psi_d}{(\tau s+1)^2+\tau^2\omega_0^2} = \underbrace{\frac{1}{\sqrt{\tau^2\omega_0^2+1}}}_{K_{11_{\text{dec}}}} \frac{\tau s+1+\tau^2\omega_0^2}{(\tau s+1)^2+\tau^2\omega_0^2}. \tag{3-12}$$

Which also shows a difference in the DC-gain of $P_{11}(s)$. This effect actually is more general than these specific cases and it proves more helpful to analyse the entire $P(s)$ structure. If the DC-gain of $P(s)$ is written out in terms as initially presented in Eq. (3-6) it means that $s = j0$ should be substituted. This results in general DC-gains of the form

$$|P(j0)| = |K| \begin{bmatrix} \frac{|\cos\psi+\tau\omega_0\sin\psi|}{\tau^2\omega_0^2+1} & \frac{|\sin\psi-\tau\omega_0\cos\psi|}{\tau^2\omega_0^2+1} \\ \frac{|\tau\omega_0\cos\psi-\sin\psi|}{\tau^2\omega_0^2+1} & \frac{|\cos\psi+\tau\omega_0\sin\psi|}{\tau^2\omega_0^2+1} \end{bmatrix}. \tag{3-13}$$

As this shows a big dependency on the choice of offset it is interesting to see how decoupling affects all DC-gains. In the case the offset is set to zero (as is currently the norm in IPC), the resulting DC-gains are

$$|P(j0)|_{\psi=0} = |K| \begin{bmatrix} \frac{1}{\tau^2\omega_0^2+1} & \frac{|-\tau\omega_0|}{\tau^2\omega_0^2+1} \\ \frac{\tau\omega_0}{\tau^2\omega_0^2+1} & \frac{1}{\tau^2\omega_0^2+1} \end{bmatrix}. \tag{3-14}$$

Now that the offset is increased to the appropriate values for low-frequency decoupling (i.e. $\psi = \psi_d$), the resulting DC-gains are calculated to be

$$|P(j0)|_{\psi=\psi_d} = |K| \begin{bmatrix} \frac{1}{\sqrt{\tau^2\omega_0^2+1}} & 0 \\ 0 & \frac{1}{\sqrt{\tau^2\omega_0^2+1}} \end{bmatrix}. \tag{3-15}$$

Now it is possible to relate the DC-gain change from $\psi = 0 \rightarrow \psi = \psi_d$ for the diagonal terms. From Eq. (3-14) and Eq. (3-15) it is clear that both of the diagonal terms show the same gain difference. The ratio between the upper diagonal elements of Eq. (3-15) and Eq. (3-14) is $\sqrt{\tau^2\omega_0^2 + 1}$. It is trivial that $\tau^2\omega_0^2 > 0$, whereby it can be concluded that $\sqrt{\tau^2\omega_0^2 + 1} > 1$, or in other words, that a gain increase is present on the diagonal terms when decoupling happens. Furthermore, the DC-gain of the diagonal terms are exactly equal to the gain $K_{11_{\text{dec}}}$ as calculated in Eq. (3-12).

3-3-2 Effect of varying τ

In the case the rotor speed, ω_0 is fixed the effect of the blade-dynamics model will change the behaviour of the coupling terms in the MBC-transformation. For now it is assumed that ω_0 is fixed at the be the rated rotor speed. This is due to the fact that IPC is most often considered to be enabled for load reduction in the above-rated region [6]. The term τ determines the placement of the pole in the first order system model described by Eq. (3-1). When it is very small ($\tau \ll 1$) the system has pole very far in the complex left-half plane, or a very fast acting pole. This indicates a fast responding system.

In the case of analysis on $K_{12_{\text{dec}}}$ this would mean that it approximates $K_{12_{\text{dec}}} \approx \omega_0\tau^2$ at low values for τ whereas it would steadily increase to about $K_{12_{\text{dec}}} \approx \tau$ for higher values of τ. Comparing this to $K_{11_{\text{dec}}} \approx 1$ for low values of τ and $K_{11_{\text{dec}}} \ll 1$ if τ would become quite large there is a trade-off present in the system. In the case that $\tau \gg 1$, the offset which decouples the system at the low-frequencies would have the inverse effect in the mid-frequency region where the roll-off is not present yet, but if τ is relatively small then $\psi = \psi_d$ would be a good choice for the offset. This is because it allows for near-perfect decoupling in the low-frequency region and it would still allow the gain of the diagonal terms to be higher than the off-diagonal terms which would ensure a certain amount of decoupling in the region where it was previously shown to be thought of as inadequate.

3-3-3 Effect of varying ω_0

In the case ω_0 is varied, τ is fixed and assumed greater than zero. Furthermore, it is assumed without loss of generality that $\omega_0 \geq 0$.

In the case the wind turbine does not rotate $\omega_0 = 0$, $K_{\text{dec}} = 0$ and as a consequence $P_{12_{\psi_d}}(s) = 0$ which automatically decouples the system (which has also been shown earlier that this happens irrespective of ψ). In the case the wind turbine has a low rotational speed ($\omega_0 \ll 1$ rad/s) $K_{12_{\text{dec}}}$ is also very small as the denominator will be dominated by the "1" term, whereas $K_{11_{\text{dec}}} \approx 1$. This means that the off-diagonal terms will have very low gains no matter the frequency region and the diagonal terms will be dominant (and as a result decoupling happens over almost the entire frequency region). Furthermore, the complex poles of the MBC-transformed system still lie close to the real-axis which means only small oscillations occur on the yaw- and tilt-moments.

When ω_0 starts increasing up until around $\pi/2$ rad/s (this equals 15RPM, which is a reasonable rated rotor speed for a wind turbine [1]) coupling starts to exist with respect to the gains of the system. As the magnitude of the complex components of the poles increases the frequency of the yaw- and tilt-moments also starts to increase. This is the point where an azimuth offset will therefore be the most useful. At rated rotor-speeds the highest coupling appears (as the turbine will not rotate any faster than that) and therefore it is the most useful region to start focussing on for decoupling. As IPC is usually implemented in the region where the rotor speed is at its rated speed, this shows that the consideration of the offset in the MBC-transformation can be very profitable from a performance viewpoint.

3-4 Verification of the low-frequency decoupling results

Now that several results have been found for a first order system, it is smart to verify them through a different analysis. If this corresponds to the analytical results described in the previous sections, it is safe to say that decoupling indeed happens under the considered circumstances. The most important part to verify is the decoupling in the low-frequency region and its relations to various τ and ψ values.

3-4-1 Gain analysis of the MBC-transformed system

In the section describing the variation of ω_0 it was noted that for low ω_0 (rotor speeds) decoupling automatically happens, whereas at higher rotor speeds decoupling is harder to show and is especially dependent on the choice of the offset. To see if this is indeed the case the gains of $|P(s)|$ as described in Eq. (3-6) are plotted for $\omega_0 \approx 1.27$ rad/s, while varying τ and the offset ψ in Figure 3-5. It should be noted that the magnitudes are normalized between a value of 0 and 1. Secondly, it should also be noted that only $P_{11}(s)$ and $P_{12}(s)$ are plotted, because $P_{11}(s) = P_{22}(s)$ and $P_{12}(s) = -P_{21}(s)$.

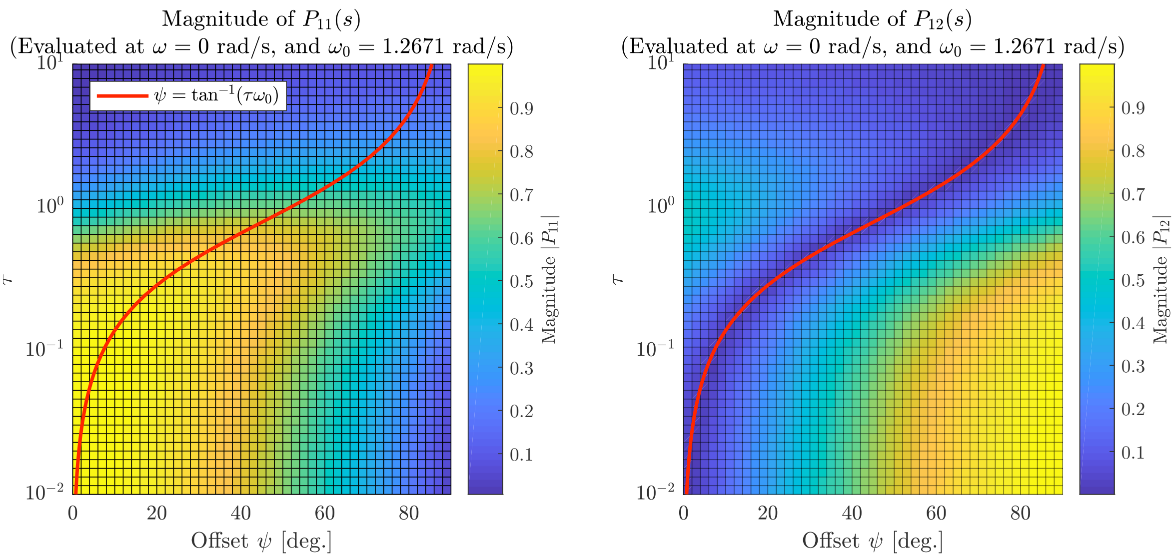

Figure 3-5: Normalized magnitude plots for $P_{11}(s)$ and $P_{12}(s)$ evaluated in the low-frequency region ($\omega = 0$ rad/s.) and for rotor speed equating to 12.1 RPM. The red line shows the theoretical result for decoupling ($\psi_d = \tan^{-1}(\tau\omega_0)$).

Several things can be observed in Figure 3-5. Firstly, in the case that τ is chosen smaller than 1 it is clear that the gain of $P_{11}(s)$ approaches 1 whereas the gain of $P_{12}(s)$ is near 0 for an offset corresponding to the results found in Chapter 3-1. However as τ becomes larger than 1, The low-frequency gain of $P_{11}(s)$ approaches that of $P_{12}(s)$ for increasing values of τ. It does correspond with what is described in the section of varying τ that the gain of the system drops as τ increases, this also shows that the chosen verification method is not appropriate for larger values of τ. Therefore in the next section the Relative Gain Array (RGA) is employed.

3-4-2 Relative Gain Array analysis of the MBC-transformed system

In the previous section the analysis was done by looking at the relative gain differences for different values of τ and ψ. A classical method to do this is by calculating the Relative Gain Array (RGA) of a system [28]. The RGA is a square complex matrix defined as

$$\mathrm{RGA}(P(s)) := P(s) \times (P(s)^{-1})^T, \tag{3-16}$$

where "$\times$" denotes the Hadamard (or Schur) product between the matrices [28]. It is a property of the RGA that the columns and rows of the RGA sum up to 1. The RGA is generally considered as a pairing of how the different gains in the system relate to each other. It is generally desired that control is not performed on RGA elements with negative values [29]. In the values considered in Figure 3-5 no negative real values were calculated for the RGA($P(s)$). Since no negative pairing was present, the norm of the RGA($P(s)$) is taken to show the consequences of the RGA. The result can be seen in Figure 3-6.

The RGA shows an even clearer result than Figure 3-5 with respect to the decoupling effects. Again, the red line is an indication of the analytically obtained result of Chapter 3-1. The

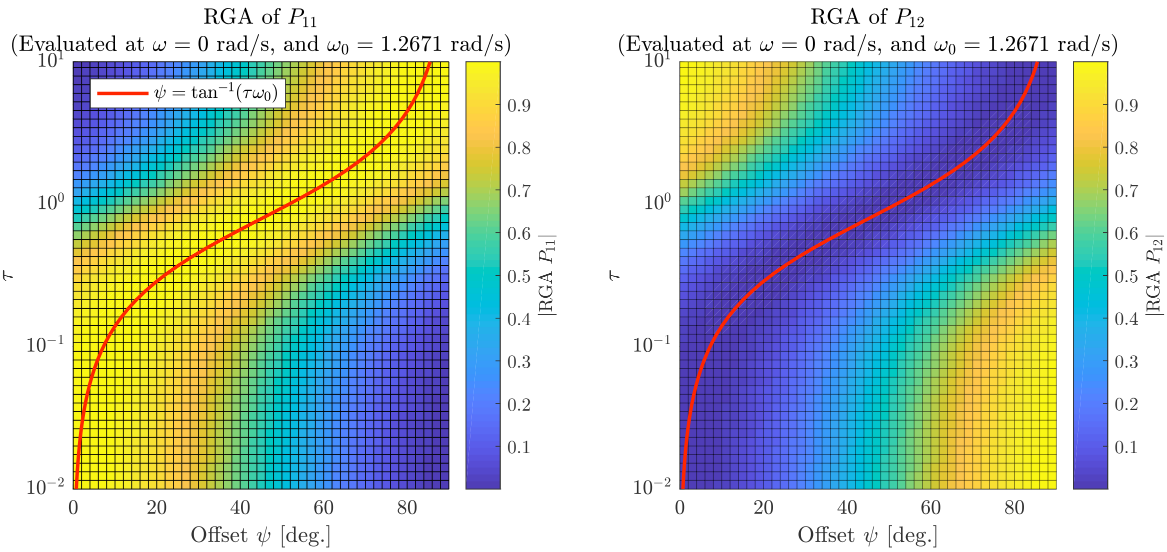

Figure 3-6: The norm of the RGA of $P_{11}(s)$ and $P_{12}(s)$ evaluated in the low-frequency region ($\omega = 0$ rad/s.) and for rotor speed equating to 12.1 RPM. The red line shows the theoretical result for decoupling ($\psi = \tan^{-1}(\tau\omega_0)$).

RGA plot now also indicates that at low values for τ and high values for ψ even inverse pairing can be seen. This inverse pairing for high values of τ was not at all obvious in Figure 3-5 but also seems to be significant if the RGA is considered. Which was also what has been derived in the previous sections.

The two plots of Figure 3-5 and 3-6 now fully corroborate the analytical results derived. Figure 3-5 shows that indeed the gains of the MBC-transformed system significantly drop when τ increases. This made it difficult to see if the decoupling was still guaranteed in this region. The RGA plot of Figure 3-6 indeed showed that this was still the case. The RGA plot also showed that inverse coupling is possible in case the offset is chosen in a wrong fashion. This would mean that tilt- and yaw-moments would be controlled by yaw- and tilt-pitch angles respectively. The RGA was still positive in these cases, which indicates that is not necessarily undesired, but is highly unintuitive to do.

3-5 Application on equal coupling between all blade-dynamics

For now, the entire analysis of the first order model has been made with respect to the most basic blade-dynamic model. In Chapter 2-4 the differences between different blade-dynamic models has been discussed. Therefore it is also important to see the effect this has on an actual system. In this section, the analysis is performed on the blade-dynamic model described in Chapter 2-4-2 (assuming equal blade cross-coupling). This means that the previous analysis changes considerably.

The main differences are that the different gains of the diagonal and off-diagonal models now play a role in decoupling the system. This also means the system has to be set up in a different way. Two different models, $g_b(s)$ and $g_c(s)$, are now needed, as described in the Eq. (2-22) and Eq. (2-23). For illustration purposes, the model is set-up as

$$\begin{cases} g_b(s) &= K_b \frac{1}{\tau_b s+1}, \\ g_c(s) &= K_c \frac{1}{\tau_c s+1}, \end{cases} \tag{3-17}$$

and subsequently these descriptions of the blade-dynamics are substituted into Eq. (2-23). As decoupling occurs on the off-diagonal, the interest is put on the upper-right term of Eq. (2-23). This becomes

$$P_{b_{c_{12}}}(s) = \frac{j}{2}\left[K_b \frac{(\tau_b s+1)\sin\psi - \tau_b\omega_0\cos\psi}{(\tau_b s+1)^2 + \tau_b^2\omega_0^2} - K_c \frac{(\tau_c s+1)\sin\psi - \tau_c\omega_0\cos\psi}{(\tau_c s+1)^2 + \tau_c^2\omega_0^2}\right]. \tag{3-18}$$

From Chapter 3-1 it became clear that decoupling can happen in different frequency regions. The argument was given that decoupling in the low-frequency region amounts to the desired decoupled characteristics. This amounts to minimization of the 2-norm of Eq. (3-18) with $s = j0$ is substituted. If this derivation is followed carefully, the following result is obtained

$$\left[K_b(1+\tau_c^2\omega_0^2) - K_c(1+\tau_b^2\omega_0^2)\right]\sin\psi - \left[K_b\tau_b\omega_0(1+\tau_c^2\omega_0^2) - K_c\tau_c\omega_0(1+\tau_b^2\omega_0^2)\right]\cos\psi = 0. \tag{3-19}$$

This has the same form as Eq. (C-1), but the multiplications are a bit more elaborate. However, an analytic solution still exists,

$$\psi = \tan^{-1}\left(\omega_0 \frac{K_b\tau_b(1+\tau_c^2\omega_0^2) - K_c\tau_c(1+\tau_b^2\omega_0^2)}{K_b(1+\tau_c^2\omega_0^2) - K_c(1+\tau_b^2\omega_0^2)}\right). \tag{3-20}$$

On first sight this seems a complicated form. The nice thing however is that it indeed agrees with the forms that were presented earlier. In case that $\tau_b = \tau_c$ and the gains are written as $K_c = \delta K_b$ which agrees with Eq. (2-24) as well as the decoupling found in Eq. (C-1).

3-6 Conclusion

The analysis of a first-order blade-dynamics model with the simplest form of coupling as discussed in Chapter 2-4 shows that a lot of different effects take place when changing the offset. Moreover, it has been shown that it is impossible to fully decouple the system by choosing one specific offset. A choice has to be made in what frequency region the offset has to be most effective.

It has been argued that when IPC decoupling in the low-frequency region is desired, this is achieved by the introduction of a pure differentiator in the origin. As a result the DC-gain of the coupling terms goes to zero. On the other hand this also introduces a zero in the diagonal terms of $P(s)$ on a non-trivial place in the complex left-half plane.

Finally, the exact effects of the choice of model-characteristics is examined. This shows that even though coupling might occur in the low-frequency region, if τ is too large (in this case meaning $\tau \gg 1$) then the decoupling achieved in the low-frequency region is negated in the mid- to high-frequency region.

In the next chapter the tools presented here are going to be applied on a more complex model. This more complex model are higher-order linearisations of a high-fidelity non-linear wind turbine model. The interest lays in extending the properties found in this chapter to these linearisations.

Chapter 4

Locating the Optimal Azimuth Offset in Higher-Order Wind Turbines

4-1 Introduction

In Chapter 3 an extensive analysis is performed on the decoupling of a first-order blade-dynamics model. The main result was the possibility of decoupling the system in certain frequency regions. It was shown that no single constant offset was able to decouple the system in the MBC-transformation over the entire frequency spectrum. As this result was only presented for a first order model it is no guarantee that this will straightforwardly translate into a high-order wind turbine model.

This chapter will look if to the possibility of extending the results previously obtained to high-order linearisations from a non-linear wind turbine model. Once linear models are obtained, the MBC-transformation is applied to it. This showcases which assumption of blade-dynamic models of Chapter 2-4 are valid.

Subsequently, the possibility of approximating this high-order wind turbine by a first order system is analysed. From Chapter 3 it is known what the ideal offset for the MBC-transformation is of a first-order model. It is investigated in this chapter whether the first order approximation can be related to the actual ideal offset.

4-2 Description of a High-Order wind turbine model

This section describes the choice of the non-linear high-fidelity model and its properties. The model under consideration is the NREL-5MW baseline reference wind turbine. The turbine's properties and possibilities for IPC (analysis) will be explained.

Table 4-1: Summary of specification of the NREL 5-MW Baseline Wind Turbine

Description	Value
Rated Power	5 MW
Rotor orientation	Upwind, 3 blades
Control	Variable speed, collective pitch
Drivetrain	High speed, multiple-stage gearbox
Rotor	126 m
Hub diameter	3 m
Hub height	90 m
Cut-in speed	3 m/s
Rated speed	11.4 m/s
Cut-out speed	25 m/s
Cut-in rotor speed	6.9 rpm
Rated rotor speed	12.1 rpm
Rated tip speed	80 m/s
Pitch-rate limit	$\|8°/s\|$

4-2-1 Description of the NREL-5MW baseline reference wind turbine

Various wind turbine models are used throughout wind turbine research fields. Currently, one of the most referenced wind turbine models is the NREL 5-MW baseline reference wind turbine model [30], which is also the model under consideration in this thesis. From now on it will be simply referred to as the "NREL 5-MW turbine".

The NREL 5-MW turbine has been established to standardize research of wind turbines and to allow for fast and convenient simulations on a high-fidelity non-linear model. The model has been designed by the National Research Energy Laboratory (NREL) in the United States of America. During the design process of the turbine model, an extensive survey was done of specifications of other turbines. An overview of the resulting wind turbine can be seen Table 4-1. For a more detailed overview of the NREL 5-MW turbine the interested reader is referred to [30].

4-2-2 Description of the FAST high-fidelity wind turbine simulation package

Next to the wind turbine model, NREL has also developed a Computer Aided Engineering (CAE) tool to simulate the coupled dynamic response of wind turbines: it is referred to as FAST (Fatigue, Aerodynamics, Structures and Turbulence). The simulation package is primarily designed for the use case of extreme and fatigue load analysis on wind turbines [31]. FAST is capable of joining aerodynamic models with control dynamic models as well as structural dynamics models. This coupling generates a high-fidelity non-linear model which can be simulated in a time-marching simulation of the wind turbine. This non-linear simulation makes use of wind-inflow (possibly turbulent) data and consequently computes turbine loads, responses as well as rotor-wake effects. Furthermore, extensive possibilities for the evaluation of the wind turbine's control system are available. This ranges from individual pitch actuation, generator-torque control as well as nacelle-yaw control [31].

Next to the non-linear simulations FAST also allows for linearisations of the wind turbine model. These linearisations give the possibility to gain extensive insight into the wind turbine's dynamics at that specific operating points. These linearisations are build up with the help of several coupled modules (AeroDyn, ServoDyn, ElastoDyn, and InflowWind).

Currently there is a difference between the ways non-linear simulations are computed and the way the linearisations are set up. Unsteady aerodynamic effects can be included in the non-linear simulations whereas it is currently impossible to include these in the calculation of the linearisations.

FAST can be run in two different ways. First in an executable format, which allows for relatively fast simulation times. The second configuration is that FAST is compiled into an S-Function block in MATLAB Simulink [31]. This S-Function block enables the inclusion of custom Fortran routines. Also, the possibility of applying complex control in the Simulink environment without the need to compile this into the executable allows for relatively fast controller iterations.

4-3 Linearisation of the NREL 5-MW wind turbine

In Chapters 2 and 3 an analysis framework has been set up to see in what way decoupling is possible by introduction of an offset in the MBC-transformation with respect to linear blade-dynamic models. Now that the choice of a high-fidelity non-linear wind turbine model has been made, this model is linearised for certain conditions.

The NREL 5-MW turbine model will be linearised under conditions where IPC is most useful. The considered wind field under which the linearisation is made is a steady wind field with a mean wind-speed of 25 m/s.

Linearisations are provided by FAST in continuous state-space form. Furthermore, the linearisation can be made at different azimuth angles. To get a clear insight in the dynamics over all rotor azimuth positions, linearisations are made at 36 distinct positions during its rotation.

Each of these linearisations results in a different state-space description. In the considered set-up activated degrees of freedom, the state-space descriptions result in a 29th order model. In the case under consideration the most important relation of states are the ones described in Figure 2-3. This means that the for the MBC-transformation the input-output interaction between the pitch angles and out-of-plane bending moments is considered. The resulting magnitude frequency responses of the linearisations are plotted in Figure 4-1.

In Chapter 2-4 the effect of the choice of the blade-dynamics model structure has been explained. This can now be related to the obtained model. Figure 4-1 essentially indicates the

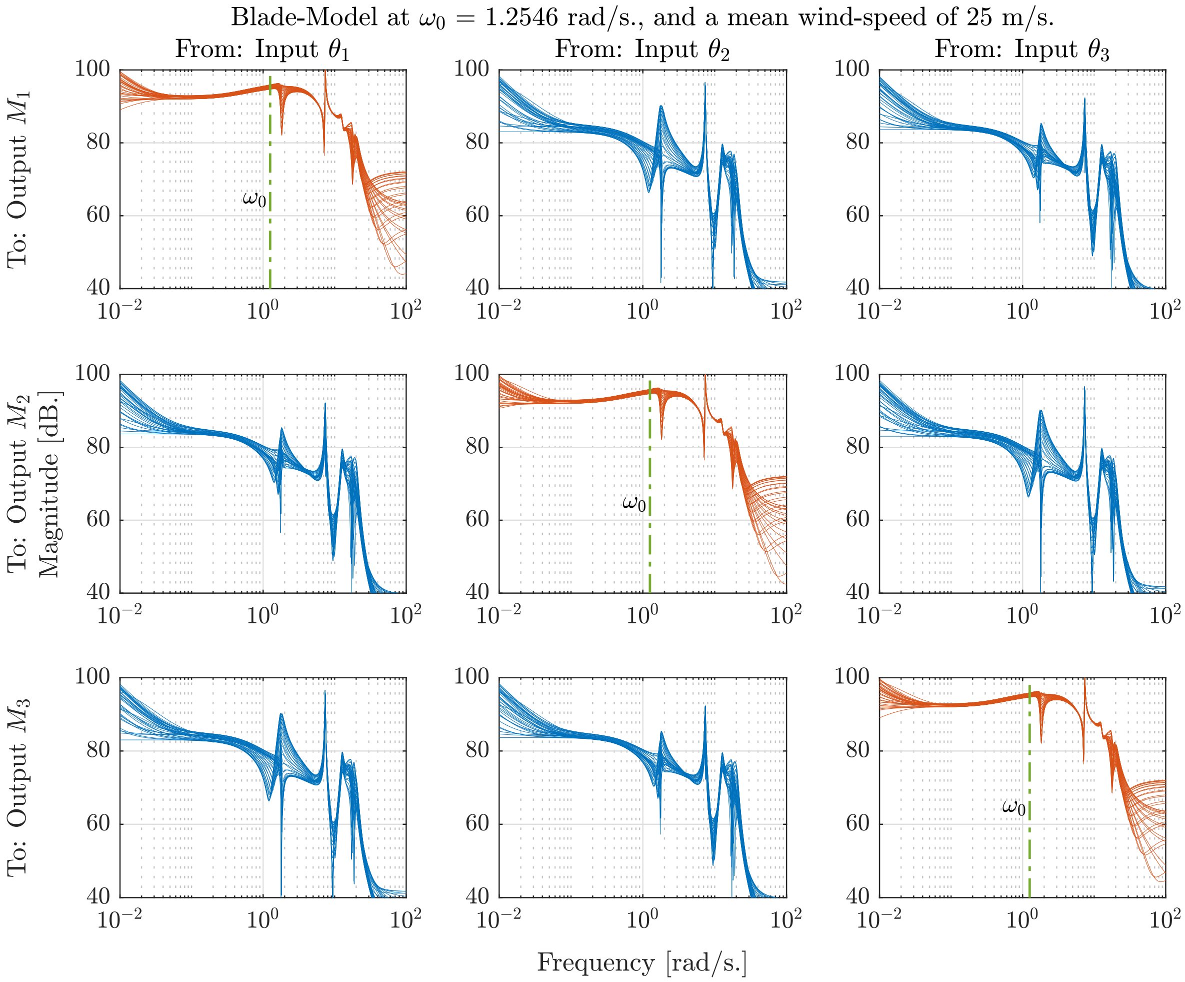

Figure 4-1: Bode magnitude plots of the NREL 5-MW turbine linearisations. The green dashed line indicates the rotational speed of the turbine. The orange plots indicate the diagonal terms, whereas the blue plots show the interplay between different blades. Each separate line is a linearisation of the wind turbine for azimuth angles over all rotor positions.

9 different transfer functions as described in Eq. (2-16). To get a first inclination as to how they relate to each other, a purely qualitative analysis is made.

It is clear that the three diagonal terms display similar dynamics. Especially around the rotational speed (ω_0) of the turbine they exhibit a 10+ dB difference compared to the off-diagonal terms. The dominance of these diagonal terms explains why the model consideration of a fully decoupled blade-dynamics model has dominated the design of IPC up until now.

However, it is also quite clear that the off-diagonal terms are non-zero and all show quite similar dynamics, which might give a good indication that the assumptions and blade-dynamic model structure of Chapter 2-4-2 could help in the explanation to find the ideal offset.

The last observation which might prove useful is that in terms of model dynamics in Figure 4-

1, the transfer functions of $\theta_3 \to M_1 \approx \theta_1 \to M_2 \approx \theta_2 \to M_3$, and $\theta_2 \to M_1 \approx \theta_3 \to M_2 \approx \theta_1 \to M_3$. This approximate equality is made on the basis of the spread in the frequency region just above the rotor speed. This type of blade-dynamic model structure relates to the assumptions made Chapter 2-4-3. Which might indicate that the interactions between the previous and next blade might be important in the analysis of the offset. Although it should be noted that the change compared to Chapter 2-4-2 is only significant in the spread just above the rotor speed frequency, which might be a reason to not consider the significant higher complexity of the model, as decoupling is desired in the lower frequency region.

4-4 MBC-transformation of the linearised wind turbine model

In the previous section the linearisations were made of the NREL 5-MW turbine at a wind-speed of 25 m/s on 10° intervals. These resulted in a 36 different 29th order state-space descriptions of the system. In Chapter 3 only "simple" 1st order systems were considered to do analysis for the MBC-transformation. This means that either the state-space systems have to be transformed into a description of the form of Chapter 2, or a full MBC-transformation has to be performed on the full state-space systems. This last point seems like to be the best option to make sure that no loss of dynamics occurs.

As a result, an analytical description of the MBC-transformation will be derived in the next section. This MBC-transformation is also able to incorporate the azimuth offset. In the subsequent section this MBC-transformation is performed on the obtained linearisation of Figure 4-1.

4-4-1 Theoretical derivation MBC-transformation for state-space models

A state-space model description is a linear model description. In the case it is a linearization of a non-linear model it is only valid in an operating region close close to the part where the dynamics are linearized. In the case of the NREL 5-MW turbine there are 36 models which describe the wind turbine dynamics at different azimuth angles. All these models describe the dynamics of the wind turbine over one rotation, this means that the state-space systems can be coupled to a switched system, dependent on rotational speed. As a result it means that to capture the full dynamics of the wind turbine in one state-space model, the state-space model obtains changing A, B, C, D matrices with respect to the azimuth angle (which in turn is dependent on time). Consequently, this results in a time-varying model of the form,

$$\begin{aligned} \dot{x}_r(t) &= A_r(\phi(t))x_r(t) + B_r(\phi(t))u_r(t) \\ y_r(t) &= C_r(\phi(t))x_r(t) + D_r(\phi(t))u_r(t). \end{aligned} \tag{4-1}$$

Where $x_r(t)$ is the state vector containing all the states present in the linearisation. The subscript r indicates that the system is in its rotating frame of reference. The input vector is referred to as $u_r(t)$, and $y_r(t)$ is the output vector. Matrices $A_r(\phi(t)),\ B_r(\phi(t)),\ C_r(\phi(t)),\ D_r(\phi(t))$ are the state-, control-, output-, and feedthrough matrices respectively. The output matrix can be partitioned into $C_r(\phi(t)) = \begin{bmatrix} C_{r_1}(\phi(t)) & C_{r_2}(\phi(t)) \end{bmatrix}$, with the dimensions of $C_{r_1}(\phi(t))$

corresponding to the dynamics dependent on the first time derivative of the system states. The dimensions of $C_{r_2}(\phi(t))$ correspond with all other states. This partitioning will become useful in transforming the system to the non-rotating frame later on. This state-space system contains many more states than the ones of interest for MBC-transformation analysis. A script has been presented in [32]. This script, `MBC3`, performs the MBC-transformation on state-space models where it should be indicated exactly what states should be MBC-transformed. For the introduction of an azimuth offset in the MBC-transformation, the `MBC3` script is modified. It presents the new non-rotating model as,

$$\begin{aligned} \dot{x}_{nr}(t) &= A_{nr}(\phi(t))x_{nr}(t) + B_{nr}(\phi(t))u_{nr}(t) \\ y_{nr}(t) &= C_{nr}(\phi(t))x_{nr}(t) + D_{nr}(\phi(t))u_{nr}(t). \end{aligned} \tag{4-2}$$

Where the subscript nr now indicates that the change into the non-rotating frame of reference has been made. The change in coordinates of the matrices is made by

$$\begin{cases} A_{nr}(\phi(t)) &= \begin{bmatrix} \hat{T}_M & 0 \\ 0 & \hat{T}_M \end{bmatrix} \left(A_r \begin{bmatrix} \hat{T}_\theta & 0 \\ \dot{\phi}\dot{\hat{T}}_\theta & \hat{T}_\theta \end{bmatrix} - \begin{bmatrix} \dot{\phi}\dot{\hat{T}}_\theta & 0 \\ \dot{\phi}^2\ddot{\hat{T}}_\theta + \ddot{\phi}\dot{\hat{T}}_\theta & 2\dot{\phi}\dot{\hat{T}}_\theta \end{bmatrix} \right) \\ B_{nr}(\phi(t)) &= \begin{bmatrix} \hat{T}_M & 0 \\ 0 & \hat{T}_M \end{bmatrix} B_r \hat{T}_u \\ C_{nr}(\phi(t)) &= \hat{T}_y \begin{bmatrix} C_{r_1}\hat{T}_\theta + \dot{\phi}C_{r_2}\dot{\hat{T}}_\theta & C_{r_2}\hat{T}_\theta \end{bmatrix}, \\ D_{nr}(\phi(t)) &= \hat{T}_y D_r \hat{T}_u. \end{cases} \tag{4-3}$$

Here all capital letters are matrices which are all dependent on $\phi(t)$. The argument is omitted to keep the transformation clear to the reader. Furthermore, it can be said that $\dot{\phi}(t) = \omega_0$, which is constant in the considered case, and $\ddot{\phi}(t) = 0$, because of the consideration that the above-rated regime is considered.

The transformation matrices indicated by the $\hat{T}$ are relatable to the classical MBC-transformation as described in Chapter 2. To be more specific, $\hat{T}_M = \left[\begin{smallmatrix} I_{\tilde{n}} & 0 \\ 0 & \tilde{T}_M \end{smallmatrix}\right]$. Where $x_r \in \mathbb{R}^{\tilde{n}+3}$ is partitioned such that the last three states of $x_r(t)$ indicate the states which are to be used in the MBC-transformation (in this case, the 3 out of plane bending moments of the blades). The same argument can be made for $\hat{T}_\theta = \left[\begin{smallmatrix} I_{\tilde{n}} & 0 \\ 0 & \tilde{T}_\theta \end{smallmatrix}\right]$. Because the MBC-transformation matrices are dependent in their argument on $\phi(t)$, the time-derivative of $\hat{T}_\theta(\phi(t))$ is derived using the chain rule. In mathematical terms this is

$$\frac{d}{dt}\left(\hat{T}_\theta(\phi(t))\right) = \underbrace{\frac{\partial \hat{T}_\theta}{\partial \phi}}_{\dot{\hat{T}}_\theta :=} \frac{\partial \phi}{\partial t} = \dot{\hat{T}}_\theta \dot{\phi}.$$

By the same idea, the second derivative $\ddot{\hat{T}}_\theta := \frac{\partial^2 \hat{T}_\theta}{\partial \phi^2}$. Lastly, the matrices $\hat{T}_u = \left[\begin{smallmatrix} I_{\tilde{m}} & 0 \\ 0 & \tilde{T}_\theta \end{smallmatrix}\right]$ (, where $u_r \in \mathbb{R}^{\tilde{m}+3}$), and $\hat{T}_y = \left[\begin{smallmatrix} I_{\tilde{p}} & 0 \\ 0 & \tilde{T}_M \end{smallmatrix}\right]$ (, where $y_r \in \mathbb{R}^{\tilde{p}+3}$).

As this thesis focusses on the effects of decoupling due to the introduction of an offset in the MBC-transformation it is important to note that the introduction of a constant offset does not change anything the described derivation. This is due to the fact that the offset is introduced as a constant addition in $\phi(t)$. This means that it drops out for $\frac{d}{dt}\phi(t)$, which preserves the transformation described in Eq. (4-3). For a full derivation of the MBC-transformation for state-space systems, the interested reader is referred to [32].

4-4-2 MBC-transformation on the NREL 5-MW Turbine

Now that the full 29th order system can be transformed by the MBC-transformation, it can be implemented on the obtained linearisations of the NREL 5-MW turbine described in Chapter 4-3. As this system has many more inputs and outputs than are needed for IPC, only the relevant dynamics are used. This means that the interaction between yaw- and tilt-moments and pitch angles are extracted from the MBC-transformed models. These yaw- and tilt- dynamics are not present in the original models. This results in Figure 4-2. In this case the MBC-transformation is performed without an offset present to set the baseline.

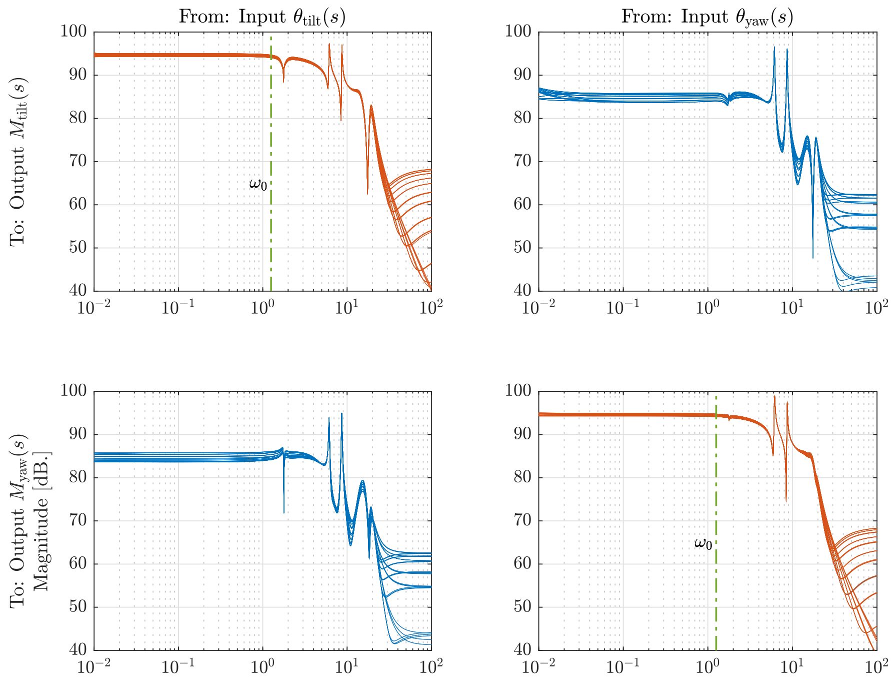

Figure 4-2: Bode magnitude plots of the MBC-transformed NREL 5-MW turbine linearisations (MBC-transformation of Figure 4-1). No azimuth offset ($\psi = 0°$) is present in the model. The green dashed line indicates the rotational speed of the turbine. The orange plots indicate the diagonal terms, whereas the blue plots show the interplay between yaw and tilt.

It is interesting to see that the model periodicity in Figure 4-2 is considerably reduced in the low-frequency region. This is a consequence of the change from a rotating frame of reference to a non-rotating frame of reference.

4-4-3 Introduction of an offset

As from Figure 4-2 it seems that significant coupling exists, it is interesting to see if this coupling can be reduced by the introduction of an azimuth offset in the MBC-transformation. For this section only two subplots of Figure 4-2 will be used. The first is $\theta_{\text{tilt}}(s) \rightarrow M_{\text{tilt}}(s)$, which will be referred to as $P_{11}(s)$, and the second one is $\theta_{\text{yaw}}(s) \rightarrow M_{\text{tilt}}(s)$, which will be referred to as $P_{12}(s)$. This is done because the other two subplots are approximately equal to $P_{11}(s)$ and $P_{12}(s)$ for the low-frequency region.

Because the interest lays in the fact that the (low-frequency) magnitude of $P_{12}(s)$ is desired to be as close to zero as possible, it is interesting to see what the effect of different offsets are on this part of the model. This is set out in Figure 4-3. A significant drop in the lower frequency region can be seen when an offset of $\psi = 19°$ is introduced. The spread between the different models is quite apparent however. A reason why this might happen is that because even for a first order model the choice of the optimal offset seemed to have a polynomial or exponential decay once it was not chosen perfectly (as can be seen in Figure 3-6). This in turn would mean that each separate model would need its own offset.

Another interesting thing is that the dynamics present between 1 and $\sim$ 15 rad/s. also seem to be affected by the offset. Which seems to hit a resonance peak at $\psi \approx 45°$ and subsequently die down when ψ increases further. Where, at $\psi = 90°$ these dynamics seem to be mitigated altogether.

Now that it is known what happens to $P_{12}(s)$ it is also needed to see the effects of the offset on the $P_{11}(s)$. The plots of $P_{11}(s)$ are set out in Figure 4-4. Several important things happen in this plot.

Firstly, there seems to be a minor increase in gain for $\psi = 19°$ as opposed to $\psi = 0°$. This is also what happened for a first order model in Chapter 3-3. The second interesting thing about the offset of 19° is that the dynamics of $P_{11}(s)$ in the region between 2 and $\sim$ 10 rad/s. is smoothed out. Whereas in this frequency region with an offset of $\psi = 45°$ it again shows a resonance peak.

Another thing that corresponds to the findings of Chapter 3 is that as the offset increases to higher values (up until 90°) the coupling slowly starts to invert. This can be seen by the fact that the DC-gain of the $\psi = 90°$ plot of Figure 4-3 is significantly higher than the gain of the $\psi = 90°$ plot of Figure 4-4.

4-4-4 Definition of decoupling

Up until now, the way that decoupling was checked for, was by checking if the DC-gain of the off-diagonal terms of $P(s)$ would be as low as possible. In the linearisation of the NREL 5-MW turbine it has been hard to calculate an exact DC-gain. That is why it is important to define the ideal decoupling due to the introduction of an azimuth offset angle.

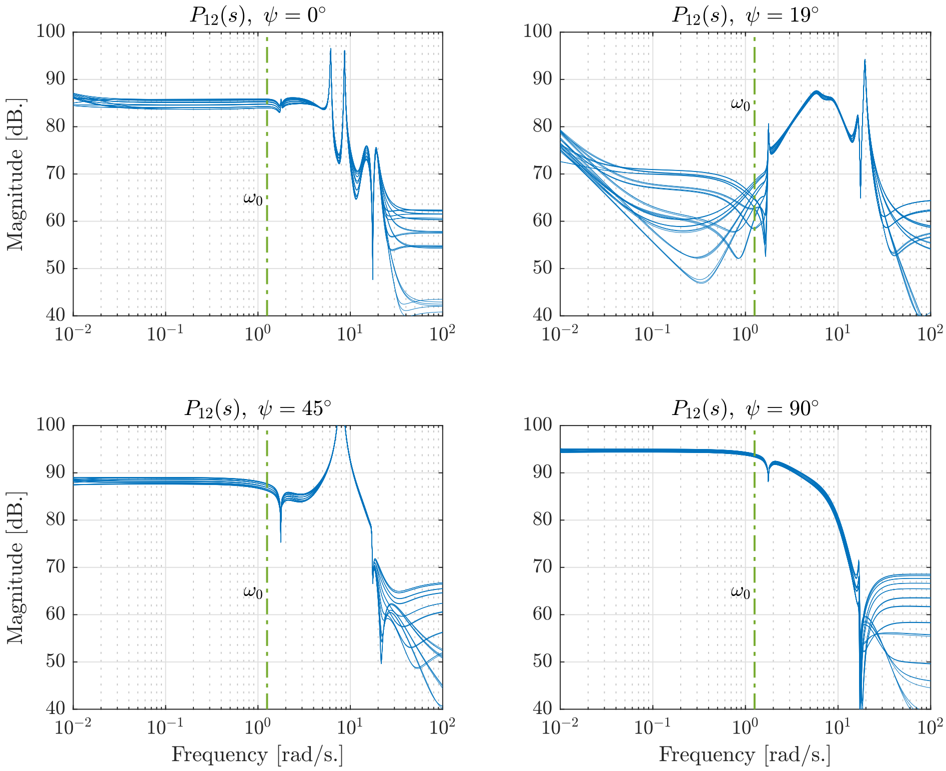

Figure 4-3: Bode magnitude plots of the MBC-transformed NREL 5-MW turbine linearisations (MBC-transformation of Figure 4-1). Only the off-diagonal model $P_{12}(s)$ is plotted for different offsets $\psi \in \{0°, 19°, 45°, 90°\}$. For $\psi = 19°$ significant lower gains are observed in the frequency region at and below ω_0, whereas for $\psi = 90°$ the gain is even increased in this region.

The low-frequency dynamics are still an important aspect to consider, because these indicate the amount of coupling in the parts where control is most effective. If the azimuth offset is changed, $P_{12}(s)$'s most significant change with respect to the low-frequency domain, is in the region from about 0.1 rad/s. to about 1 rad/s. This can be seen in Figure 4-3 for the offset $\psi = 19°$.

It is also apparent in previous plots that the gain of the 36 different linear approximations vary significantly in various regions. In order to take this into account with the definition of decoupling an averaging amount of the different linearisations is desired. At this point the superscript i in $P_{12}^i(s)$ indicates which of the 36 different linearisations is used.

A way to combine the above noted observations in the definition of ideal decoupling, is to consider the average off-diagonal magnitude in the region from 0.1 to 1 rad/s. As this is all relative, the absolute magnitude is not necessary and a normalized magnitude gives an appropriate indication of decoupling.

In mathematical terms this translates to

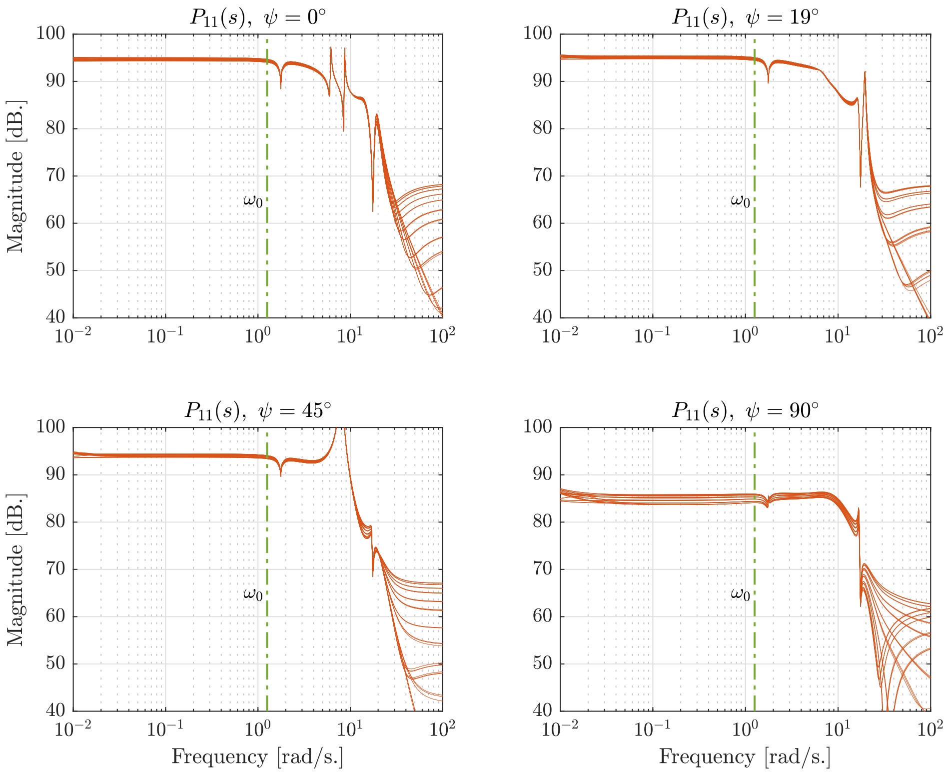

Figure 4-4: Bode magnitude plots of the MBC-transformed NREL 5-MW turbine linearisations (MBC-transformation of Figure 4-1). Only the off-diagonal model $P_{11}(s)$ is plotted for different offsets $\psi \in \{0°, 19°, 45°, 90°\}$. There does not seem a lot of difference in the low-frequency region for the offsets $\psi = 0°, 19°, 45°$, but for $\psi = 90°$ the gain decrease is significant.

$$\eta(\psi) := \frac{1}{n_{\text{lin}}} \sum_{i=1}^{n_{\text{lin}}} \frac{1}{\omega_{\max} - \omega_{\min}} \int_{\omega_{\min}}^{\omega_{\max}} P_{12}^{i}(j\omega, \psi) \mathrm{d}\omega. \tag{4-4}$$

Where $n_{\text{lin}} = 36$ is the amount of linear models, and $\omega_{\min}$ and $\omega_{\max}$ signify the minimum and maximum frequency between which the decoupling is desired. In this case $\omega_{\min} = 0.1$, $\omega_{\max} = 1$. To normalize Eq. (4-4), the infinity norm is used. This means $||\eta(\psi)||_{\infty} = \max_{\psi} \eta(\psi)$. This means the ideal $\psi_{5\text{MW}}$ for decoupling the linearized NREL 5-MW turbine model is defined as

$$\psi_{5\text{MW}} := \arg\min_{\psi} \frac{\eta(\psi)}{||\eta(\psi)||_{\infty}}. \tag{4-5}$$

Now that the mathematical framework is set out, it helps in the clarification to plot the result. In Figure 4-5, $\eta(\psi)/||\eta(\psi)||_{\infty}$ is plotted for different values of ψ. The green line indicates the ψ-value for which the minimum is found. Now that is clear that the ideal decoupling according to the definition of Eq. (4-5) is found to be $\psi_{5\text{MW}} = 19°$ the following step is to see whether this can be linked to the results obtained in the previous chapters.

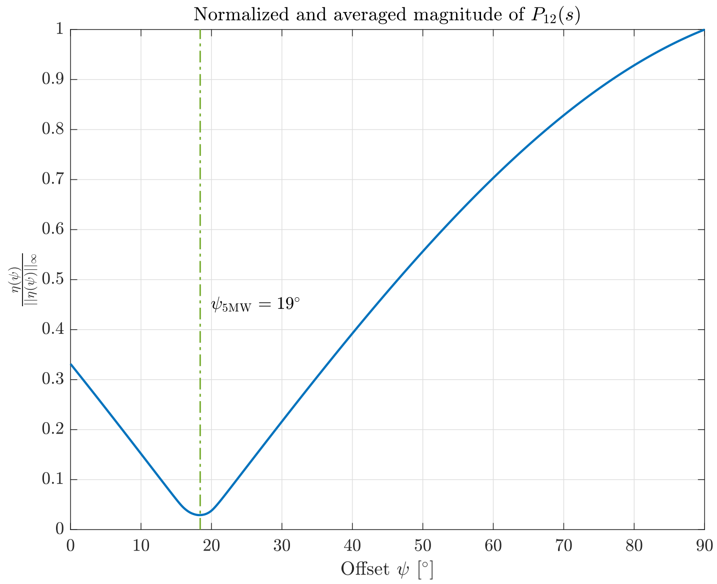

Figure 4-5: A plot of the minimization function of Eq. (4-5) is plotted against ψ. The green dashed line indicates the minimum value found for $\psi_{5\mathrm{MW}} = 19°$.

4-5 First-order model approximation of the NREL 5-MW Turbine

As discussed earlier, it is interesting to see if the complexity of the higher-order linearized model can be approximated by a simplified model to provide a faster way of finding the ideal offset for the MBC-transformation. The simplified model will be assumed to be a first-order model. This would amount to finding first-order linear models which correspond roughly to the models of Figure 4-1.

Equal Coupling Blade-Dynamic Model Structure

For this approximation a certain blade-dynamics model structures should be chosen. In Chapter 4-3 several model structures have been discussed and why it might be relevant to consider them. In the case of a first order approximation of every of the 9 models the most important consideration is the gain and the time constant frequency. The approximation which approximates the gains and the breaking point as well as possible can be seen in Figure 4-6. This has been an heuristic way of tuning the model.

The approximation of the diagonal models are indicated by the black solid line and are all the same. The off-diagonal models are indicated by the black dashed line and are also all the same. As this fits the blade-dynamic model structure well over all different models, this type of blade-dynamic model is considered (as explained in Chapter 2-4-2). The reason why the more complex model structure as discussed in 2-4-3 is not used is because the gains and breaking points correspond very well in all the off-diagonal models. The slight difference this would make would not weigh up against the severe increase in model complexity. The transfer function expressions in Figure 4-6 are described as

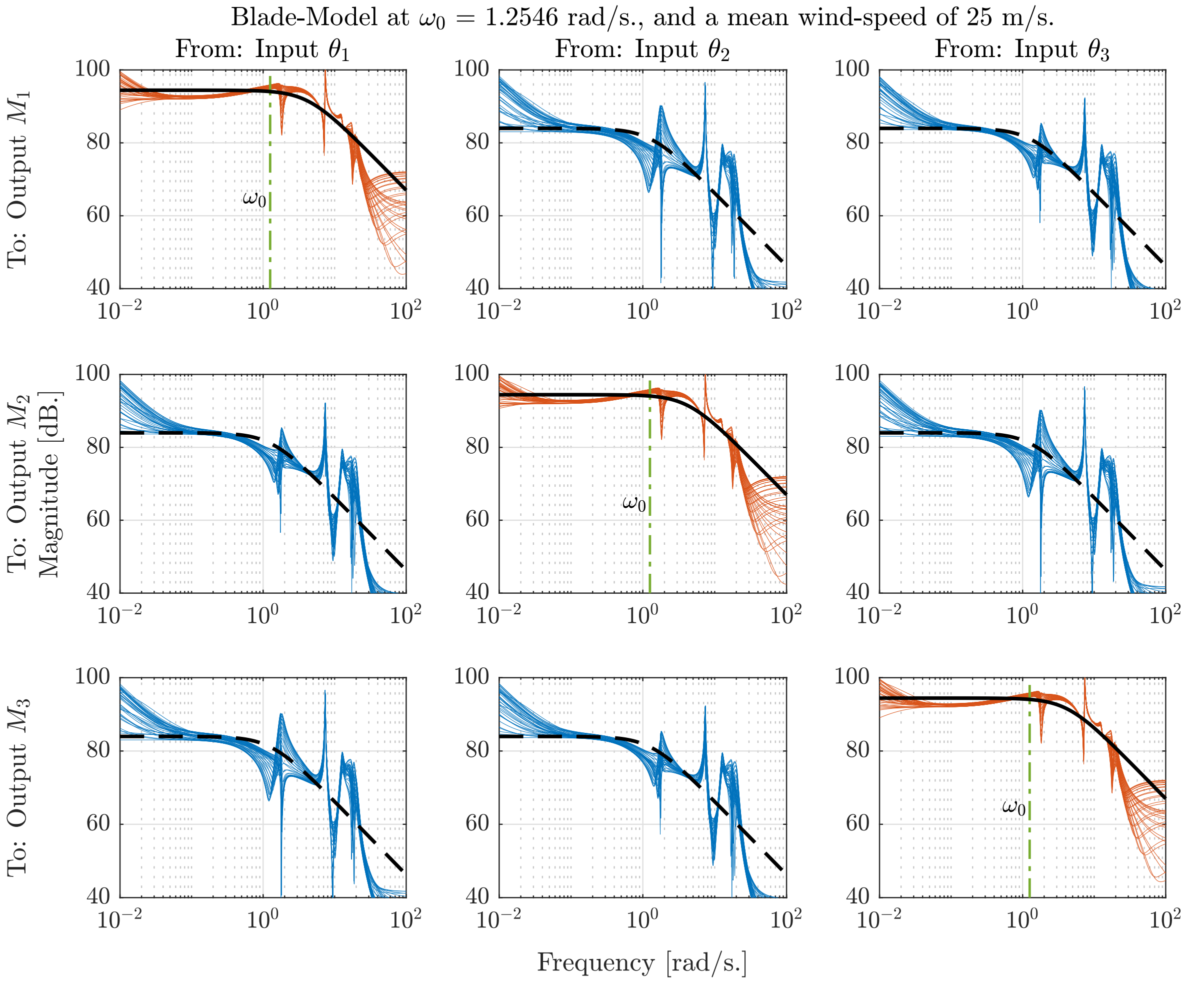

Figure 4-6: Bode magnitude plots NREL 5-MW turbine linearisations with first-order model approximations. The green dashed line indicates the rotational speed of the turbine. The orange plots indicate the diagonal terms, whereas the blue plots show the interplay between different blades. The fits on the diagonal are indicated by the black solid line and are all the same, and are decribed by $g_b(s) = \frac{5.27 \cdot 10^4}{0.2353s+1}$. The fits on the off-diagonal are indicated by the black dashed line and are all the same as well, and defined by $g_c(s) = \frac{1.58 \cdot 10^4}{0.7692s+1}$.

$$\begin{aligned} g_b(s) &= \frac{5.27 \cdot 10^4}{0.2353s+1}, \\ g_c(s) &= \frac{1.58 \cdot 10^4}{0.7692s+1}, \end{aligned} \tag{4-6}$$

corresponding to the notation of Eq. (2-22). Where τ of $g_b(s)$ (0.2353) is chosen such that the breaking point is at $\omega_{g_b} = 4.25$ rad/s., and τ for $g_c(s)$ (0.7692) the breaking point is at $\omega_{g_c} = 1.3$ rad/s. These values are obtained in a heuristic fashion in order to make a proper fit of Figure 4-1.

It is now possible to continue with the model of Eq. (4-6) and put it through the MBC-transformation to obtain a model described by Eq. (2-23). Because the interest currently is if the obtained model has the same approximate decoupling azimuth offset as the NREL 5-MW turbine an overview is presented with the discovered maximum decoupling. This overview is presented in Figure 4-7, where ψ is varied from 0° to 90°.

The lowest point of the approximations is indicated by the black dashed line, which is found for $\psi = 19°$. Two important characteristics can be seen in the variation of the linear model structure. First, this value corresponds with the analytical form of Eq. (3-20). Secondly, the ideal differentiator which is found for a fully decoupled blade-dynamic model structure (which could be seen in Figure 3-3) is not possible anymore.

The ideal decoupling value of $\psi = 19°$ of the 1st order model approximation corresponds with the value found for the linearisation of the NREL 5-MW turbine. This gives a good indication that the ideal offset for decoupling for the linearisation of a turbine can be found by approximating it with a first order approximation.

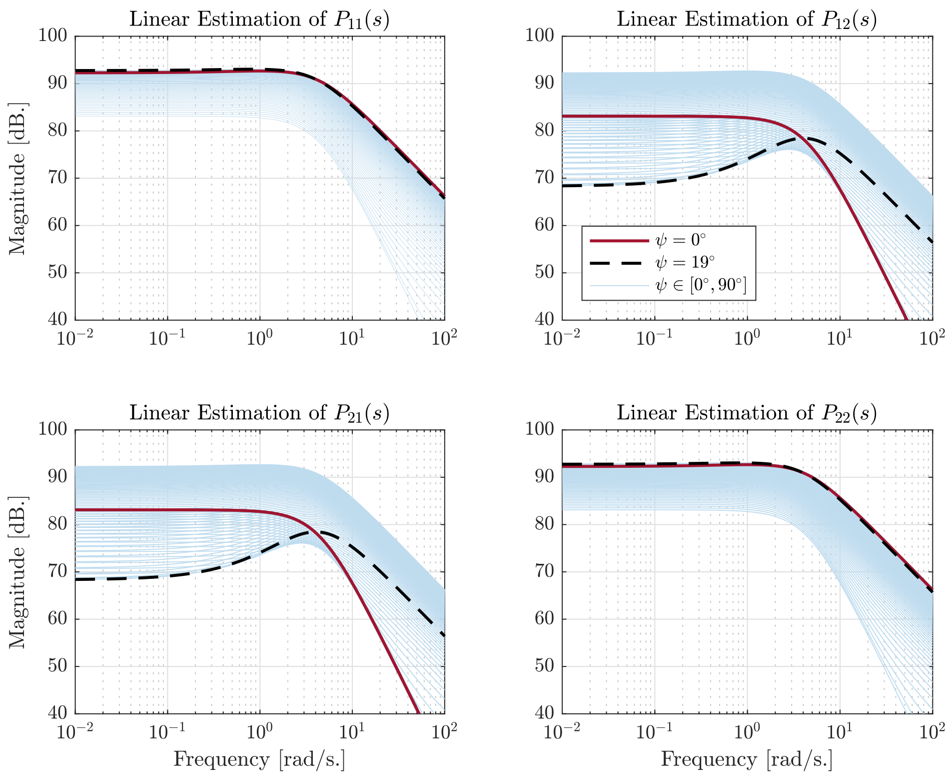

Figure 4-7: The MBC-transformed first-order linear approximations of the NREL 5-MW turbine. The black dashed line indicates the maximum decoupling achieved ($\psi = 19°$), the blue lines indicate the different offset values ($\psi \in [0°, 90°]$), and the red line indicates the baseline ($\psi = 0°$).

Figure 4-2 and Figure 4-7 are both plots of MBC-transformed systems. Because the first order model is used as an approximation of the higher-order model for finding the offset, it is also interesting to see how the MBC-transformed dynamics relate to each other. This is seen in Figure 4-8 for an offset of $\psi = 19°$.

Figure 4-8 shows that there is a gain difference of about 2 - 3dB. on the diagonal. This is probably due to the fact that the model of Eq. (4-6) is found by manual tuning and is very

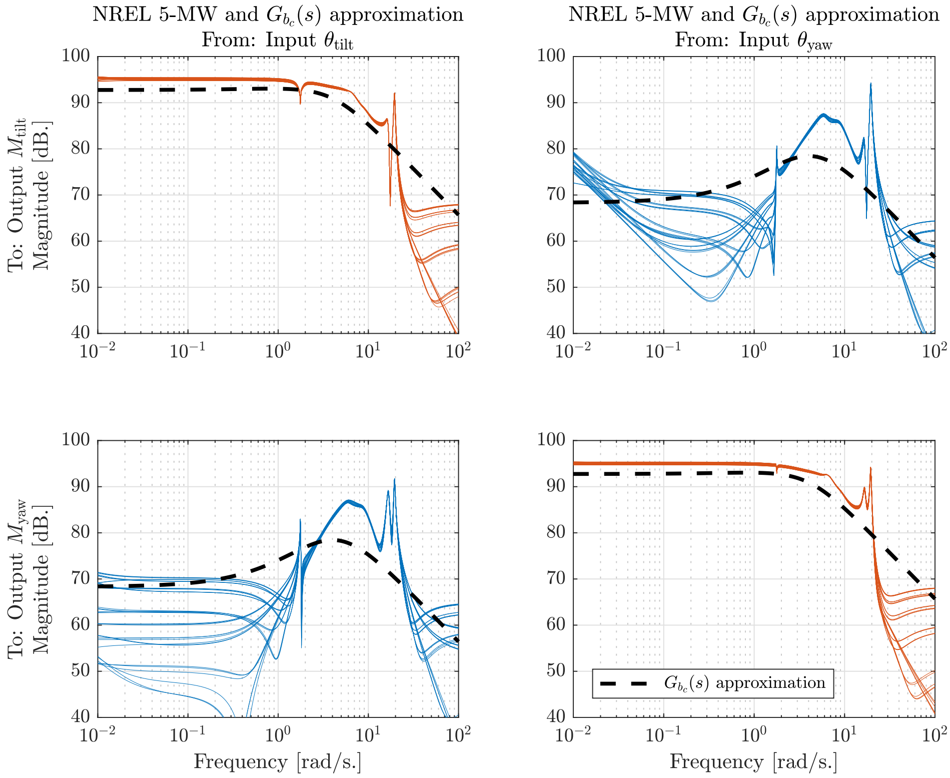

Figure 4-8: Comparing the MBC-transformation of NREL 5-MW turbine with a first-order approximation (with blade-dynamic model structure $G_{b_c}(s)$) with an offset of $\psi = 19°$.

sensitive to small changes. The roll-off in high frequencies does correspond with the linearisation of the NREL 5-MW turbine. The off-diagonal shows a larger variation, but this is also due to the effect that the 36 different models seem to be very sensitive to the offset chosen and because each separate model will have its own specific ideal decouple offset.

This variation in dynamics of 36 different 29th order models can never be approximated by a first-order model. But the first-order model does serve as a good approximation in finding the ideal offset of the higher order complex model.

Diagonal Blade-Dynamic Model Structure

The literature generally makes use of the fully decoupled blade-dynamic model structure as described in Eq. (2-17). In the previous section it has been argued that a more appropriate choice is the choice of a blade-dynamic model structure of the form Eq. (2-22). This has been applied as an approximation to the NREL 5-MW turbine and found the same offset.

It is also interesting to see how much it differs from the blade-dynamic model structure classically applied to the wind turbine. This would mean that the approximation made in Figure 4-6 changes and the off-diagonal terms (the black dashed lines) are removed. This would only remain the black solid lines described by $g_b(s) = \frac{5.27 \cdot 10^4}{0.2353s+1}$ in Eq. (4-6). If this model is transformed to the non-rotating frame, and the ideal offset is found it amounts to an offset of $\psi_d = \tan^{-1}(\omega_0 \tau) = 16.4°$. In Figure 4-9 the same plot as Figure 4-8 is made, but with an offset of $\psi = 16.4°$ and the $G_b(s)$ model structure applied to the approximation.

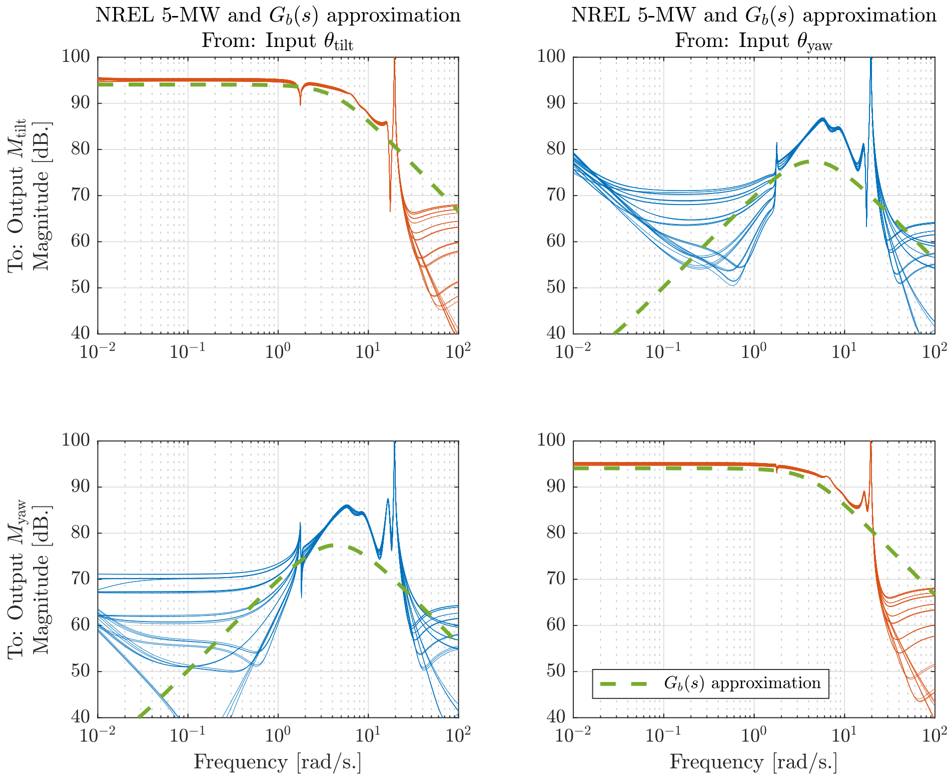

Figure 4-9: Comparing the MBC-transformation of NREL 5-MW turbine with a first order approximation (with blade-dynamic model structure $G_b(s)$) with an offset of $\psi = 16.4°$.

Figure 4-9 shows that an ideal differentiator in the low frequency-region on the off-diagonal shows up in the approximation. This is also what was deduced that would happen in Chapter 3-2. Although it does not happen to the higher-order linearisations. The diagonal model seems to correspond better in terms of gains compared to Figure 4-8. To make the comparison a bit easier to do, $P_{11}(s)$ and $P_{12}(s)$ of Figure 4-8 and of Figure 4-9 are plotted together in Figure 4-10.

In Figure 4-10 it becomes clear that indeed the gain of $P_{11}(s)$ is better for the case of the $G_b(s)$ model approximation. The difference in the low-frequency gain of the $P_{12}(s)$ seem to agree with the $G_{b_c}(s)$ model structure a bit better, because the linearisation of the NREL 5-MW turbine does not have an ideal differentiator in their low-frequency domain, whereas the decoupled blade-dynamic model does. The difference in dynamics seen in the $P_{12}(s)$ plots of Figure 4-10 also indicate that the offset of $\psi = 19°$ is indeed a better value to decouple the system. This agrees with the results found in Figure 4-5.

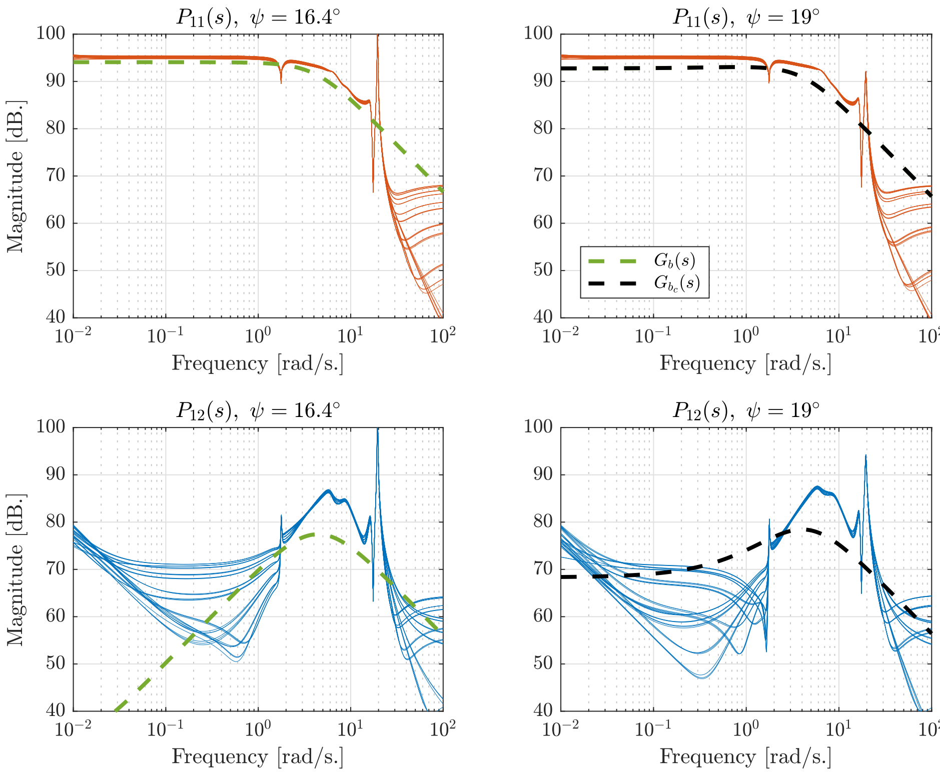

Figure 4-10: Comparing the MBC-transformation of NREL 5-MW turbine with different first-order approximations. Specifically the ones done in Figure 4-8 and Figure 4-9.

4-6 Conclusion

This Chapter has extended the theoretical basis set out of the previous Chapters to the actual application on a high-fidelity wind turbine model. The application of the MBC-transformation to this higher-order model could be done in a relatively fast fashion. The blade-dynamics of the higher order model correspond in different ways to the different blade-dynamics models earlier considered.

The increased complexity of the higher-order model meant that a metric had to be defined by which decoupling could be quantified. This was due to the fact that the lower-frequency dynamics of the linearisations of the non-linear model do not have a easily determinable DC-gain. After the definition of the new decoupling metric, an ideal offset was found by varying the offset from $\psi = 0°$ to $\psi = 90°$.

The blade-dynamics model (specifically $G_{b_c}(s)$) allowed for the approximation of the high-order wind turbine model with a first-order model. Although the approximation did not produce an accurate picture of the MBC-transformed system dynamics, it did provide an opportunity to find a fast approximation of the ideal azimuth offset needed in the MBC-transformation to decouple the yaw and tilt moments.

Finally, the $G_{b_c}(s)$ model approximation was compared with a $G_b(s)$ model approximation, because the $G_b(s)$ is the model structure classically considered in the literature. The $G_b(s)$ model approximation had a 2.6° difference from the ideal offset. This can in turn be compared to the decrease in decoupling compared to the ideal decoupling as plotted in Figure 4-5. Here it is found that $\frac{\eta(16.4)}{\eta(19)} \approx 1.44$. This means that even though the deviation from the ideal offset is just 2.6°, the increase in gain compared to the ideal decoupling is almost 44%. This justifies the use of the small increase in complexity of the $G_{b_c}(s)$ model structure compared to the $G_b(s)$ model structure.

Chapter 5

Identification, Simulation and Analysis

Everything up to this point has focussed on analysing linear models to get a good grasp on the properties of the introduction of an offset in the MBC-transformation. In this chapter, the NREL 5-MW turbine's characteristics in the non-linear domain will be used. This is done to see if the ideal offset as found in the previous chapter translates into the non-linear domain and what the consequences are for applying control on the turbine using the offset.

The first part of this chapter identifies frequency response estimates of MBC-transformed dynamics of the non-linear wind turbine. After these are analysed, the full non-linear system is simulated with and without the offset to see what effect this has the system. Subsequently, the sensitivity function of the system is set up to relate this to the results of the simulation. Finally, a conclusion is presented.

5-1 Identification

In this section the interest is in identifying the MBC-transformed dynamics of the system. This provides the possibility of comparing the effect of the offset on the linearised model (of for example Figure 4-2) with the true dynamics.

This identification for a non-parametric spectral model is done on the NREL 5-MW turbine which is implemented in an open-loop setup as can be seen in Figure 5-1. The non-linear NREL 5-MW turbine model is denoted by the "WT" block. The mean pitch angle $\bar{\theta}$ and torque τ_e are determined from controllers based on the operating conditions. The identification is performed $(\theta_{\text{yaw}}(t),\ \theta_{\text{tilt}}(t)) \rightarrow (M_{\text{yaw}}(t),\ M_{\text{tilt}}(t))$ where it is applied for the offset range $\psi \in [0°, 90°]$.

The system is excited with two independent Random Binary Signals (RBS) of different seeds with an amplitude of 1 deg and clock period of $N_c = 1$ [33]. During the first identification it was found that the unfiltered excitation signals produced faulty simulation results. As a consequence a bandpass filter $\mathcal{B}$ was implemented at cut-off frequencies 10^{-3} rad/s and 10^2 rad/s. The sampling frequency was set to $\omega_s = 125$Hz, and the total simulation time was 2200s. In this case the first 200s were discarded to get rid of the transient effects from the data.

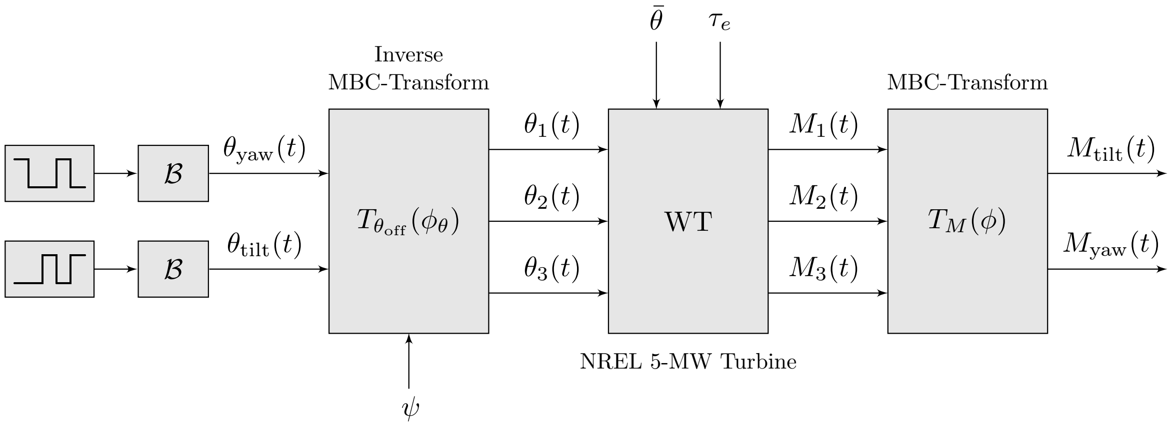

Figure 5-1: The model being considered for identification of a spectral model of the non-linear NREL 5-MW turbine (the "WT" block in the figure) model. The wind turbine is controlled in an open-loop set-up by steady-state collective pitch angle $\bar{\theta}$, and generator torque τ_e. The system is excited by Random Binary Signals (RBS) which are fed through a bandpass filter $\mathcal{B}$ to result in two distinct excitation angles $\theta_{\text{yaw}}(t)$, $\theta_{\text{tilt}}(t)$. This identification is performed for different offset ψ. The identification is performed from $(\theta_{\text{yaw}}(t),\ \theta_{\text{tilt}}(t)) \rightarrow (M_{\text{yaw}}(t),\ M_{\text{tilt}}(t))$. The identification is performed at a wind-speed of 25m/s.

For the obtained data Power Spectral Densities (PSDs) were calculated. A Hamming window was applied to reduce spectral leakage. Furthermore, frequency averaging was applied to reduce variance effects of the random signals (a frequency which might not have been actuated as much as other frequencies). This was done with the help of the Predictor-Based-Subspace-IDentification (PBSID) toolbox [34]. The PSDs were calculated for the non-rotating tilt- and yaw-pitch angles to the tilt- and yaw-moments. The results of this identification for the offsets $\psi \in \{0°, 14°, 19°, 22°\}$ are shown in Figure 5-2. The top plot relates to $P_{11}(s)$, and the bottom plot relates to $P_{12}(s)$ in previous chapters. The ideal decoupling offset was defined as the offset which minimises the off-diagonal components in the low-frequency region. It is clear from Figure 5-2 that this happens for $\psi = 19°$ which corresponds nicely with the results found in Chapter 4.

Furthermore, from Figure 5-2 it becomes clear that for frequencies larger than ~ 5 rad/s the effect of the offset is negligible. Or on the contrary, even has a deteriorating effect on the decoupling. This agrees with the results found, even for first order systems.

5-2 Simulation

Now that the non-linear (de)coupling dynamics are identified, the goal is to see what effect this has on simulations of the full system. This section first sets up the simulation with pre-

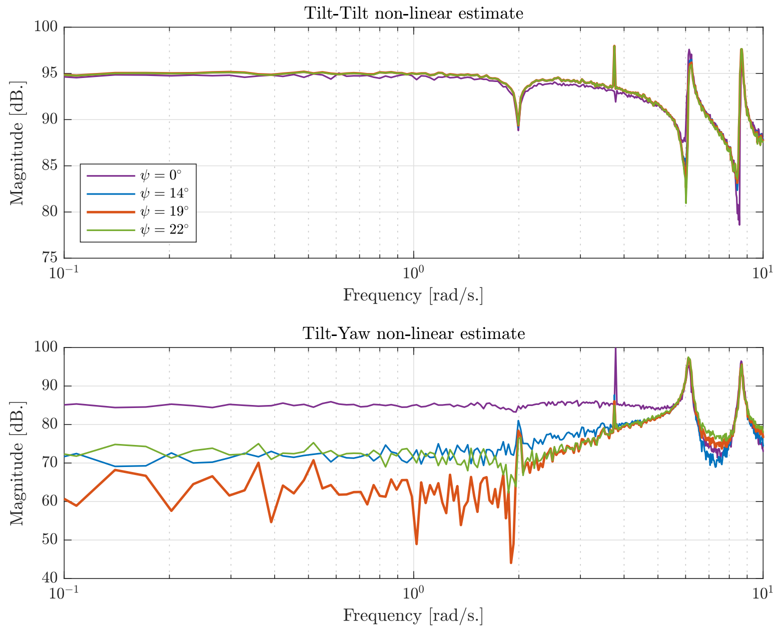

Figure 5-2: Results of the non-linear spectral identification of the set-up of Figure 5-1 for offsets $\psi \in \{0°, 14°, 19°, 22°\}$. Where the cross-coupling was miminized for an offset $\psi = 19°$. In the high frequency region the difference is reduced and the ideal decoupling there is at $0°$.

liminary load spectrum results, after which the direct comparison is made between the effect of the offset on the results.

This simulation was set up using the NREL 5-MW turbine in a closed-loop setting using a MATLAB Simulink compiled version of FAST. The IPC considered is implemented as shown in Figure 5-3. Here, the NREL 5-MW block is the turbine model described above, and the IPC is formed by two fully decoupled integrators with integrator gains K_{tilt}, K_{yaw} acting on the tilt- and yaw-moments respectively. This type of setup was chosen, because in literature the initial controllers for IPC are often basic integrator action with the assumption that the system is fully decoupled [6, 18]. For this specific setup the values $K_{\text{yaw}} = K_{\text{tilt}} = 1 \cdot 10^{-8}$ as a baseline case.

The system in the form of Figure 5-3 is simulated for a wind speed of 25 m/s and for a $\psi = 0°$ as well as a simulation with $\psi = 19°$. Mean pitch and torque control values, as in Figure 5-1, are implemented in parallel with the IPC. As was seen throughout the thesis, the incorporation of an offset in the MBC-transformation has the effect of changing the gains of the system. For a controlled system, this has as a consequence that the cross-over frequency also shifts. In the case of $\psi = 0°$, the integrator gains were chosen as $K_{\text{yaw}} = K_{\text{tilt}} = 1 \cdot 10^{-8}$. To compensate for the gain change, for $\psi = 19°$ the cross-over frequency is kept the same if the integrator gains are slightly reduced to $K_{\text{yaw}} = K_{\text{tilt}} = 0.95 \cdot 10^{-8}$.

The results of these simulations with respect to the OoP bending moments can be seen in Figure 5-4a. Here the PSD [33] is plotted against the frequencies. The baseline of when IPC is fully disabled shows to have a big peak in its fatigue loads at a 1P (or ω_0) frequency. This

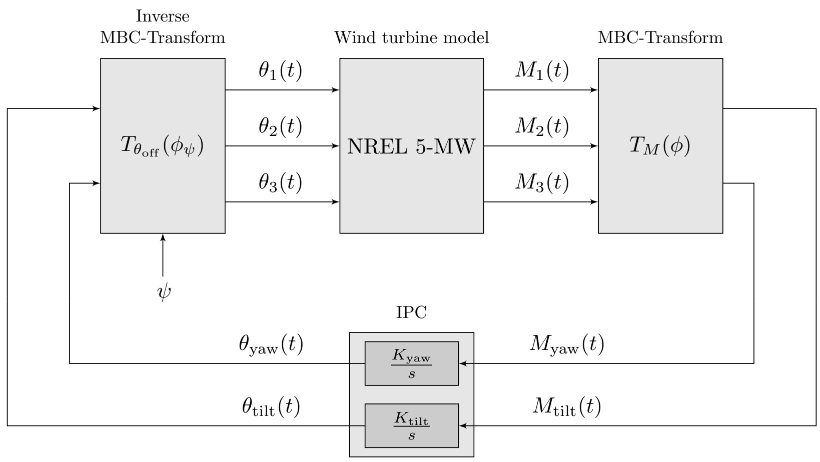

Figure 5-3: The setup used for running the simulation. The NREL 5-MW block is a `MATLAB/Simulink` compiled version of the NREL 5-MW turbine combined with FAST. This simulation is run for $\psi = 0°$ and $\psi = 19°$. $K_{\text{yaw}} = K_{\text{tilt}} = 1 \cdot 10^{-8}$ for $\psi = 0°$, and $K_{\text{yaw}} = K_{\text{tilt}} = 0.95 \cdot 10^{-8}$ for $\psi = 19°$.

shows the usefulness of IPC. This reduction in OoP bending moments through IPC comes at the cost of extra actuation of the blades, as can be seen in Figure 5-4b. This has also been suggested in the literature [13].

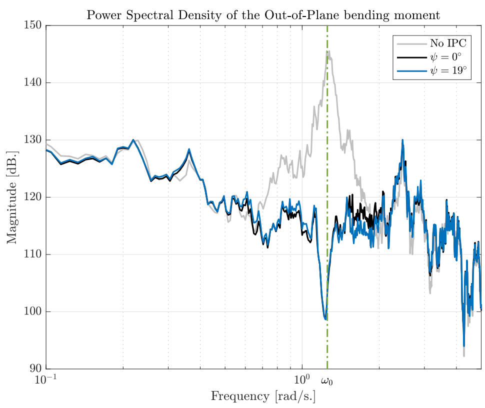

(a) PSD of the OoP bending moments. A significant reduction can be observed when IPC is present.

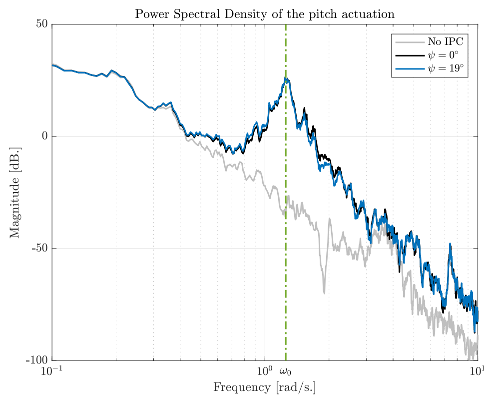

(b) PSD of the pitch actuation. A significant increase in pitch actuation is observed when IPC is present.

Figure 5-4: Power Spectral Densities (PSD)s of OoP bending moments and the pitch actuation of the blades. The PSDs are plotted for when IPC is turned off, for IPC with no offset in the MBC-transformation present and for an offset of $\psi = 19°$ in the MBC-transformation. The difference between "No IPC" and the rest is significant. The difference between $\psi = 0°$ and $\psi = 19°$ is hard to read out from the plots.

In Figure 5-4 it is hard to distinguish the exact differences between $\psi = 0°$ and $\psi = 19°$. To see exact differences between these simulations the PBSID toolbox is once again used. Here the ratio between the cross-spectral density with the PSD is calculated to obtain a frequency domain estimate of the transfer function [34]. This means that for the frequency dependent

OoP bending moments of the blades for no offset $M_{\psi=0^\circ}(s)$ can be related to the frequency dependent OoP bending moments of an offset of $\psi = 19^\circ$, or $M_{\psi=19^\circ}(s)$. This would result in a frequency domain estimate of the transfer function describing $\frac{M_{\psi=19^\circ}(s)}{M_{\psi=0^\circ}(s)}$.

The same can be said for the pitching actuation of the blades. The frequency dependent pitching of the blades for no offset $\Theta_{\psi=0^\circ}(s)$ can be related to the frequency dependent pitching of the blades for an offset of $\psi = 19^\circ$, or $\Theta_{\psi=19^\circ}(s)$. This would result in a frequency domain estimate of the transfer function describing $\frac{\Theta_{\psi=19^\circ}(s)}{\Theta_{\psi=0^\circ}(s)}$.

The frequency domain estimates of these transfer functions are given by Figure 5-5. In Figure 5-5a, this is done for the OoP bending moments. There seems to be an increase of the bending moments in the low frequency region as well as a significant drop just around 1-1.3 rad/s, which represents the 1P frequency. The transient in the high frequency region subsequently seems to go to 0dB. Which means that the loads experienced in the high-frequency region with and without offset is the same.

For the pitch actuation the results seem to be more significant. In Figure 5-5b there seems to be a slight increase in pitch actuation in region of 0.4-1 rad/s. However, at the same time, the pitch actuation of the offset $\psi = 19^\circ$ attenuates and stays below the pitch actuation compared to when no offset is present in the high-frequency region.

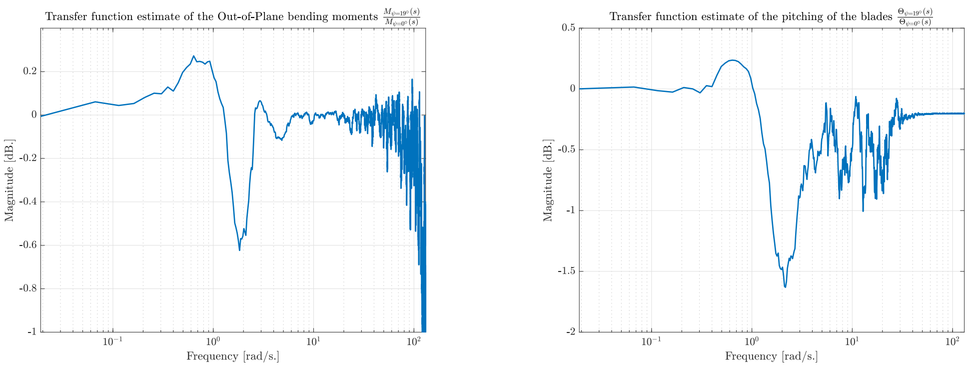

(a) A frequency domain estimate of the transfer function $\frac{M_{\psi=19^\circ}(s)}{M_{\psi=0^\circ}(s)}$.

(b) A frequency domain estimate of the transfer function $\frac{\Theta_{\psi=19^\circ}(s)}{\Theta_{\psi=0^\circ}(s)}$.

Figure 5-5: Frequency domain estimates of the transfer function relating the OoP bending moments and the pitch actuation signals. These signals relate the difference between an offset in the MBC-transformation of $\psi = 0^\circ$ with $\psi = 19^\circ$. Both plots seem to indicate an amplification peak around $\omega \approx 0.65$ rad/s. This is subsequently followed by a more significant attenuation of both estimates. The bending moments return to 0dB in the high-frequency region, whereas the pitch actuation remains lower. Which implies that with less pitch actuation the same loads are observed.

Combining these results, it can be concluded that in the high-frequency region with less pitch actuation the same load spectrum is present for the offset $\psi = 19^\circ$ as opposed to the case when no offset is present. In the next section an extensive analysis will be given on the performance of the controller on the system, which helps to interpret the obtained results.

5-3 Sensitivity analysis

In previous chapters several reasons for introducing an offset in the MBC-transformation have been set out. The reasons were mainly related to the cross-coupling of the MBC-transformed dynamics. These coupled dynamics were reduced to make easier control synthesis possible, because a decoupled system allows for control synthesis of separate SISO control loops.

In the previous section for the first time in this thesis, control has been applied on the system. The results seem to indicate that the decoupling has an effect on the pitch and load dynamics of the system. However, no analysis has been performed up until this point on the effect of the offset on the controlled system.

5-3-1 Sensitivity function

A classical method to assess the performance of a controller is by analysing the sensitivity function of the system. For a closed loop system the sensitivity function shows several. This includes among other things how well the system is able to attenuate disturbances, and the sensitivity of the closed-loop transfer function to the relative plant model error [28].

The classical (negative) feedback control loop model is given in Figure 5-6. This control loop aims for the output y to track a reference signal r. The error term $e = r - y$ is provided to the controller K. The controller provides an input signal u. Input disturbance d_2 is added to the input signal u. The addition of these two signals is then fed into the plant G. An output disturbance signal d_1 is added to the output of the plant to result in the final output signal y.

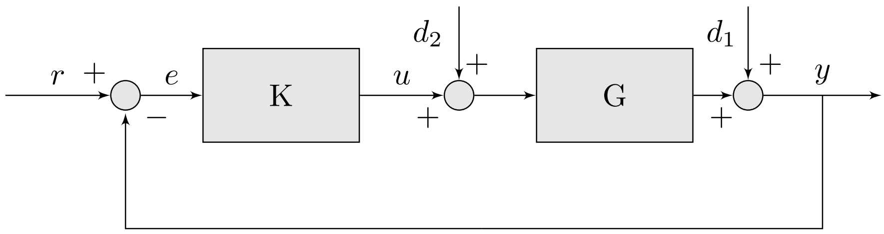

Figure 5-6: Feedback control loop for tracking a reference signal r. The output y is subtracted from the reference of r. This results in the error signal e. The error signal is subsequently the input for the controller K, which provides an input signal u into the plan G. There are two disturbance signals, d_1 and d_2 which work on the output and the input respectively.

The sensitivity function for this classic control loop is defined as,

$$S = (I + GK)^{-1} = \begin{cases} \frac{y}{d_1}, & \text{for } r = d_2 = 0, \\ \frac{e}{r}, & \text{for } d_1 = d_2 = 0. \end{cases} \tag{5-1}$$

Here it becomes clear why the sensitivity function relates to disturbance rejection. It directly gives a measure of how the error relates to the reference signal, or how the output disturbance relates itself to the output signal. This is valid for both SISO and MIMO systems.

For MIMO systems, the sensitivity function can give information on the effectiveness of control through the ratio $\frac{||e||_2}{||r||_2}$ (or $\frac{||y||_2}{||d_1||_2}$). It can be derived that

$$\underline{\sigma}(S(j\omega)) \leq \frac{||e(\omega)||_2}{||r(\omega)||_2} \leq \bar{\sigma}(S(j\omega)). \tag{5-2}$$

Where $\underline{\sigma}(S(j\omega))$ indicates the smallest singular value, and $\bar{\sigma}(S(j\omega))$ the largest singular value of $S(j\omega)$. The singular values correspond to the directions corresponding with the smallest and the biggest gains of $S(j\omega)$ [28].

The bandwidth for SISO systems is generally defined as the point where the sensitivity function $S(j\omega)$ crosses -3dB (or $1/\sqrt{2}$) from lower magnitudes. Colloquially this means that the bandwidth is defined as the frequency up until which feedback control is effective. For MIMO systems there is a so-called bandwidth region. This is the region between the frequencies where $\underline{\sigma}(S)$ (the "best-case" direction) and $\bar{\sigma}(S)$ (the "worst-case" direction) crosses the -3dB.

Furthermore, the maximum and mimimum singular value of a system denote the maximum and minimum gain of the system in certain directions. These directions can in turn be determined by looking at matrices obtained by the Singular Value Decomposition (SVD) of the system [28].

All the theory discussed can now be applied on the system under consideration to see what effect the offset in the MBC-transformation has on the controlled system.

5-3-2 Application on IPC

In the previous section the classic (feedback) control structure (as shown in Figure 5-6) was used to derive the sensitivity function with its respective properties. The model of Figure 2-3 can turned into the form of Figure 5-6. In the case of IPC there is positive feedback, and the controller consists of two separate integrators. If all this is combined, Figure 5-7 is obtained. Here r is set to zero, because the loads are supposed to be minimised. d_1 and d_2 indicate any disturbances acting on the in- and output respectively.

In the case of positive feedback, the sensitivity function changes from the form presented Eq. (5-1) into $S = (I - GK)^{-1}$. This sign change does not change any of the other properties discussed earlier. The plant G is now the transfer function from the tilt- and yaw-moments to the tilt- and yaw-pitch angles, which has been referred to as $P(s)$ throughout the thesis. The IPC used in the simulations were two disconnected integrators. As a consequence, the sensitivity function can be denoted as

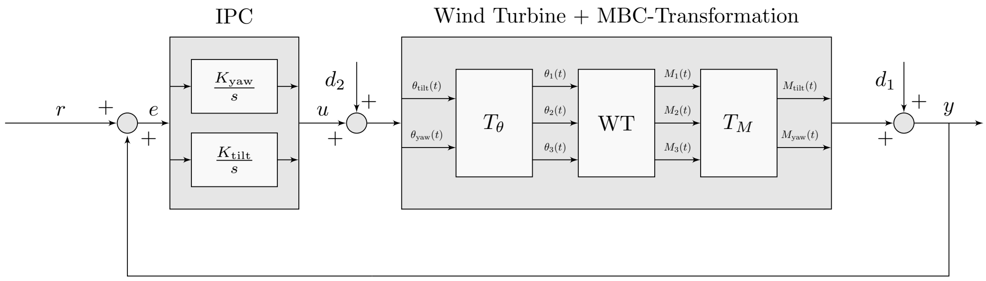

Figure 5-7: Combining the classic feedback control model of Figure 5-6 with the considered IPC loop of Figure 2-3. The feedback is positive in the case of IPC.

$$S(s) = \begin{bmatrix} 1 - \frac{K_{\text{tilt}}}{s} P_{11}(s) & -P_{12}(s) \\ -P_{21}(s) & 1 - \frac{K_{\text{yaw}}}{s} P_{22}(s) \end{bmatrix}^{-1}. \tag{5-3}$$

In this case the wind turbine under consideration is the NREL 5-MW turbine. Once again the linearisation of Chapter 4-3 is used. This time a method of state-space model averaging is used. The method of state-space averaging is a summation of all 36 different A is made, after which each value is divided by 36. This same is done for the B, C, D matrices. Even though this method is not without its limitations [35], it suffices for the present analysis. It allows a combination with the theory of Chapter 4-4-1, and is also present in the `MBC3` script of [32]. Which means that the 36 different linearisations are transformed into one single system approximating the average of the 36 linearisations. This provides a 29th order description of $P(s)$ which can be substituted into Eq. (5-3). Together with the controllers applied in Chapter 5-2 (meaning $K_{\text{yaw}} = K_{\text{tilt}} = 1 \cdot 10^{-8}$) the sensitivity function can be fully set up. (More accurate methods for averaging have recently been proposed and might prove for more accurate analysis [35].)

This allows for the comparison of the effect of the offset on the sensitivity function. In different sections of this thesis the ideal offset was found to be $\psi = 19°$. When an offset is introduced, this changes the gain of the open-loop system. As a consequence the gains of the integrators are scaled appropriately to guarantee that the cross-over frequency of the open-loop dynamics remains on the same frequency. In case of the sensitivity function, the comparison between these values can be made. In Figure 5-8 the minimum and maximum singular values of Eq. (5-3) are plotted.

In Figure 5-8 the sensitivity function of the plant without an offset has a significant spread. This results in a bandwidth region (of $\omega_b \in [0.38, 0.65]$). In the case the offset is chosen to be $\psi = 19°$ there is almost no difference between the minimum and maximimum singular values. This results in a single bandwidth frequency of $\omega_b = 0.47$ rad/s.

As described earlier, the mimimum and maximum singular values specify the extreme gains of a system. In the case they (nearly) coincide it has as a consequence that no matter what input direction is chosen, the gain of the system will be the same. In the case of the sensitivity function this means that no matter the output direction of the plant, control will always be

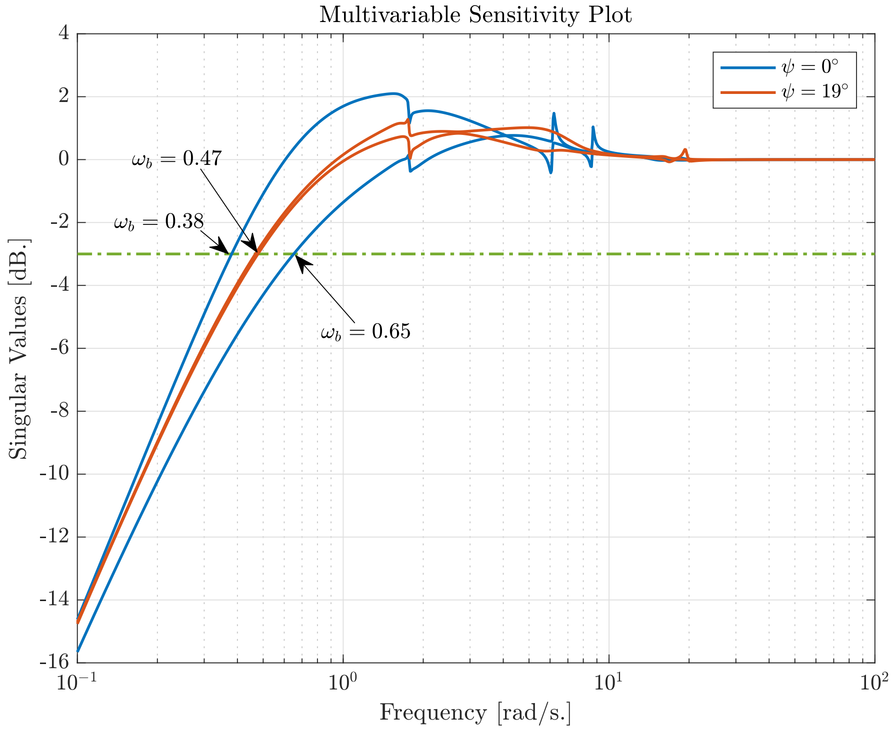

Figure 5-8: The sensitivity function of the average linearised NREL 5-MW turbine is plotted for $\psi \in \{0°, 19°\}$. The green line signifies the line of -3dB (bandwidth). For $\psi = 0°$ a bandwidth between $\omega = 0.38$ rad/s and $\omega = 0.65$ rad/s is found. For $\psi = 19°$ the bandwidth coincides on the frequency $\omega = 0.47$ rad/s.

just as effective. Or in other words, that no matter the output direction, the attenuation of the error as a result of IPC is the same.

The obtained result can now be related to the RGA. If the RGA shows that the system is sufficiently decoupled, this can be combined with the effect that the sensitivity function properties to justify certain control properties. The RGA of the system at $\omega = 0.47$ rad/s is calculated to be

$$|\text{RGA}(P_{\psi=0°}(j0.47))| = \begin{bmatrix} 0.9052 & 0.0948 \\ 0.0948 & 0.9052 \end{bmatrix}, \ |\text{RGA}(P_{\psi=19°}(j0.47))| = \begin{bmatrix} 0.9997 & 0.0003 \\ 0.0003 & 0.9997 \end{bmatrix}. \tag{5-4}$$

Here it should be noted that the norm is justified because all the real values of the RGA are positive and no negative coupling is therefore present in the RGA. In Eq. (5-4) it is clear that the system for $\psi = 19°$ is as good as decoupled compared to when the offset is not present.

Technically, the RGA for the case that no offset is present should be calculated at the frequencies $\omega = 0.38$ rad/s and $\omega = 0.65$. If this is done, the value of the RGA deviates less than 1% from the values found in Eq. (5-4). Therefore, the value of $\omega = 0.47$ rad/s was chosen.

Furthermore, to make conclusions for the entire region up until $\omega_b = 0.47$ rad/s, the RGA should be known up until that value. A property of the RGA is that the columns and rows sum up two 1 [28]. For this reason it is sufficient for a 2×2 system to look at one row, therefore in Figure 5-9 the first row of the RGA of an offset of $\psi = 19°$ is plotted. In Figure 5-9 it is visible that near perfect decoupling is achieved up until around $\omega \approx 3.5$ rad/s.

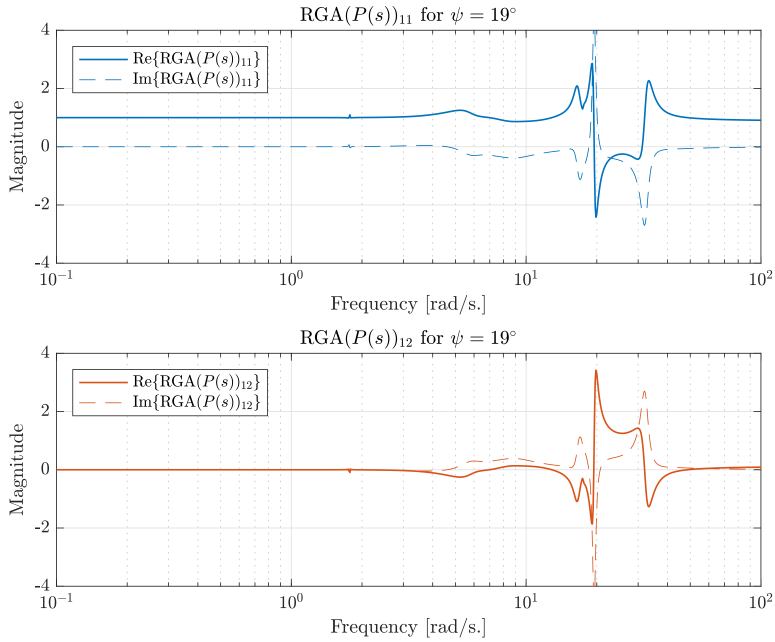

Figure 5-9: The first row of the RGA of the average NREL 5-MW turbine with an offset of $\psi = 19°$. Here it is seen that the system is fully decoupled up until around $\omega \approx 3.5$ rad/s. In the low-frequency region it is also observable that the imaginary component is a negligible component, whereas when the decoupling breaks down it becomes also more prevalent.

As a small side note, the RGA also provides the possibility to analyse the high-frequency coupling as well. It has been noticed that the RGA reaches its asymptote just under $\omega = 100$ rad/s. Therefore, this frequency is taken as the high-frequency estimation. In Eq. (5-5) the decoupling is seen as happening better for an offset of $\psi = 0°$ as opposed to $\psi = 19°$. This corresponds to the results found for a first-order, as was found in Eq. (3-7).

$$|\text{RGA}(P_{\psi=0°}(j100))| = \begin{bmatrix} 1 & 0 \\ 0 & 1 \end{bmatrix}, \ |\text{RGA}(P_{\psi=19°}(j100))| = \begin{bmatrix} 0.9103 & 0.0911 \\ 0.0911 & 0.9103 \end{bmatrix} \tag{5-5}$$

5-3-3 Effects on the system

The RGA of the system indicates decoupling of the system at least until the bandwidth frequency. This means that the control that is applied to result in θ_{tilt} is dominated by M_{tilt}. The same thing can be said for the yaw-component. As a consequence, choosing a diagonal controller is justified (as was done in Chapter 5-2 and in Figure 5-7).

This diagonal controller chosen with the control gains to be $K_{\text{tilt}} = K_{\text{yaw}}(= 0.95 \cdot 10^{-8})$ resulted in a sensitivity function where nearly $\underline{\sigma}(S(j\omega)) \approx \bar{\sigma}(S(j\omega))$ for $\omega \leq \omega_b$. Consequently, the controller applied on the tilt-component is the exact same controller which is applied on the yaw-component. These components are (almost fully) decoupled. The fact that these two controllers result in the exact same sensitivity function for $\omega \leq \omega_b$ seems to indicate that the tilt- and yaw- dynamics in the low frequency region are equal to each other.

This corroborates the approximation made in Figure 4-6. Because it was based on the blade-dynamic model of Eq. (2-22), which resulted in Eq. (2-23), which had on the diagonal the same dynamic model for $P_{11}(s)$ and $P_{22}(s)$. As a consequence this seems to be true for low frequencies up until about $\omega = 0.8$ rad/s (as can be seen in Figure 5-8). This indicates that the bandwidth could be increased to a higher frequency by changing the controller. Furthermore, the fact that the RGA in Figure 5-9 indicates that the system is (as good as) decoupled until about 3.5 rad/s could mean that with more advanced controller synthesis an even higher bandwidth than 0.8 rad/s is possible.

This can be related to the simulations performed in Chapter 5-2. The results seen in Figure 5-5b indicate that there is a reduction in pitch actuation in high frequencies for the basic controller. This drop starts at a frequency of $\omega = 1$ rad/s. This corresponds to the frequency where the sensitivity function in Figure 5-8 crosses the 0dB line. This point in the sensitivity function signifies where the error signal e or where the disturbance signal d_1 starts being amplified.

5-4 Conclusion

At the start of the chapter a spectral analysis of the non-linear MBC-transformed system has been made to identify the effect of introducing an offset in the MBC-transformation. This resulted in finding that the offset which decouples the non-linear system in the low-frequency domain corresponded with the offset that decouples the system made by a first-order approximation of the linearised dynamics.

Subsequently, a simulation was carried out by implementing a very basic decoupled controller consisting of only an integrator to see if with the help of this controller the effects of the offset could be seen. It does however seem to indicate that there is a decrease in pitch actuation action in the high-frequency region.

In the final section an analysis of the sensitivity function is performed, together with an evaluation of the RGA. These two finding do indeed seem to confirm the fact that the type of (decoupled) control performed is justified for the offset of $\psi = 19°$ whereas for the offset $\psi = 0°$ this is not straightforwardly justified. This section also showed that an increase in bandwidth is possible by modifying the controller applied to the system.

When relating the simulation results with the sensitivity function analysis it seems to show that the actuation drop seems to correspond to the point where the sensitivity function crosses the 0dB line. This means that from the point where the system starts to amplify the error signal/output disturbances, the actuation is decreased for the system with $\psi = 19°$, which is a positive effect.

As the basic controller with the same integrator gains applied to the system has shown a decrease in actuation signal in the high-frequency region a more careful controller synthesis can prove to increase the usefulness of the offset even more. This is due to the fact that the current controller just makes use of one of a big variety of loop shaping options. Furthermore, the offset has presented the possibility to increasing the bandwidth of the controller as opposed to the case where no offset is present.

Chapter 6

Conclusion and Recommendations

In Chapter 1-2 the goal of this thesis was set out through stating the different problems currently encountered in the literature. The main problem was a lack of insight in the effects of the offset in the MBC-transformation. This lack of insight was mainly due to the fact no extensive analysis had been carried out.

The research performed has provided a variety of results which contribute in different ways to an understanding of the introduction of an offset in the MBC-transformation. This chapter discusses these results and in what way they contribute in acquiring a deeper understanding of the effects of this offset. After the results are presented, several recommendations for future research are proposed.

The conclusion is split up in two sections. First, the general conclusions made through analytical analysis are set out, after which the results of the application on a high-order wind turbine model are explained.

6-1 Analytical results

Several clarifications and results have come up during the analytical analysis of introducing an offset in the MBC-transformation. Firstly, It has become clear why the offset is usually applied in the inverse MBC-transformation. It is shown that it does not matter where it is applied except for a sign change. What does matter however, is the choice of blade-dynamic model structure. The initial assumption of a fully decoupled blade-dynamic model structure is evaluated, and it is seen that the MBC-transformed system changes considerably when assuming different blade-dynamic model structures. Furthermore, it is shown that this changes the value obtained of the ideal offset to decouple the MBC-transformed system. As a result, it is very important to make a thorough assessment of the system before choosing the blade-dynamic model structure.

An important result is that for the most basic blade-dynamic model structure with a basic linear model, it is impossible to decouple the system over the entire frequency region. This result extends to more complex blade-dynamic model structures. Consequently, for the system it should be clear in what frequency region decoupling is desired. Because the basic MBC-transformation maps the 1P harmonics to 0P or the DC-gain of the system, decoupling is desired in the low frequency region.

Another result is that the offset in the MBC-transformation can change the location of the zeros of the elements of the MBC-transformed system. If the offset is chosen such that the location of the zeros of the off-diagonal components of the MBC-transformed system are located at low frequencies, the DC-gain of these off-diagonal components decreases, and as a result the decoupling increases.

This is verified by determining the RGA of the system for different offsets. The RGA indeed shows that the values of the offset which decouples the system correspond to the location which places the zeros of the off-diagonals at the origin. The RGA furthermore shows that small deviations from the ideal offset result in a polynomial/exponential decrease in decoupling, as well as that the coupling can even invert by choosing certain values of the offset.

6-2 High-fidelity non-linear model results

With respect to the high-fidelity model, a number of results carry over from the analytical case as well as new results have been found with respect to the introduction of an offset in the MBC-transformation. One of these results is that the approximation of higher-order linearised models is possible by first-order models. The ideal offset for decoupling the MBC-transformed system for these first-order approximations corresponds with the higher-order model. As a result, it allows for the possibility of using an analytic form to calculate the ideal offset in a relatively fast fashion.

In the literature it has been stated that fully decoupled dynamics provide a valid blade-dynamic model structure for IPC without deteriorating the performance of the controller all that much [18]. This assumption is not valid. The dynamics of the pitching a specific blade does have a non-negligible effect on the resulting moments of the other blades. In the case these coupled dynamics are taken into account, it results in significantly better approximations of the ideal offset for the MBC-transformation. This is because a small deviation reduces the performance of decoupling polynomially/exponentially in the higher-order linearisations.

A number of these results also carry over to the spectral estimates of the high-fidelity non-linear model. The offset which decouples these spectral estimates is the same as the offset which decouples the linearisations of high-fidelity non-linear model. Consequently, the offset which decouples the spectral estimates can also be found with the first-order approximations of these linearisations. Furthermore, small deviations from the ideal offset for the spectral estimates also significantly decreases the decoupling. Which is also seen in the first-order model analysis of the MBC-transformation.

In the sensitivity analysis of a basic controller on the system it is found that a significant gain difference exists (depending on the directionality of the input) for the case when no offset is applied. This result signifies that choosing two exactly equal SISO controllers does not result in ideal performance. By introducing the offset, this dependency on the directionality of the gain reduces significantly. This offset also decreases the peak of the sensitivity function, whereby making the controller more robust and justifying the use of two controllers with equal gains, resulting in similar sensitivity dynamics. The ideal offset which minimises the gain difference of the sensitivity function, corresponds with the offset which decoupled the tilt- and yaw-moments.

A reduction in pitch actuation in the high-frequency region is identified from non-linear simulations. The frequency where this pitch actuation starts to be attenuated corresponds with the frequency where the sensitivity function indicates that amplification of the error signal and disturbances start to happen. This is an important result because increased pitch actuation due to IPC can cause significant stresses on pitch actuators [13]. The introduction of the offset in the MBC-transformation indicates that this can help alleviate high-frequency pitch actuation without affecting the PSD of the loads in that frequency region.

6-3 Recommendations for future research

1. *Data-driven approach to finding the ideal offset.*
   The method of finding the ideal offset for the wind turbine is currently done by setting up a metric which is defined depending on the linear dynamics of the system. These linear dynamics were in turn found by the linearisation of a high-fidelity non-linear model, which could be approximated with first-order models. This first-order approximation was done in a heuristic fashion and showed promising results in finding the ideal offset using lower-order parametrisable models. It is interesting to see if there is a more rigorous way of approximating these linearisations such that the ideal offset can be identified using a data-driven technique.

   A second possibility is to extend this towards a method which is able to find the ideal offset in a data-driven manner without the need of linearisations. Different data-driven optimisation methods already exist, for example Extremum Seeking Control (ESC) has proven itself a good contender in different applications of wind turbine control optimisation [36]. The definition of a suitable performance-/cost-function is important to enable performance assessment of the the offset in a data-driven manner.

2. *More advanced controller synthesis based on the decoupled tilt- and yaw-dynamics.*
   In this thesis a basic integrator controller with a fixed gain has been employed to showcase the difference in performance for the offset. As the effect of the offset becomes better understandable, it can be employed as the basis for controller synthesis. As a result from the decoupling, the tilt-to-tilt and yaw-to-yaw dynamics would provide the

main dynamics for controller design. This can increase the performance of the IPC as opposed to the ones implemented in this thesis.

3. *Analytic consequences of non-constant offsets.*
   Throughout the thesis, the assumption was made that a constant non-varying offset is made of the form $\phi_\theta(t) = \omega_0 t + \psi$. In the analysis of the offset on the linearisations of the high-fidelity non-linear model there were 36 different models present, all describing the dynamics on different azimuth angles. During the analysis, the models reacted differently to the same offset. This might indicate that making ψ dependent on the azimuth angle could help in further decoupling over the entire rotating frame.

4. *Varying the results over different wind speeds and under different wind conditions.*
   Currently, the non-linear simulation has only been run at wind speeds of 25m/s and with one (type of) wind field. This has proven to be useful for an initial understanding, but in the generalisation of the findings it is useful to vary the turbulent wind fields for statistical reliability of the findings. Furthermore, as the wind speed varies it could be that offset is only dependent of ω_0, the wind speed itself, or of a combination of both.

Appendix A

MBC-Derivation

In this Appendix the mathematical details of the MBC-transformation are set out. This is done, because they are needed for later derivations of the effects of offsets in the MBC-transformation. The goal of the derivation is to arrive at a matrix relating the tilt- and yaw-pitch angles to the tilt- and yaw-moments as described in Eq. (2-7). To do be able to do this, first certain Laplace transformations are needed. After these will be defined, the derivation of the MBC-transformation can be completed.

A-1 Laplace transforms

The formula for the azimuth angle forms the basis Laplace transform and is for that reason repeated here. It was defined to be $\phi(t) = \omega_0 t$, where ω_0 was the constant rotational speed of the wind turbine. This can now be used to write the Laplace transform of Eq. (2-7). This is done with the help of the following identities. Where $y(t)$ is an arbitrary function of time.

$$\mathcal{L}\left[y(t)\cos(\omega_0 t)\right] = \mathcal{L}\left[y(t)\frac{e^{j\omega_0 t}+e^{-j\omega_0 t}}{2}\right] = \frac{1}{2}\left[Y(s+j\omega_0)+Y(s-j\omega_0)\right], \quad \text{(A-1)}$$

$$\mathcal{L}\left[y(t)\sin(\omega_0 t)\right] = \mathcal{L}\left[y(t)\frac{e^{-j\omega_0 t}-e^{j\omega_0 t}}{2}\right] = \frac{j}{2}\left[Y(s+j\omega_0)-Y(s-j\omega_0)\right], \quad \text{(A-2)}$$

In case there is an offset in the sines or cosines (as can be seen in some terms of $T_M(t)$ and $T_\theta(t)$), the following trigonometric identities might come in useful.

$$\cos(\omega_0 t+\alpha) = \cos(\omega_0 t)\cos(\alpha) - \sin(\omega_0 t)\sin(\alpha), \quad \text{(A-3)}$$

$$\sin(\omega_0 t+\alpha) = \sin(\omega_0 t)\cos(\alpha) + \cos(\omega_0 t)\sin(\alpha) \quad \text{(A-4)}$$

The Laplace transform of the cosines and sines with offsets will also be useful in the following parts. The derivation for both the sine and cosine are made below. First, the derivation is made for the offset in the cosine,

$$
\begin{aligned}
\mathcal{L}\left[y(t)\cos(\omega_0 t+\alpha)\right] &= \mathcal{L}\left[y(t)\left[\cos(\omega_0 t)\cos(\alpha)-\sin(\omega_0 t)\sin(\alpha)\right]\right] &\text{(A-5)}\\
&= \cos(\alpha)\underbrace{\mathcal{L}\left[y(t)\cos(\omega_0 t)\right]}_{\text{Eq. (A-1)}}-\sin(\alpha)\underbrace{\mathcal{L}\left[y(t)\sin(\omega_0 t)\right]}_{\text{Eq. (A-2)}}\\
&= \frac{\cos\alpha}{2}\left[Y(s+j\omega_0)+Y(s-j\omega_0)\right]\\
&\quad -\frac{j\sin\alpha}{2}\left[Y(s+j\omega_0)-Y(s-j\omega_0)\right]\\
&= \frac{\cos\alpha-j\sin\alpha}{2}Y(s+j\omega_0)+\frac{\cos\alpha+j\sin\alpha}{2}Y(s-j\omega_0) &\text{(A-6)}\\
&= \frac{1}{2}\left[e^{-j\alpha}Y(s+j\omega_0)+e^{j\alpha}Y(s-j\omega_0)\right]. &\text{(A-7)}
\end{aligned}
$$

Secondly, the derivation is made for the sine with an offset,

$$
\begin{aligned}
\mathcal{L}\left[y(t)\sin(\omega_0 t+\alpha)\right] &= \mathcal{L}\left[y(t)\left[\sin(\omega_0 t)\cos(\alpha)+\cos(\omega_0 t)\sin(\alpha)\right]\right] &\text{(A-8)}\\
&= \cos(\alpha)\underbrace{\mathcal{L}\left[y(t)\sin(\omega_0 t)\right]}_{\text{Eq. (A-2)}}+\sin(\alpha)\underbrace{\mathcal{L}\left[y(t)\cos(\omega_0 t)\right]}_{\text{Eq. (A-1)}}\\
&= \frac{j\cos\alpha}{2}\left[Y(s+j\omega_0)-Y(s-j\omega_0)\right]\\
&\quad +\frac{\sin\alpha}{2}\left[Y(s+j\omega_0)+Y(s-j\omega_0)\right]\\
&= \frac{\sin\alpha+j\cos\alpha}{2}Y(s+j\omega_0)+\frac{\sin\alpha-j\cos\alpha}{2}Y(s-j\omega_0) &\text{(A-9)}\\
&= \frac{j}{2}\left[e^{-j\alpha}Y(s+j\omega_0)-e^{j\alpha}Y(s-j\omega_0)\right]. &\text{(A-10)}
\end{aligned}
$$

A-2 Completing the MBC-transform

It is now possible to apply the different Laplace transforms to get the MBC-transforms of the linearized model as described above. When taking the Laplace transform of Eq. (2-5) the following is obtained (with the help of Eq. (A-7) and Eq. (A-10)),

$$
\begin{bmatrix}\Theta_1(s)\\ \Theta_2(s)\\ \Theta_3(s)\end{bmatrix} = \underbrace{\frac{1}{2}\begin{bmatrix}1 & 1 & j & -j\\ e^{-j\frac{2\pi}{3}} & e^{j\frac{2\pi}{3}} & je^{-j\frac{2\pi}{3}} & -je^{j\frac{2\pi}{3}}\\ e^{-j\frac{4\pi}{3}} & e^{j\frac{4\pi}{3}} & je^{-j\frac{4\pi}{3}} & -je^{j\frac{4\pi}{3}}\end{bmatrix}}_{\mathcal{T}_\theta}\begin{bmatrix}\Theta_{\text{tilt}}(s+j\omega_0)\\ \Theta_{\text{tilt}}(s-j\omega_0)\\ \Theta_{\text{yaw}}(s+j\omega_0)\\ \Theta_{\text{yaw}}(s-j\omega_0)\end{bmatrix}. \tag{A-11}
$$

As was discussed in Chapter 2-2-2 a fully decoupled linear wind turbine model was assumed to describe the dynamics of the blades. The Laplace transformed expression of Eq. (2-8) is

$$
\begin{bmatrix}M_1(s)\\ M_2(s)\\ M_3(s)\end{bmatrix} = \begin{bmatrix}g_b(s) & 0 & 0\\ 0 & g_b(s) & 0\\ 0 & 0 & g_b(s)\end{bmatrix}\begin{bmatrix}\tilde{\Theta}_1(s)\\ \tilde{\Theta}_2(s)\\ \tilde{\Theta}_3(s)\end{bmatrix}. \tag{A-12}
$$

Substituting the obtained transformations for $\Theta_1(s)$ to $\Theta_3(s)$ from Eq. (A-11) (with $I_3 = \left[\begin{smallmatrix}1&0&0\\0&1&0\\0&0&1\end{smallmatrix}\right]$),

$$\begin{bmatrix}M_1(s)\\M_2(s)\\M_3(s)\end{bmatrix} = \frac{1}{2}g_b(s)I_3\begin{bmatrix}1 & 1 & j & -j\\ e^{-j\frac{2\pi}{3}} & e^{j\frac{2\pi}{3}} & je^{-j\frac{2\pi}{3}} & -je^{j\frac{2\pi}{3}}\\ e^{-j\frac{4\pi}{3}} & e^{j\frac{4\pi}{3}} & je^{-j\frac{4\pi}{3}} & -je^{j\frac{4\pi}{3}}\end{bmatrix}\begin{bmatrix}\Theta_{\text{tilt}}(s+j\omega_0)\\\Theta_{\text{tilt}}(s-j\omega_0)\\\Theta_{\text{yaw}}(s+j\omega_0)\\\Theta_{\text{yaw}}(s-j\omega_0)\end{bmatrix}. \tag{A-13}$$

If $s+j\omega_0$ and $s-j\omega_0$ are entered as arguments into Eq. (A-13) two new equations are obtained which come in useful later.

$$\begin{bmatrix}M_1(s+j\omega_0)\\M_2(s+j\omega_0)\\M_3(s+j\omega_0)\end{bmatrix} = \frac{1}{2}g_b(s+j\omega_0)I_3\begin{bmatrix}1 & 1 & j & -j\\ e^{-j\frac{2\pi}{3}} & e^{j\frac{2\pi}{3}} & je^{-j\frac{2\pi}{3}} & -je^{j\frac{2\pi}{3}}\\ e^{-j\frac{4\pi}{3}} & e^{j\frac{4\pi}{3}} & je^{-j\frac{4\pi}{3}} & -je^{j\frac{4\pi}{3}}\end{bmatrix}\begin{bmatrix}\Theta_{\text{tilt}}(s+2j\omega_0)\\\Theta_{\text{tilt}}(s)\\\Theta_{\text{yaw}}(s+2j\omega_0)\\\Theta_{\text{yaw}}(s)\end{bmatrix} \tag{A-14}$$

and

$$\begin{bmatrix}M_1(s-j\omega_0)\\M_2(s-j\omega_0)\\M_3(s-j\omega_0)\end{bmatrix} = \frac{1}{2}g_b(s-j\omega_0)I_3\begin{bmatrix}1 & 1 & j & -j\\ e^{-j\frac{2\pi}{3}} & e^{j\frac{2\pi}{3}} & je^{-j\frac{2\pi}{3}} & -je^{j\frac{2\pi}{3}}\\ e^{-j\frac{4\pi}{3}} & e^{j\frac{4\pi}{3}} & je^{-j\frac{4\pi}{3}} & -je^{j\frac{4\pi}{3}}\end{bmatrix}\begin{bmatrix}\Theta_{\text{tilt}}(s)\\\Theta_{\text{tilt}}(s-2j\omega_0)\\\Theta_{\text{yaw}}(s)\\\Theta_{\text{yaw}}(s-2j\omega_0)\end{bmatrix}. \tag{A-15}$$

It is possible to combine this all into a big matrix equation such that a relation for the frequency shifted moments are related.

$$\begin{bmatrix}M_1(s+j\omega_0)\\M_2(s+j\omega_0)\\M_3(s+j\omega_0)\\M_1(s-j\omega_0)\\M_2(s-j\omega_0)\\M_3(s-j\omega_0)\end{bmatrix} = \frac{1}{2}\begin{bmatrix}g_b(s+j\omega_0) & 0 & 0 & 0 & 0 & 0\\ 0 & g_b(s+j\omega_0) & 0 & 0 & 0 & 0\\ 0 & 0 & g_b(s+j\omega_0) & 0 & 0 & 0\\ 0 & 0 & 0 & g_b(s-j\omega_0) & 0 & 0\\ 0 & 0 & 0 & 0 & g_b(s-j\omega_0) & 0\\ 0 & 0 & 0 & 0 & 0 & g_b(s-j\omega_0)\end{bmatrix}$$
$$\begin{bmatrix}1 & 1 & j & -j & 0 & 0 & 0 & 0\\ e^{-j\frac{2\pi}{3}} & e^{j\frac{2\pi}{3}} & je^{-j\frac{2\pi}{3}} & -je^{j\frac{2\pi}{3}} & 0 & 0 & 0 & 0\\ e^{-j\frac{4\pi}{3}} & e^{j\frac{4\pi}{3}} & je^{-j\frac{4\pi}{3}} & -je^{j\frac{4\pi}{3}} & 0 & 0 & 0 & 0\\ 0 & 0 & 0 & 0 & 1 & 1 & j & -j\\ 0 & 0 & 0 & 0 & e^{-j\frac{2\pi}{3}} & e^{j\frac{2\pi}{3}} & je^{-j\frac{2\pi}{3}} & -je^{j\frac{2\pi}{3}}\\ 0 & 0 & 0 & 0 & e^{-j\frac{4\pi}{3}} & e^{j\frac{4\pi}{3}} & je^{-j\frac{4\pi}{3}} & -je^{j\frac{4\pi}{3}}\end{bmatrix}\begin{bmatrix}\Theta_{\text{tilt}}(s+2j\omega_0)\\\Theta_{\text{tilt}}(s)\\\Theta_{\text{yaw}}(s+2j\omega_0)\\\Theta_{\text{yaw}}(s)\\\Theta_{\text{tilt}}(s)\\\Theta_{\text{tilt}}(s-2j\omega_0)\\\Theta_{\text{yaw}}(s)\\\Theta_{\text{yaw}}(s-2j\omega_0)\end{bmatrix} \tag{A-16}$$

The final step that rests is to obtain the relation from $M_{\text{tilt}}, M_{\text{yaw}}$ to the yaw- and tilt-pitch angles in the Laplace domain is to make the Laplace transformation of Eq. (2-2).

$$
\begin{bmatrix} M_{\text{tilt}}(s) \\ M_{\text{yaw}}(s) \end{bmatrix} = \frac{2}{6} \begin{bmatrix} 1 & e^{-j\frac{2\pi}{3}} & e^{-j\frac{4\pi}{3}} & 1 & e^{j\frac{2\pi}{3}} & e^{j\frac{4\pi}{3}} \\ j & je^{-j\frac{2\pi}{3}} & je^{-j\frac{4\pi}{3}} & -j & -je^{j\frac{2\pi}{3}} & -je^{j\frac{4\pi}{3}} \end{bmatrix} \begin{bmatrix} M_1(s+j\omega_0) \\ M_2(s+j\omega_0) \\ M_3(s+j\omega_0) \\ M_1(s-j\omega_0) \\ M_2(s-j\omega_0) \\ M_3(s-j\omega_0) \end{bmatrix} \tag{A-17}
$$

From the Laplace transformation it becomes clear why the frequency shifted equation as build up in Eq. (A-16) was made. This can now be substituted in the Laplace transform of the tilt- and yaw-moments as described in Eq. (A-17). The full description then becomes

$$
\begin{aligned}
\begin{bmatrix} M_{\text{tilt}}(s) \\ M_{\text{yaw}}(s) \end{bmatrix} = \frac{2}{12} & \begin{bmatrix} 1 & e^{-j\frac{2\pi}{3}} & e^{-j\frac{4\pi}{3}} & 1 & e^{j\frac{2\pi}{3}} & e^{j\frac{4\pi}{3}} \\ j & je^{-j\frac{2\pi}{3}} & je^{-j\frac{4\pi}{3}} & -j & -je^{j\frac{2\pi}{3}} & -je^{j\frac{4\pi}{3}} \end{bmatrix} \\
& \begin{bmatrix}
g_b(s+j\omega_0) & g_b(s+j\omega_0) & jg_b(s+j\omega_0) & -jg_b(s+j\omega_0) & 0 & 0 & 0 & 0 \\
e^{-j\frac{2\pi}{3}} g_b(s+j\omega_0) & e^{j\frac{2\pi}{3}} g_b(s+j\omega_0) & je^{-j\frac{2\pi}{3}} g_b(s+j\omega_0) & -je^{j\frac{2\pi}{3}} g_b(s+j\omega_0) & 0 & 0 & 0 & 0 \\
e^{-j\frac{4\pi}{3}} g_b(s+j\omega_0) & e^{j\frac{4\pi}{3}} g_b(s+j\omega_0) & je^{-j\frac{4\pi}{3}} g_b(s+j\omega_0) & -je^{j\frac{4\pi}{3}} g_b(s+j\omega_0) & 0 & 0 & 0 & 0 \\
0 & 0 & 0 & 0 & g_b(s-j\omega_0) & g_b(s-j\omega_0) & jg_b(s-j\omega_0) & -jg_b(s-j\omega_0) \\
0 & 0 & 0 & 0 & e^{-j\frac{2\pi}{3}} g_b(s-j\omega_0) & e^{j\frac{2\pi}{3}} g_b(s-j\omega_0) & je^{-j\frac{2\pi}{3}} g_b(s-j\omega_0) & -je^{j\frac{2\pi}{3}} g_b(s-j\omega_0) \\
0 & 0 & 0 & 0 & e^{-j\frac{4\pi}{3}} g_b(s-j\omega_0) & e^{j\frac{4\pi}{3}} g_b(s-j\omega_0) & je^{-j\frac{4\pi}{3}} g_b(s-j\omega_0) & -je^{j\frac{4\pi}{3}} g_b(s-j\omega_0)
\end{bmatrix}
\begin{bmatrix} \Theta_{\text{tilt}}(s+2j\omega_0) \\ \Theta_{\text{tilt}}(s) \\ \Theta_{\text{yaw}}(s+2j\omega_0) \\ \Theta_{\text{yaw}}(s) \\ \Theta_{\text{tilt}}(s) \\ \Theta_{\text{tilt}}(s-2j\omega_0) \\ \Theta_{\text{yaw}}(s) \\ \Theta_{\text{yaw}}(s-2j\omega_0) \end{bmatrix}
\end{aligned} \tag{A-18}
$$

To get a clearer picture of what is actually happening in Eq. (A-18) the $g_b(\ldots)$ terms are omitted from the big matrix and the multiplication of the two constant matrices is performed after which the multiplication of the $g_b(\ldots)$ will be reintroduced in its proper form.

It should be noted that this matrix multiplication and subsequent cancelling of the columns performed below is just there to indicate the dropping out of many different terms. The actual mathematical multiplication was carried out with care using the full matrix as described in Eq. (A-18).

$$
\begin{aligned}
& \begin{bmatrix} 1 & e^{-j\frac{2\pi}{3}} & e^{-j\frac{4\pi}{3}} & 1 & e^{j\frac{2\pi}{3}} & e^{j\frac{4\pi}{3}} \\ j & je^{-j\frac{2\pi}{3}} & je^{-j\frac{4\pi}{3}} & -j & -je^{j\frac{2\pi}{3}} & -je^{j\frac{4\pi}{3}} \end{bmatrix}
\begin{bmatrix}
1 & 1 & j & -j & 0 & 0 & 0 & 0 \\
e^{-j\frac{2\pi}{3}} & e^{j\frac{2\pi}{3}} & je^{-j\frac{2\pi}{3}} & -je^{j\frac{2\pi}{3}} & 0 & 0 & 0 & 0 \\
e^{-j\frac{4\pi}{3}} & e^{j\frac{4\pi}{3}} & je^{-j\frac{4\pi}{3}} & -je^{j\frac{4\pi}{3}} & 0 & 0 & 0 & 0 \\
0 & 0 & 0 & 0 & 1 & 1 & j & -j \\
0 & 0 & 0 & 0 & e^{-j\frac{2\pi}{3}} & e^{j\frac{2\pi}{3}} & je^{-j\frac{2\pi}{3}} & -je^{j\frac{2\pi}{3}} \\
0 & 0 & 0 & 0 & e^{-j\frac{4\pi}{3}} & e^{j\frac{4\pi}{3}} & je^{-j\frac{4\pi}{3}} & -je^{j\frac{4\pi}{3}}
\end{bmatrix} = \\
& \begin{bmatrix} 0 & 3 & 0 & -3j & 3 & 0 & 3j & 0 \\ 0 & 3j & 0 & 3 & -3j & 0 & 3 & 0 \end{bmatrix}
\end{aligned} \tag{A-19}
$$

Now that it has become clear that many terms drop out in the multiplication of the constant matrices the multiplication performed in Eq. (A-18) ends up as (where all the zero columns of the matrix in Eq. (A-19) will be omitted).

$$
\begin{bmatrix} M_{\text{tilt}}(s) \\ M_{\text{yaw}}(s) \end{bmatrix} = \frac{1}{2} \begin{bmatrix} 0 & 1 & 0 & -j & 1 & 0 & j & 0 \\ 0 & j & 0 & 1 & -j & 0 & 1 & 0 \end{bmatrix} \begin{bmatrix} \Theta_{\text{tilt}}(s+2j\omega_0) \\ \Theta_{\text{tilt}}(s) \\ \Theta_{\text{yaw}}(s+2j\omega_0) \\ \Theta_{\text{yaw}}(s) \\ \Theta_{\text{tilt}}(s) \\ \Theta_{\text{tilt}}(s-2j\omega_0) \\ \Theta_{\text{yaw}}(s) \\ \Theta_{\text{yaw}}(s-2j\omega_0) \end{bmatrix} =
$$

$$
\frac{1}{2} \begin{bmatrix} 1 & -j & 1 & j \\ j & 1 & -j & 1 \end{bmatrix} \begin{bmatrix} \Theta_{\text{tilt}}(s) \\ \Theta_{\text{yaw}}(s) \\ \Theta_{\text{tilt}}(s) \\ \Theta_{\text{yaw}}(s) \end{bmatrix} \tag{A-20}
$$

Now that has become clear what is cancelled against each other, the derivation is continued with the $g_b(s+j\omega_0), g_b(s-j\omega_0)$ terms in their proper places.

$$
\begin{bmatrix} M_{\text{tilt}}(s) \\ M_{\text{yaw}}(s) \end{bmatrix} = \frac{1}{2} \begin{bmatrix} g_b(s+j\omega_0) & -jg_b(s+j\omega_0) & g_b(s-j\omega_0) & jg_b(s-j\omega_0) \\ jg_b(s+j\omega_0) & g_b(s+j\omega_0) & -jg_b(s-j\omega_0) & g_b(s-j\omega_0) \end{bmatrix} \begin{bmatrix} \Theta_{\text{tilt}}(s) \\ \Theta_{\text{yaw}}(s) \\ \Theta_{\text{tilt}}(s) \\ \Theta_{\text{yaw}}(s) \end{bmatrix} =
$$

$$
\begin{bmatrix} \frac{g_b(s-j\omega_0)+g_b(s+j\omega_0)}{2} & j\frac{g_b(s-j\omega_0)-g_b(s+j\omega_0)}{2} \\ -j\frac{g_b(s-j\omega_0)-g_b(s+j\omega_0)}{2} & \frac{g_b(s-j\omega_0)+g_b(s+j\omega_0)}{2} \end{bmatrix} \begin{bmatrix} \Theta_{\text{tilt}}(s) \\ \Theta_{\text{yaw}}(s) \end{bmatrix} \tag{A-21}
$$

Here the final form has been derived. This form is used as the basis of the different variations made on the MBC-transformation.

Appendix B

Offset Derivation MBC-Transformation

In this Appendix, the exact mathematical consequences of the introduction of an offset in the MBC-transformation are discussed. First it is discussed in the context of an offset being present in the Inverse MBC-transformation, then in the normal MBC-transformation and finally in the case it is present in both the MBC-transformations. This Appendix serves as the mathematical derivations of Chapter 2-3.

B-1 Offset in the inverse MBC-transformation

As was shown in Figure 2-5 the offset in the inverse MBC-transformation has as a consequence that the derivation changes, because one of the matrices which is used in the derivation changes. The change in the matrix is described in Eq. (2-10).

The change described in Figure 2-5 and Eq. (2-10) means that the inverse MBC-transformation is changed a little bit, while the MBC-transformation (Eq. (2-2)) remains exactly the same. This also means that in terms of the Laplace transforms that Eq. (A-11) also changes a little bit.

$$\begin{bmatrix} \Theta_1(s) \\ \Theta_2(s) \\ \Theta_3(s) \end{bmatrix} = \underbrace{\frac{1}{2}\begin{bmatrix} e^{-j\psi_\theta} & e^{j\psi_\theta} & je^{-j\psi_\theta} & -je^{j\psi_\theta} \\ e^{-j(\frac{2\pi}{3}+\psi_\theta)} & e^{j(\frac{2\pi}{3}+\psi_\theta)} & je^{-j(\frac{2\pi}{3}+\psi_\theta)} & -je^{j(\frac{2\pi}{3}+\psi_\theta)} \\ e^{-j(\frac{4\pi}{3}+\psi_\theta)} & e^{j(\frac{4\pi}{3}+\psi_\theta)} & je^{-j(\frac{4\pi}{3}+\psi_\theta)} & -je^{j(\frac{4\pi}{3}+\psi_\theta)} \end{bmatrix}}_{\mathcal{T}_{\theta_{\text{off}}}} \begin{bmatrix} \Theta_{\text{tilt}}(s+j\omega_0) \\ \Theta_{\text{tilt}}(s-j\omega_0) \\ \Theta_{\text{yaw}}(s+j\omega_0) \\ \Theta_{\text{yaw}}(s-j\omega_0) \end{bmatrix} \quad \text{(B-1)}$$

While Eq. (A-17) remains the same transformation. As a result the multiplication performed in Eq. (A-19) now changes, because of the change the block diagonal matrices. This means that the new multiplication ends up as:

$$\begin{bmatrix} 1 & e^{-j\frac{2\pi}{3}} & e^{-j\frac{4\pi}{3}} & 1 & e^{j\frac{2\pi}{3}} & e^{j\frac{4\pi}{3}} \\ j & je^{-j\frac{2\pi}{3}} & je^{-j\frac{4\pi}{3}} & -j & -je^{j\frac{2\pi}{3}} & -je^{j\frac{4\pi}{3}} \end{bmatrix} \begin{bmatrix} \mathcal{T}_{\theta_{\text{off}}} & 0 \\ 0 & \mathcal{T}_{\theta_{\text{off}}} \end{bmatrix} = \begin{bmatrix} 0 & 3e^{j\psi_\theta} & 0 & -3je^{j\psi_\theta} & 3e^{-j\psi_\theta} & 0 & 3je^{-j\psi_\theta} & 0 \\ 0 & 3je^{j\psi_\theta} & 0 & 3e^{j\psi_\theta} & -3je^{-j\psi_\theta} & 0 & 3e^{-j\psi_\theta} & 0 \end{bmatrix} \tag{B-2}$$

Which means that the final form as was seen in Eq. (2-9) without the offset changes into the following form with the offset:

$$\begin{bmatrix} M_{\text{tilt}}(s) \\ M_{\text{yaw}}(s) \end{bmatrix} = \begin{bmatrix} \frac{e^{-j\psi_\theta} g_b(s-j\omega_0)+e^{j\psi_\theta} g_b(s+j\omega_0)}{2} & j\frac{e^{-j\psi_\theta} g_b(s-j\omega_0)-e^{j\psi_\theta} g_b(s+j\omega_0)}{2} \\ -j\frac{e^{-j\psi_\theta} g_b(s-j\omega_0)-e^{j\psi_\theta} g_b(s+j\omega_0)}{2} & \frac{e^{-j\psi_\theta} g_b(s-j\omega_0)+e^{j\psi_\theta} g_b(s+j\omega_0)}{2} \end{bmatrix} \begin{bmatrix} \Theta_{\text{tilt}}(s) \\ \Theta_{\text{yaw}}(s) \end{bmatrix} \tag{B-3}$$

B-2 Offset in the MBC-transformation

If the offset is now introduced in the MBC-transformation, a description of the form of Figure 2-6 and Eq. (2-12) is obtained. Once again, this changes the derivation slightly. In this case a change in phase occurs in Eq. (A-17) (or in other words, an extra term $e^{j\psi_M}$ is introduced). If the Laplace transforms calculations are followed carefully with the help of Eq. (A-7) and Eq. (A-10) we obtain the new form of Eq. (A-17),

$$\begin{bmatrix} M_{\text{tilt}}(s) \\ M_{\text{yaw}}(s) \end{bmatrix} = \frac{2}{6} \begin{bmatrix} e^{-j\psi_M} & e^{-j(\frac{2\pi}{3}+\psi_M)} & e^{-j(\frac{4\pi}{3}+\psi_M)} & e^{j\psi_M} & e^{j(\frac{2\pi}{3}+\psi_M)} & e^{j(\frac{4\pi}{3}+\psi_M)} \\ je^{-j\psi_M} & je^{-j(\frac{2\pi}{3}+\psi_M)} & je^{-j(\frac{4\pi}{3}+\psi_M)} & -je^{j\psi_M} & -je^{j(\frac{2\pi}{3}+\psi_M)} & -je^{j(\frac{4\pi}{3}+\psi_M)} \end{bmatrix} \begin{bmatrix} \tilde{M}_1(s+j\omega_0) \\ \tilde{M}_2(s+j\omega_0) \\ \tilde{M}_3(s+j\omega_0) \\ \tilde{M}_1(s-j\omega_0) \\ \tilde{M}_2(s-j\omega_0) \\ \tilde{M}_3(s-j\omega_0) \end{bmatrix}. \tag{B-4}$$

As Eq. (A-11) remains unchanged, just one matrix in the multiplication of Eq. (A-19) changes, namely

$$\begin{bmatrix} e^{-j\psi_M} & e^{-j(\frac{2\pi}{3}+\psi_M)} & e^{-j(\frac{4\pi}{3}+\psi_M)} & e^{j\psi_M} & e^{j(\frac{2\pi}{3}+\psi_M)} & e^{j(\frac{4\pi}{3}+\psi_M)} \\ je^{-j\psi_M} & je^{-j(\frac{2\pi}{3}+\psi_M)} & je^{-j(\frac{4\pi}{3}+\psi_M)} & -je^{j\psi_M} & -je^{j(\frac{2\pi}{3}+\psi_M)} & -je^{j(\frac{4\pi}{3}+\psi_M)} \end{bmatrix} \begin{bmatrix} \mathcal{T}_\theta(s) & 0 \\ 0 & \mathcal{T}_\theta(s) \end{bmatrix} = \begin{bmatrix} 0 & 3e^{-j\psi_M} & 0 & -3je^{-j\psi_M} & 3e^{j\psi_M} & 0 & 3je^{j\psi_M} & 0 \\ 0 & 3je^{-j\psi_M} & 0 & 3e^{-j\psi_M} & -3je^{j\psi_M} & 0 & 3e^{j\psi_M} & 0 \end{bmatrix}. \tag{B-5}$$

As a result the final part of the MBC-transformation can be finilized as

$$\begin{bmatrix} M_{\text{tilt}}(s) \\ M_{\text{yaw}}(s) \end{bmatrix} = \begin{bmatrix} \frac{e^{j\psi_M} g_b(s-j\omega_0)+e^{-j\psi_M} g_b(s+j\omega_0)}{2} & j\frac{e^{j\psi_M} g_b(s-j\omega_0)-e^{-j\psi_M} g_b(s+j\omega_0)}{2} \\ -j\frac{e^{j\psi_M} g_b(s-j\omega_0)-e^{-j\psi_M} g_b(s+j\omega_0)}{2} & \frac{e^{j\psi_M} g_b(s-j\omega_0)+e^{-j\psi_M} g_b(s+j\omega_0)}{2} \end{bmatrix} \begin{bmatrix} \Theta_{\text{tilt}}(s) \\ \Theta_{\text{yaw}}(s) \end{bmatrix}. \tag{B-6}$$

B-3 Offset in both the MBC-transformations

If the offset is now introduced in both the MBC-transformations, a description of the form of Figure 2-7 and Eq. (2-10) and Eq. (2-12) is obtained. If the derivation is made once more, but now with both offsets being present one will see that in Eq. (A-19) both matrices will change in the respective ways they did in Eq. (B-2), and Eq. (B-5). This results in the following multplication

$$\begin{bmatrix} e^{-j\psi_M} & e^{-j(\frac{2\pi}{3}+\psi_M)} & e^{-j(\frac{4\pi}{3}+\psi_M)} & e^{j\psi_M} & e^{j(\frac{2\pi}{3}+\psi_M)} & e^{j(\frac{4\pi}{3}+\psi_M)} \\ je^{-j\psi_M} & je^{-j(\frac{2\pi}{3}+\psi_M)} & je^{-j(\frac{4\pi}{3}+\psi_M)} & -je^{j\psi_M} & -je^{j(\frac{2\pi}{3}+\psi_M)} & -je^{j(\frac{4\pi}{3}+\psi_M)} \end{bmatrix} \begin{bmatrix} \mathcal{T}_{\theta_{\text{off}}} & 0 \\ 0 & \mathcal{T}_{\theta_{\text{off}}} \end{bmatrix} =$$
$$\begin{bmatrix} 0 & 3e^{j(\psi_\theta-\psi_M)} & 0 & -3je^{j(\psi_\theta-\psi_M)} & 3e^{-j(\psi_\theta-\psi_M)} & 0 & 3je^{-j(\psi_\theta-\psi_M)} & 0 \\ 0 & 3je^{j(\psi_\theta-\psi_M)} & 0 & 3e^{j(\psi_\theta-\psi_M)} & -3je^{-j(\psi_\theta-\psi_M)} & 0 & 3e^{-j(\psi_\theta-\psi_M)} & 0 \end{bmatrix}. \quad \text{(B-7)}$$

This means that not all that much changes if the offset is in the regular part or in the inverse part of the MBC-transformation, because the offsets are just subtracted from each other in the phase shift. This also means that the final part of the transformations can be written as

$$\begin{bmatrix} M_{\text{tilt}}(s) \\ M_{\text{yaw}}(s) \end{bmatrix} = \begin{bmatrix} \frac{e^{-j(\psi_\theta-\psi_M)}g_b(s-j\omega_0)+e^{j(\psi_\theta-\psi_M)}g_b(s+j\omega_0)}{2} \\ -j\frac{e^{-j(\psi_\theta-\psi_M)}g_b(s-j\omega_0)-e^{j(\psi_\theta-\psi_M)}g_b(s+j\omega_0)}{2} \end{bmatrix} \cdots$$
$$\begin{bmatrix} j\frac{e^{-j(\psi_\theta-\psi_M)}g_b(s-j\omega_0)-e^{j(\psi_\theta-\psi_M)}g_b(s+j\omega_0)}{2} \\ \frac{e^{-j(\psi_\theta-\psi_M)}g_b(s-j\omega_0)+e^{j(\psi_\theta-\psi_M)}g_b(s+j\omega_0)}{2} \end{bmatrix} \begin{bmatrix} \Theta_{\text{tilt}}(s) \\ \Theta_{\text{yaw}}(s) \end{bmatrix}. \quad \text{(B-8)}$$

Appendix C

Analytical Derivation Ideal Offset First-Order Approximation

In Chapter 3-1 a description is given to decouple the 1st-order MBC-transformed system. As discussed there, it can be done by considering different frequency regions. One where $\omega \ll \omega_0$, $\omega \approx \omega_0$, and $\omega \gg \omega_0$.

For the low-frequency region, the term $(\tau\omega \sin\psi)^2 \approx 0$ which means the ideal offset can be calculated as

$$\begin{aligned} \omega \ll \omega_0 \quad &\Rightarrow \quad \arg\min_\psi |P_{12}(j\omega)| \approx \arg\min_\psi \sqrt{(\sin\psi - \tau\omega_0 \cos\psi)^2} \\ &\Leftrightarrow \quad \sin\psi - \tau\omega_0\cos\psi = 0 \\ &\Leftrightarrow \quad \sin\psi = \tau\omega_0 \cos\psi \\ &\Leftrightarrow \quad \tan\psi = \tau\omega_0 \\ &\Leftrightarrow \quad \psi = \tan^{-1}(\tau\omega_0). \end{aligned} \tag{C-1}$$

It is important to state that this is only valid for $\psi \in \left[-\frac{\pi}{2}, \frac{\pi}{2}\right]$ rad. For the case that $\omega \gg \omega_0$ a similar dropout happens in the numerator of Eq. (3-5), but this time it is due to the fact that $(\tau\omega\sin\psi)^2 \gg (\sin\psi - \tau\omega_0\cos\psi)^2$ whereby making this second term negligible in its contribution to the magnitude. As a result the ideal offset in the high-frequency region is

$$\begin{aligned} \omega \gg \omega_0 \quad &\Rightarrow \quad \arg\min_\psi |P_{12}(j\omega)| \approx \arg\min_\psi \sqrt{(\tau\omega\sin\psi)^2} \\ &\Rightarrow \quad \psi = 0. \end{aligned} \tag{C-2}$$

This leaves the region where $\omega \approx \omega_0$. In this case it is significantly more laborious to see if a definite single ideal offset exists which allows for a maximum amount of decoupling. Even though the derivation is laborious it is still possible analytically and it goes as follows,

$$
\begin{array}{rcl}
\omega \approx \omega_0 & \Rightarrow & \arg\min_\psi |P_{12}(j\omega)| \\
& = & \arg\min_\psi \sqrt{(\sin\psi - \tau\omega_0\cos\psi)^2 + (\tau\omega\sin\psi)^2} \\
& = & \arg\min_\psi (\sin\psi - \tau\omega_0\cos\psi)^2 + (\tau\omega\sin\psi)^2 \\
& = & \arg\min_\psi \left(\sin^2\psi - 2\tau\omega_0\sin\psi\cos\psi + \tau^2\omega_0^2\cos^2\psi + \tau^2\omega^2\sin^2\psi\right) \\
& \overset{\omega=\omega_0}{=} & \arg\min_\psi \left(\sin\psi\left(\sin\psi - 2\tau\omega_0\cos\psi\right) + \tau^2\omega_0^2\right) \\
& \Rightarrow & \frac{\mathrm{d}}{\mathrm{d}\psi}\left(\sin\psi\left(\sin\psi - 2\tau\omega_0\cos\psi\right) + \tau^2\omega_0^2\right) = 0 \\
& = & 2\sin\psi\cos\psi - 2\tau\omega_0\cos^2\psi + 2\tau\omega_0\sin^2\psi \\
& = & \sin(2\psi) - 2\tau\omega_0\cos(2\psi) = 0 \\
& \Leftrightarrow & \sin(2\psi) = 2\tau\omega_0\cos(2\psi) \\
& \Leftrightarrow & \tan(2\psi) = 2\tau\omega_0 \\
& \Leftrightarrow & \psi = \frac{\tan^{-1}(2\tau\omega_0)}{2}, \text{ valid for } \psi \in \left[-\frac{\pi}{2}, \frac{\pi}{2}\right].
\end{array}
\tag{C-3}
$$

Bibliography

[1] E. Hau, *Wind turbines: fundamentals, technologies, application, economics*. Springer Science & Business Media, 2013.

[2] "GWEC global wind statistics 2017." http://gwec.net/wp-content/uploads/2018/04/Global-Cumulative-Installed-Wind-Capacity-2001-2017.jpg. Accessed: 2017-06-19.

[3] P. Agreement, "United nations framework convention on climate change," *Paris, France*, 2015.

[4] L. Y. Pao and K. E. Johnson, "Control of wind turbines," *IEEE Control Systems*, vol. 31, no. 2, pp. 44–62, 2011.

[5] F. D. Bianchi, R. J. Mantz, and H. De Battista, *Wind Turbine Control Systems, Principles, Modelling and Gain Scheduling Design*. Springer, 2007.

[6] E. Bossanyi, "Individual blade pitch control for load reduction," *Wind energy*, vol. 6, no. 2, pp. 119–128, 2003.

[7] E. W. E. Association *et al.*, "Wind energy–the facts. a guide to the technology, economics and future of wind power," *Earthscan, London, UK*, 2009.

[8] M. H. Hansen, "Aeroelastic instability problems for wind turbines," *Wind Energy*, vol. 10, no. 6, pp. 551–577, 2007.

[9] G. F. Franklin, J. D. Powell, A. Emami-Naeini, and J. D. Powell, *Feedback control of dynamic systems*, vol. 3. Addison-Wesley Reading, MA, 1994.

[10] G. Bir, "Multiblade coordinate transformation and its application to wind turbine analysis," in *ASME Wind Energy Symposium*, pp. 1–15, 2008.

[11] T. Van Engelen, "Design model and load reduction assessment for multi-rotational mode individual pitch control (higher harmonics control)," in *European Wind Energy Conference*, pp. 27–2, 2006.

[12] E. Solingen and J. Wingerden, "Linear individual pitch control design for two-bladed wind turbines," *Wind Energy*, vol. 18, no. 4, pp. 677–697, 2015.

[13] M. Jelavić, V. Petrović, and N. Perić, "Estimation based individual pitch control of wind turbine," *Automatika*, vol. 51, no. 2, pp. 181–192, 2010.

[14] J. Ehlers, A. Diop, and H. Bindner, "Sensor selection and state estimation for wind turbine controls," in *45th AIAA Aerospace Sciences Meeting and Exhibit*, p. 1019, 2007.

[15] E. A. Bossanyi, P. A. Fleming, and A. D. Wright, "Validation of individual pitch control by field tests on two-and three-bladed wind turbines," *IEEE Transactions on Control Systems Technology*, vol. 21, no. 4, pp. 1067–1078, 2013.

[16] E. Solingen, P. A. Fleming, A. Scholbrock, and J. Wingerden, "Field testing of linear individual pitch control on the two-bladed controls advanced research turbine," *Wind Energy*, vol. 19, no. 3, pp. 421–436, 2016.

[17] M. D. Spencer, K. A. Stol, C. P. Unsworth, J. E. Cater, and S. E. Norris, "Model predictive control of a wind turbine using short-term wind field predictions," *Wind Energy*, vol. 16, no. 3, pp. 417–434, 2013.

[18] Q. Lu, R. Bowyer, and B. L. Jones, "Analysis and design of coleman transform-based individual pitch controllers for wind-turbine load reduction," *Wind Energy*, vol. 18, no. 8, pp. 1451–1468, 2015.

[19] M. Vali, J.-W. van Wingerden, and M. Kühn, "Optimal multivariable individual pitch control for load reduction of large wind turbines," in *American Control Conference (ACC), 2016*, pp. 3163–3169, IEEE, 2016.

[20] E. Bossanyi and D. Witcher, "Controller for 5mw reference turbine," *Project UpWind, Bristol, England, Tech. Rep*, 2009.

[21] I. Houtzager, J. van Wingerden, and M. Verhaegen, "Wind turbine load reduction by rejecting the periodic load disturbances," *Wind Energy*, vol. 16, no. 2, pp. 235–256, 2013.

[22] A. Pamososuryo, "Enhancement of conventional ipc decoupling by inclusion of an azimuth offset.," Master's thesis, Delft University of Technology, The Netherlands, 2018.

[23] W. Johnson, *Helicopter theory.* Courier Corporation, 2012.

[24] R. Miller, "Helicopter control and stability in hovering flight," *Journal of the Aeronautical Sciences*, vol. 15, no. 8, pp. 453–472, 1948.

[25] R. P. Coleman and A. M. Feingold, "Theory of self-excited mechanical oscillations of helicopter rotors with hinged blades," 1957.

[26] K. H. Hohenemser and S.-K. Yin, "Some applications of the method of multiblade coordinates," *Journal of the American Helicopter Society*, vol. 17, no. 3, pp. 3–12, 1972.

[27] P. Caselitz, W. Kleinkauf, T. Krüger, J. Petschenka, M. Reichardt, and K. Störzel, "Reduction of fatigue loads on wind energy converters by advanced control methods," in *EWEC-CONFERENCE-*, pp. 555–558, BOOKSHOP FOR SCIENTIFIC PUBLICATIONS, 1997.

[28] S. Skogestad and I. Postlethwaite, *Multivariable feedback control: analysis and design*, vol. 2. Wiley New York, 2007.

[29] P. Grosdidier, M. Morari, and B. R. Holt, “Closed-loop properties from steady-state gain information,” *Industrial & engineering chemistry fundamentals*, vol. 24, no. 2, pp. 221–235, 1985.

[30] J. Jonkman, S. Butterfield, W. Musial, and G. Scott, “Definition of a 5-mw reference wind turbine for offshore system development,” tech. rep., National Renewable Energy Lab.(NREL), Golden, CO (United States), 2009.

[31] J. M. Jonkman and M. L. Buhl Jr, “Fast user’s guide-updated august 2005,” tech. rep., National Renewable Energy Laboratory (NREL), Golden, CO., 2005.

[32] G. S. Bir, “User’s guide to mbc3: Multi-blade coordinate transformation code for 3-bladed wind turbine,” tech. rep., National Renewable Energy Laboratory (NREL), Golden, CO., 2010.

[33] L. Ljung, “System identification,” in *Signal analysis and prediction*, pp. 163–173, Springer, 1998.

[34] V. M. van Wingerden J. W., “Closed loop identification of mimo hammerstein models using ls-svm,” in *in Proceedings of the 15th IFAC conference on system identification (SYSID 2009), Saint Malo, France, July 2009*, 2009.

[35] v. W. J. W. Mulders S.P., “On the averaging in the multi-blade coordinate transformations for wind turbines: a $\mathcal{H}_\infty$ model matching approach.,” in *in Proceedings of the 2018 IEEE Conference on Control Technology and Applications (CCTA)*, 2018.

[36] Y. Tan, W. Moase, C. Manzie, D. Nešić, and I. Mareels, “Extremum seeking from 1922 to 2010,” in *Control Conference (CCC), 2010 29th Chinese*, pp. 14–26, IEEE, 2010.

Glossary

List of Acronyms

CPC	Collective Pitch Control
DCSC	Delft Center for Systems and Control
ESC	Extremum Seeking Control
EWEA	European Wind Energy Association
FAST	Fatigue, Aerodynamics, Structures and Turbulence
GWEC	Global Wind Energy Council
HAWT	Horizontal Axis Wind Turbine
IPC	Individual Pitch Control/Individual Pitch Controller
LCoE	Levelised Cost of Energy
LQG	Linear Quadratic Gaussian
MBC	Multi-Blade Coordinate
MPC	Model Predictive Control
MIMO	Multiple-Input Multiple-Output
NREL	National Renewable Energy Laboratory
OoP	Out-of-Plane
PBSID	Predictor-Based-Subspace-IDentification
PI	Proportional Integral
PSD	Power Spectral Density
RBS	Random Binary Signals

RGA Relative Gain Array

SISO Single-Input Single-Output

SVD Singular Value Decomposition